Quarterly Reviews of Biophysics **35**, 4 (2002), pp. 369–430. © 2002 Cambridge University Press
DOI: 10.1017/S0033583502003815 Printed in the United Kingdom

What vibrations tell us about proteins

Andreas Barth* and Christian Zscherp

Institut für Biophysik, Johann Wolfgang Goethe-Universität, Theodor Stern-Kai 7, Haus 74, D-60590 Frankfurt am Main, Germany

Abstract. This review deals with current concepts of vibrational spectroscopy for the investigation of protein structure and function. While the focus is on infrared (IR) spectroscopy, some of the general aspects also apply to Raman spectroscopy. Special emphasis is on the amide I vibration of the polypeptide backbone that is used for secondary-structure analysis. Theoretical as well as experimental aspects are covered including transition dipole coupling. Further topics are discussed, namely the absorption of amino-acid side-chains, $^{1}H/^{2}H$ exchange to study the conformational flexibility and reaction-induced difference spectroscopy for the investigation of reaction mechanisms with a focus on interpretation tools.

* Address for correspondence (present address): Andreas Barth, Institute of Biochemistry and Biophysics, The Arrhenius Laboratories for Natural Sciences, Stockholm University, SE-106 91 Stockholm, Sweden.
Tel.: +46 8 16 2452; Fax: +46 8 15 5597; E-mail: Andreas.Barth@dbb.su.se

1. Introduction

The average yeast protein has more than 20 000 vibrational degrees of freedom, the normal modes of vibration.[1] In general, a normal mode couples movements of several internal coordinates (bond lengths and bond angles). For many of them, the number of contributing internal coordinates is small, some even are dominated by only one internal coordinate, like many C═O stretching vibrations. These vibrations involve only a few atoms and are thus localized on a small portion of a protein, for example on the functional group of an amino-acid side-chain. It is these group vibrations that are the most valuable for the spectroscopist when she or he wants to reveal the molecular secrets of proteins because group vibrations are reporters of group structure and group environment.

Abbreviations: ATR, attenuated total reflection; δ, in-plane bending vibration; IR, infrared; NMA, *N*-methylacetamide; ν, stretching vibration; TDC, transition dipole coupling; TDM, transition dipole moment.

[1] This estimate is based on the following: the average yeast protein consists of 500 amino acids (Netzer & Hartl, 1997). As the average number of atoms per amino acid is 15 (according to their relative abundance in *E. coli*, Table 5-3 in Lehninger, 1987), the total number of atoms adds up to 7500. Each atom has 3 degrees of freedom, which gives more than 20 000 degrees of freedom for the whole protein. While 6 degrees correspond to the translational and rotational movements of the whole protein, all the rest are vibrational degrees of freedom, i.e. the normal modes of vibration of the protein.

Given the vast number of normal modes, the vibrational spectrum is complex with many of the vibrational bands overlapping. Therefore, attempts to extract meaningful information from the spectrum may appear futile. However, we will see that this is not the case. On the one hand it is often possible to select a spectral region that provides answers to specific questions. A suitable region would be one where the same kind of normal mode of the many repeat units in a protein dominates the spectrum. An example is the amide I region, dominated by signals of the backbone C=O vibrations, that encodes the secondary structure of a protein. On the other hand, with special difference techniques it is possible to observe only those groups that actively participate in a catalytic reaction – with a sensitivity high enough to detect one out of the many thousands of normal modes. This mode reports exclusively on the events in the vicinity of the vibrating group and it is possible to follow the fate of that group in the course of a protein reaction in time-resolved experiments.

The vibrational spectrum of biomolecules can be observed using Raman scattering (reviewed by Spiro & Gaber, 1977; Callender & Deng, 1994; Robert, 1996; Carey, 1998, 1999; Deng & Callender, 1999) and the absorption of IR light (reviewed by Arrondo *et al.* 1993; Goormaghtigh *et al.* 1994a; Haris & Chapman, 1994; Siebert, 1995). It is usually plotted against the wavenumber $\tilde{\nu} = 1/\lambda$ (in units of cm^{-1}) which is the inverse of the wavelength λ. We will focus here on IR spectroscopy. IR light can be absorbed by a molecular vibration when the frequencies of light and vibration coincide. The frequency of the vibration and the probability of absorption depend on the strength and polarity of the vibrating bonds and are thus influenced by intra- and intermolecular effects. As pointed out by Deng & Callender (1999), vibrational spectroscopy is exceptionally sensitive to changes in bond strength since a change of 0·02% can be easily detected. (This is a cautious estimate based on a spectral resolution of 5 cm^{-1}.) As bond energy and bond length are directly related, bond distortions in the course of a catalytic reaction can be monitored with an astonishing accuracy. They concluded: 'although an oversimplification, it can be said that the resolution of vibrational spectroscopy picks up where diffraction and multidimensional nuclear magnetic resonance (NMR) techniques leave off, at approximately 0·2 Å, and extends down to much lower lengths'.

Thus, a wealth of information about structure and environment of amino-acid side-chains, bound ligands or cofactors, and the protein backbone can be deduced from the spectral parameters: band position, bandwidth and absorption coefficient. This makes vibrational spectroscopy a valuable tool for the investigation of protein structure (reviewed by Arrondo *et al.* 1993; Goormaghtigh *et al.* 1994a–c; Jackson & Mantsch, 1995; Siebert, 1995; Arrondo & Goñi, 1999), of the molecular mechanism of protein reactions (reviewed by Siebert, 1990, 1995; Rothschild, 1992; Mäntele, 1993b, 1995; Gerwert, 1993, 1999; Maeda, 1995; Slayton & Anfinrud, 1997; Fahmy *et al.* 2000a; Jung, 2000; Vogel & Siebert, 2000; Wharton, 2000; Barth & Zscherp, 2000; Zscherp & Barth, 2001; Breton, 2001; Fahmy, 2001; Kim & Barry, 2001) and of protein folding, unfolding and misfolding (Fabian *et al.* 1999; Reinstädler *et al.* 1999; Schultz, 2000; Troullier *et al.* 2000, Kauffmann *et al.* 2001, reviewed by Dyer *et al.* 1998; Arrondo & Goñi, 1999). Its advantages are a large application range from small soluble proteins to large membrane proteins, a high time resolution down to 1 μs with moderate effort, and relatively low costs.

In this review, we summarize theory and applications of the IR spectroscopy of proteins, i.e. general principles of IR absorption, the absorption of the protein constituents and current applications. Some of the more theoretical chapters may be difficult for readers not familiar with quantum mechanics. We have taken care, however, that the physical principles will become clear without that background.

2. IR spectroscopy – general principles

2.1 Vibrations

The simple two-atomic oscillator illustrates well some of the fundamental principles that govern the relationship between the vibrational spectrum of a molecule and its structure and environment. The frequency, ν, of a two-atomic oscillator is given by

$$\nu = (k/m_r)^{0.5}/2\pi,$$

where k is the force constant between the two atoms, and m_r the reduced mass ($1/m_r = 1/m_1 + 1/m_2$). The frequency rises when the force constant increases, that is when the electron density in the bond between the two atoms increases. Any inter- or intramolecular factor that alters the electron density in the bonds will affect the vibrational spectrum. The second important influence on the frequency is the mass of vibrating atoms, the larger the mass, the slower the vibration. This effect is often used as a tool for the interpretation of spectra, when the sample is isotopically labelled in order to shift the frequency of vibrations that involve the labelled atoms.

2.2 Information that can be derived from the vibrational spectrum

Chemical structure. The chemical structure of a molecule is the dominating effect that determines the vibrational frequencies via the strengths of the vibrating bonds and the masses of the vibrating atoms. This effect may seem to be of minor relevance to biophysicists since the chemical structure of a protein cannot be deduced from the vibrational spectrum and will often be inert in biophysical investigations. However, changes to the protonation state of side-chains is an important exception and protonation and deprotonation are often an essential part of catalytic mechanisms. Here, vibrational spectroscopy seems to be the method of choice since the protonation state of most side-chains is reflected in the spectrum. Some examples from IR spectroscopy are given: protonation of Asp and Glu residues accompanies proton pumping by bacteriorhodopsin (reviewed by Rothschild, 1992; Gerwert, 1993, 1999; Maeda, 1995; Heberle, 1999), electron transfer reactions (reviewed by Mäntele, 1995), Ca^{2+} release from Ca^{2+}-ATPase (Barth *et al.* 1997), and seems to provide a mechanism of charge compensation when the negatively charged ATP binds to Ca^{2+}-ATPase (Von Germar *et al.* 2000). As for Asp and Glu residues, the protonation state of other catalytically active side-chains can be characterized by IR spectroscopy, as done for example for His and Tyr residues of photosystem II (Hienerwadel *et al.* 1997; Noguchi *et al.* 1999) and bacteriorhodopsin (Dollinger *et al.* 1986; Rothschild *et al.* 1986; Roepe *et al.* 1987).

Other examples for an alteration of chemical structure in biophysical experiments are protein modifications like phosphorylation and chemical reactions that are catalysed by enzymes (Fisher *et al.* 1980; Barth *et al.* 1991; White *et al.* 1992; Raimbault *et al.* 1997; reviewed by Wharton, 2000).

Redox state. Redox reactions are the basis of the energy-delivering processes in living organisms. They affect the electron density distribution of a given molecule and thus will alter its vibrational spectrum, which can probably be seen best in model studies that investigate isolated biological cofactors. An example is the investigation of the cofactors involved in photosynthesis (Mäntele *et al.* 1988; Bauscher *et al.* 1990; Nabedryk *et al.* 1990; Bauscher & Mäntele, 1992) that allowed the assignment and molecular interpretation of signals in the protein spectra

to specific molecular groups of cofactors and, in consequence, statements about their protein environment (reviewed by Mäntele, 1993a, 1995; Nabedryk, 1996; Breton, 2001).

Bond lengths and bond strength. Vibrational frequencies of stretching vibrations are a direct function of the force constants of the vibrating bonds and are therefore correlated to a number of other physico-chemical parameters like bond length and bond strength. Empirical relationships between these parameters have been established (reviewed by Palafox, 1998; Deng & Callender, 2001) and can be rationalized in terms of a simple modification of the Morse potential (Bürgi & Dunitz, 1987). These correlations are very helpful for the interpretation of spectra since they enable a detailed understanding of the molecular mechanism of enzyme catalysis.

The relationship between stretching frequency and bond strength, ΔH, has been used to study serine proteases and proteins that are targets for antibiotics (White & Wharton, 1990; Chittock *et al.* 1999). These proteins form an acyl-enzyme intermediate, the breakdown of which depends on the interactions with the acyl-enzyme ester carbonyl (for vibrational spectroscopy studies see Tonge & Carey, 1989; White & Wharton, 1990). In case of the dihydrocinnamoyl-chymotrypsin acyl-enzyme intermediate, a non-bonded conformation and a productive conformation were identified, of which the carbonyl stretching wavenumbers differ by 39 cm^{-1} (White & Wharton, 1990). From this a difference in carbonyl bond strength of 26·9 kJ mol^{-1} was deduced with the productive conformation having the weaker bond. Since this bond weakening is directed towards the transition state (formal single bond) it reduces the activation energy of deacylation and it is estimated that the rate of deacylation increases by a factor of $5{\cdot}3 \times 10^4$ with respect to the non-bonded conformation. This rate increase upon interaction with a single substrate group represents, in this case, approximately half of the rate enhancement by enzymic catalysis.

The approach towards the transition state in the ground state of rapidly decaying acyl-enzymes was expressed in terms of C═O bond-length changes in a related series of Raman experiments (Tonge & Carey, 1992). Here a decrease of the acyl-enzyme C═O frequency of 54 cm^{-1} was found to correlate with an $1{\cdot}63 \times 10^4$-fold increase in deacylation rate and an increase of the C═O bond length by 0·025 Å, which is 11% of what is expected on going from a formal double bond in the substrate to a formal single bond in the transition state. Very small changes in bond length therefore have dramatic effects on reaction rates.

Correlations obtained from a normal mode analysis of phosphates and vanadates (Deng *et al.* 1998b) have been used to quantify bond length and bond order of a vanadate transition-state analogue for the ATP hydrolysis reaction catalysed by myosin (Deng *et al.* 1998a) and of the phosphate groups of GTP and GDP bound to Ras (Wang *et al.* 1998; Cheng *et al.* 2001). Ras is involved in signalling and acts as a switch when it hydrolyses GTP. One result is that the P—O bond between the β- and the γ-phosphate of GTP is lengthened by 0·005 Å and weakened by 0·012 valence units already in the ground state by the interaction between GTP and Ras (Cheng *et al.* 2001).

Bond angles and conformation. Vibrations are often coupled and this coupling depends on details of the molecular geometry which has enabled frequency–geometry correlations for a number of chemical groups (reviewed by Palafox, 1998). Coupling therefore often provides insight into the three-dimensional (3D) structure of molecules. A simple example are the two coupled CO vibrations in the COO^- group. Their coupling and thus the frequency of the two stretching modes (normally observed near 1400 and 1570 cm^{-1}) depends upon the electron density in, and the angle between, the two CO bonds. In the hypothetical extreme cases of angles of 90° and 180°, coupling is zero for 90° but is strongest for 180°. In addition, coupling is strongest

when the two bonds oscillate with the same frequency and therefore depends on the electron density distribution in the carboxylate group. As a consequence, the frequencies of the two modes may shift considerably upon cation chelation (Deacon & Phillips, 1980; Tackett, 1989; Nara *et al.* 1994) which can be explained by changes of bond lengths and angles (Nara *et al.* 1996). The effects depend upon the mode of chelation and have been valuable in studies of several Ca^{2+}-binding proteins (Nara *et al.* 1994; Fabian *et al.* 1996b; Mizuguchi *et al.* 1997a).

Similarly, the frequencies of the asymmetric and the symmetric stretching vibrations of phosphate and vanadate groups give information on the angle between the P—O or V—O bonds (Deng *et al.* 1998b) which has been exploited in the above-mentioned studies on myosin (Deng *et al.* 1998a) and Ras (Wang *et al.* 1998; Cheng *et al.* 2001).

A final example are the amide groups of the protein backbone. The Coulomb interactions between them couple the amide oscillators and this depends on the 3D structure of the protein backbone. As discussed in more detail below, this coupling renders the amide I band sensitive to secondary structure.

Hydrogen bonding. Hydrogen bonds stabilize protein structure and are essential for catalysis. Vibrational spectroscopy is one of the few methods that directly report on the strength of hydrogen bonds. As a general rule, hydrogen bonding lowers the frequency of stretching vibrations, since it lowers the restoring force, but increases the frequency of bending vibrations since it produces an additional restoring force (Colthup *et al.* 1975). Linear dependencies between the enthalpy of hydrogen bond formation, ΔH, and the frequency of stretching vibrations [Badger and Bauer relationships (Badger & Bauer, 1937)] have been found for several groups (reviewed by Tonge *et al.* 1996; Deng & Callender, 1999, 2001). For example, for C═O groups a downshift of 1 cm^{-1} corresponds to a favourable binding enthalpy of approximately 1·6–2·6 kJ mol^{-1} for several aliphatic compounds (for methyl acetate, a model for Asp and Glu, 1·7 kJ mol^{-1}). In Raman studies (reviewed by Callender & Deng, 1994), favourable binding enthalpies with respect to water, as large as -60 kJ mol^{-1}, have been detected for C═O groups of substrates bound to enzymes. One example given by Callender and Deng is pyruvate binding to lactate dehydrogenase which leads to a downshift of the pyruvate C═O band of 35 cm^{-1}. This large shift corresponds to a change in bond length of only 0·02 Å! Formation of a single hydrogen bond to a C═O group leads to a 20 cm^{-1} downshift for the methyl acetate–water complex in an argon matrix (Maes & Zeegers-Huyskens, 1983; Maes *et al.* 1988) and of 25 cm^{-1} for propionic acid in an ethanol/hexane (1:200) mixture (Dioumaev & Braiman, 1995).

Phosphate groups are of considerable interest for biological spectroscopy since they are a component of DNA and of many substrates for enzymes. Hydrogen bonding to PO_2^- groups lowers the observed band position of the symmetric stretching vibration by 3–20 cm^{-1}, and of the antisymmetric stretching vibration by 20–34 cm^{-1} (Brown & Peticolas, 1975; Arrondo *et al.* 1984; Pohle *et al.* 1990; George *et al.* 1994) with a single hydrogen bond contributing 16 cm^{-1} in a nitrogen matrix (George *et al.* 1994). Hydrogen bonding results in two effects (Pohle *et al.* 1990): (i) less electron density in the P—O bonds and (ii) a relaxation of phosphate geometry towards the ideal tetrahedral form due to the reduced Coulomb repulsion. The overall effect of hydrogen bonding is considerably smaller for the symmetric stretching vibration since here the two effects partly compensate whereas they add for the antisymmetric stretching vibration.

Electric fields. Similarly to hydrogen bonding, the electric field produced by the environment modifies the electron density distribution of a given molecule. A strong electric field has been

detected, for example, in the active site of dehalogenase where it strongly polarizes the product of the catalytic reaction (Carey, 1998). For carboxyl groups in the absence of hydrogen bonding (bands above 1740 cm^{-1}), there is an inverse correlation of the C═O stretching frequency with the dielectric constant ε (Dioumaev & Braiman, 1995).

Conformational freedom. Besides band position and band intensity, the third spectral parameter, the bandwidth, is also useful for a molecular interpretation. Due to its short characteristic timescale, in the order of 10^{-13} s, vibrational spectroscopy provides a snapshot of the sample conformer population. As the band position for a given vibration is usually slightly different for every conformer, heterogeneous band broadening is the consequence. Flexible structures will thus give broader bands than rigid structures and the bandwidth is a measure of conformational freedom. It is possible to relate bandwidth with entropy and thus to quantify entropic effects in catalysis (Deng & Callender, 1999).

For molecules that bind to proteins, the restriction of conformational freedom is a natural consequence of binding. This reduces the bandwidth (Alben & Caughey, 1968; Belasco & Knowles, 1980; Fisher *et al.* 1980), often by a factor of 2 (Wharton, 2000). For example, phosphate bands of GTP become sharper when the nucleotide binds to Ras (Cepus *et al.* 1998; Wang *et al.* 1998) and ubiquinone is in a more rigid environment when bound to cytochrome bo_3 (Hellwig *et al.* 1999). Binding of a molecule may also confer enhanced rigidity to more distant parts of the protein. Binding of a substrate analogue to the binary complex of lactate dehydrogenase and NADH affects the environment of NADH since band narrowing of NADH Raman bands has been observed (Deng & Callender, 1999). As a final example, the bandwidth has been used to characterize the environment of the phosphorylated Asp residue of the sarcoplasmic reticulum Ca^{2+}-ATPase (Barth & Mäntele, 1998). From the small bandwidth of the ν(C═O) band it was concluded that this group is not exposed to solvent water but exhibits defined interactions with the protein environment.

2.3 Absorption of IR light

IR absorption is caused by the interaction of electromagnetic waves with molecular vibrations. To be more specific, the electric field vector, $E(t)$, of the electromagnetic wave couples with the dipole moment, $\mu(t)$, of the molecule. A simple classical picture is that of two vibrating point charges $+q$ and $-q$ connected by a spring. If the frequencies of light and vibration are the same, the electric field will amplify the movement of the partial charges. The vibrational frequency, however, remains unaffected. This simple picture already illustrates two important findings: (i) the frequencies of light and of the vibration have to coincide for absorption to occur and (ii) the larger the point charges $+q$ and $-q$, the stronger the interaction with the electric field.

In the quantum mechanical world, the discrete energy levels of a harmonic oscillator are separated by $h\nu$ with ν being the vibrational frequency. An IR photon with this energy, $h\nu$, can be absorbed by the oscillator which then goes from the ground-energy level to the first excited level in a typical IR experiment. The spacing of energy levels by $h\nu$ ensures that light can only be absorbed when light frequency and vibrational frequency coincide (this rule strictly applies only to the harmonic oscillator).

According to Fermi's golden rule, the transition probability between the two vibrational levels is proportional to the square of the transition dipole moment (TDM). For a transition from the vibrational level n to level m of the electronic ground state ψ_0, this quantity can be

written as given below (Cantor & Schimmel, 1980) using the Born–Oppenheimer approximation that separates the nuclear wavefunctions ϕ_n and ϕ_m from the electronic wavefunction ψ_0 and using $\mathbf{U} = \boldsymbol{\mu}(t)E(t)$ for the operator of the interaction potential $\mathbf{U}$, where $E(t)$ is the electric field of the electromagnetic wave and $\boldsymbol{\mu}(t)$ the dipole moment operator (bold print indicates operators):

$$\mathrm{TDM} = \langle \psi_0 \phi_m | \boldsymbol{\mu} | \psi_0 \phi_n \rangle.$$

Further calculation shows that the TDM can then be split into an electronic and a nuclear term that gives rise to the two selection rules: The nuclear term is zero except for $m = n \pm 1$ and represents the selection rule that vibrational transitions only occur to the next vibrational level: $\Delta n = \pm 1$. This is strictly valid only for the harmonic oscillator. For spectroscopy in the mid-IR spectral range at room temperature, the large majority of oscillators are not thermally excited; they are in the vibrational ground state and IR absorption leads to a transition to the first excited state. For this transition of a diatomic oscillator the TDM is then given by

$$\mathrm{TDM} = \langle \boldsymbol{\partial\mu}/\boldsymbol{\partial \mathbf{R}}(R_0) \rangle (h/8\pi^2 m_\mathrm{r} \nu)^{0.5},$$

where h is Planck's constant, m_r the reduced mass of the diatomic oscillator ($1/m_\mathrm{r} = 1/m_1 + 1/m_2$) and ν the frequency of oscillation.

The right term is the nuclear contribution. The left term represents the electronic contribution and is the expectation value for the change of dipole moment at the equilibrium position R_0 calculated with the electronic wavefunctions. It gives rise to the second selection rule that IR absorption only takes place when the dipole moment of the molecule changes with the vibration. The larger the change, the stronger the absorption. Often a large change is correlated with a large bond polarity. This can be visualized in the simple classical picture above with vibrating partial charges $+q$ and $-q$. Here, the dipole moment at a given distance R between the partial charges is $\mu = qR$. The change of dipole moment at any distance is: $\partial\mu/\partial R = q$. This shows that the larger the partial charges, i.e. the larger the bond polarity, the stronger will be the absorption of IR light. For example, strong bands are observed for C═O vibrations, weak bands for C═C vibrations in molecules like HFC═CH_2 or no absorption for molecules like H_2C═CH_2. Factors such as a change in environment that alter the bond polarity will lead to a change in intensities of absorbance bands.

3. Protein IR absorption

3.1 Amino-acid side-chain absorption

General remarks. Amino-acid side-chain absorption provides valuable information when the mechanism of protein reactions is investigated. This is because side-chains are often at the heart of the molecular reaction mechanism. Often, in a single experiment, it is possible to follow the fate of several individual groups that are involved in the reaction. The aim of this kind of research is to identify the catalytically important side-chains and to deduce their environmental and structural changes from the spectrum in order to understand the molecular reaction mechanism. As discussed above, information that may be obtained is, for example, on the protonation state, coordination of cations and hydrogen bonding.

Table 1 gives an overview of the IR absorption of amino-acid side-chains in ^1H_2O and ^2H_2O (Barth, 2000b), see also further compilations of IR bands (Chirgadze *et al.* 1975;

Table 1. *Overview of amino-acid side-chain IR bands* (*Barth, 2000b*)

Assignments	Band position/cm^{-1}, ($\varepsilon/M^{-1}\,cm^{-1}$) in ^1H_2O	Band position/cm^{-1}, ($\varepsilon/M^{-1}\,cm^{-1}$) in ^2H_2O	Remarks
Cys, ν(SH)	2551	*1849*	
Asp, ν(C═O)	1716 (280)	*1713* (*290*)	Without H-bond up to 1762 cm^{-1} observed in proteins (Fahmy *et al.* 1993). Single H-bond shifts 25 cm^{-1} down. Above ~1740 cm^{-1} inverse correlation of ν(C═O) with ε (dielectric constant) (Dioumaev & Braiman, 1995)
Glu, ν(C═O)	1712 (220)	*1706* (*280*)	Expected to be up to 50 cm^{-1} higher without H-bond. See also Asp ν(C═O)
Asn, ν(C═O)	1677–1678 (310–330)	*1648* (*570*)	Up to 1704 cm^{-1} in proteins (Cao *et al.* 1993)
Arg, $\nu_{as}(CN_3H_5^+)$	1652–1695 (420–490)	*1605–1608* (*460*)	Position depends on the salt bridge between Arg and other residues only for ^1H_2O not for ^2H_2O. In ^1H_2O near 1672 cm^{-1} without salt bridge. In proteins up to 1695 cm^{-1} (^1H_2O) and down to 1595 cm^{-1} (^2H_2O) (Chirgadze *et al.* 1975; Berendzen & Braunstein, 1990; Rüdiger *et al.* 1995; Braiman *et al.* 1999)
Gln, ν(C═O)	1668–1687 (360–380)	*1635–1654* (*550*)	Between 1659 and 1696 cm^{-1} in proteins (Hienerwadel *et al.* 1997)
Arg, $\nu_s(CN_3H_5^+)$	1614–1663 (300–340)	*1581–1586* (*500*)	Position depends on the salt bridge between Arg and other residues only for ^1H_2O not for ^2H_2O. In ^1H_2O near 1635 cm^{-1} without salt bridge. In deuterated proteins down to 1576 cm^{-1} (Chirgadze *et al.* 1975; Braiman *et al.* 1999)
$HisH_2^+$, ν(C═C)	1631 (250)	*1600* (*35*), *1623* (*16*)	Only one strong band observed for 4-methylimidazole at 1633 (H_2O) and 1605 cm^{-1} (^2H_2O) (Hasegawa *et al.* 2000)
Lys, $\delta_{as}(NH_3^+)$	1626–1629 (60–130)	*1201*	^2H_2O band position based on shift observed for CH_3NH_3Cl and $CH_3N^2H_3Cl$
Tyr—OH, ν(CC) δ(CH)	1614–1621 (85–150)	*1612–1618* (*160*)	ε estimated relative to 1517 cm^{-1} band, Tyr or *p*-cresol
Asn, $\delta(NH_2)$	1612–1622 (140–160)		
Trp, ν(CC), ν(C═C)	1622	*1618*	
Tyr—O^-, ν(CC)	1599–1602 (160)	*1603* (*350*)	Tyr or *p*-cresol
Tyr—OH, ν(CC)	1594–1602 (70–100)	*1590–1591* (*<50*)	ε estimated relative to 1517 cm^{-1} band, Tyr or *p*-cresol
Gln, $\delta(NH_2)$	1586–1610 (220–240)	*1163*	
HisH, ν(C═C)	1575, 1594 (70)	*1569, 1575*	Doublet due to the two protonated tautomers of His
Asp, $\nu_{as}(COO^-)$	1574–1579 (290–380)	*1584* (*820*)	May shift +60/−40 cm^{-1} (Tackett, 1989; Nara *et al.* 1994) upon cation chelation, in extreme cases band position as for ν(C═O) (Deacon & Phillips, 1980)
Glu, $\nu_{as}(COO^-)$	1556–1560 (450–470)	*1567* (*830*)	See Asp $\nu_{as}(COO^-)$
Lys, $\delta_s(NH_3^+)$	1526–1527 (70–100)	*1170*	^2H_2O band position based on shift observed for CH_3NH_3Cl and $CH_3N^2H_3Cl$
Tyr—OH, ν(CC), δ(CH)	1516–1518 (340–430)	*1513–1517* (*500*)	Tyr or *p*-cresol
Trp, ν(CN), δ(CH), δ(NH)	1509		Indole IR spectrum
Tyr—O^-, ν(CC), δ(CH)	1498–1500 (700)	*1498–1500* (*650*)	Tyr or *p*-cresol
Trp, ν(CC), δ(CH)	1496		Trp Raman spectrum, observed in the indole IR spectrum at 1487 cm^{-1}

[*continued overleaf*

Table 1 (*cont.*)

Assignments	Band position/cm^{-1}, ($\varepsilon/M^{-1}\,cm^{-1}$) in ^1H_2O	Band position/cm^{-1}, ($\varepsilon/M^{-1}\,cm^{-1}$) in ^2H_2O	Remarks
Phe, ν(CC ring)	1494 (80)		
$\delta_{as}(CH_3)$	1445–1480		
Trp, δ(CH), ν(CC), ν(CN)	1462	*1455* (*200*)	ε estimated from comparison with the 1517 cm^{-1} Tyr band (Fabian *et al.* 1994)
His^-, $\delta(CH_3)$, ν(CN)	1439	*1439*	Observed for 4-methylimidazole with a strong contribution of $\delta(CH_3)$. Thus, position for His may differ
Pro, ν(CN)	1400–1465		Sensitive to backbone conformation (Johnston & Krimm, 1971; Caswell & Spiro, 1987)
$\delta(CH_2)$	1425–1475		Good group frequency, normally at 1463, near 1425 cm^{-1} and more intense when next to a C═O group (Colthup *et al.* 1975)
Trp, δ(NH), ν(CC), δ(CH)	1412–1435	*1382*	^1H_2O: higher number for Raman spectrum of Trp, lower number for IR imidazole spectrum. ^2H_2O: Raman spectrum of Trp
Gln, ν(CN)	1410	*1409*	
Glu, $\nu_s(COO^-)$	1404 (316)	*1407*	See Asp $\nu_s(COO^-)$
Asp, $\nu_s(COO^-)$	1402 (256)	*1404*	May shift $+60/-90$ cm^{-1} upon cation chelation (Tackett, 1989), in extreme cases band position as for ν(C—O) of COOH group (Deacon & Phillips, 1980). Band position of Asp in ^2H_2O estimated from shift observed for CH_3COO^-
$\delta_s(CH_3)$	1375 or (1368, 1385)		1 band for 1 CH_3 group, 2 bands for 2 adjacent groups (Val, Leu), narrower than $\delta_{as}(CH_3)$ but same intensity (Colthup *et al.* 1975). Insensitive to hydrocarbon chain conformation (Lewis & McElhaney, 1996)
Trp	1352–1361		Higher number for Raman spectrum of Trp, lower number for IR imidazole spectrum
Trp	1334–1342	*1334* (*100*)	^1H_2O: higher number for Raman spectrum of Trp, lower number for IR imidazole spectrum. ^2H_2O: IR spectrum of Trp in protein
δ(CH)	1315–1350		
Trp, δ(NH), ν(CN), δ(CH)	1276		Indole IR spectrum
Tyr—O^-, ν(C—O), ν(CC)	1269–1273 (580)		Tyr or *p*-cresol
Asp, Glu, δ(COH)	1264–1450	*955–1058*	Hydrogen bonded (1058 and 1450 cm^{-1}) and free (955 and 1264 cm^{-1}) CH_3COOH
Trp, δ(CH), ν(CC)	1245		Indole IR spectrum
Tyr—OH ν(C—O), ν(CC)	1235–1270 (200)	*1248–1265* (*150*)	Tyr or *p*-cresol, band sensitive to H-bonding, 3–11 cm^{-1} lower in ^2H_2O, ε in ^2H_2O estimated from comparison with 1517 cm^{-1} band
His, δ(CH), ν(CN), δ(NH)	1217, 1229, 1199	*1217, 1223, 1239*	Values are for His^-, HisH and $HisH_2^+$, respectively
Trp, ν(CC)	1203		Indole IR spectrum
Ser, δ(COH) or $\delta(CO^2H)$, ν(CO)	1181–1420	*875–985*	Band position sensitive to hydrogen bonding
$\gamma_w(CH_2)$	1170–1382		Couples with adjacent CH_2 groups (Colthup *et al.* 1975). Sensitive to hydrocarbon chain conformation (Lewis & McElhaney, 1996)

Tyr—OH, δ(COH)	1169–1260 (200)	*913*	Tyr or *p*-cresol, band sensitive to H-bonding for OH group, 256 cm^{-1} lower for O^2H group
Asp, Glu, ν(C—O)	1160–1253	*1250–1300*	Range in ^1H_2O from band position in aqueous solution near 1250 cm^{-1} (Sengupta & Krimm, 1985; Venyaminov & Kalnin, 1990a) and shift observed for hydrogen bonded and free CH_3COOH (Pinchas & Laulicht, 1971). Band position in ^2H_2O from shifts relative to ^1H_2O of hydrogen bonded (data not shown) and free CH_3COOH (Pinchas & Laulicht, 1971)
His, ν(CN), δ(CH)	1104, 1090, 1106, 1094	*1104, 1096, 1107, 1110*	Values are for His^-, N1-, N3-protonated HisH and $HisH_2^+$, respectively
Trp, δ(CH), ν(NC)	1092		Indole IR spectrum
Trp, ν(NC), δ(CH), ν(CC)	1064		Indole IR spectrum
$\gamma_t(CH_2)$	1063–1295		Weak, couples with adjacent CH_2 groups, but in phase mode at 1300 cm^{-1} good group frequency (Colthup *et al.* 1975)
Thr, ν(C—O)	1075–1150		2 bands expected
Ser, ν(C—O)	1030	*1023*	
Trp, ν(CC), δ(CH)	1012–1016	*1012*	
Ser, ν(CO) or ν(CC)	983		
Ser, ν(CO), $\delta(CO^2H)$		*940*	
Thr, $\delta(CO^2H)$		*865–942*	
$\gamma_r(CH_2)$	724–1174		Couples with adjacent CH_2 groups, in phase mode at 724 cm^{-1} most intense (Colthup *et al.* 1975)

If available, parameters of IR spectra of amino-acid side-chains are given. If not, data are taken from IR spectra of model compounds or from Raman spectra. Band positions are given for H_2O and ^2H_2O, the latter are indicated with italics. The shift upon $H/^2H$ exchange is given when a compound in both solvents is compared in the original work. The listing of internal coordinate contributions to a normal mode is according to their contribution to the potential energy of the normal mode (if specified in the literature). If the contribution of an internal coordinate to the potential energy of a normal vibration is $\geqslant 70\%$ only that coordinate is listed. Two coordinates are listed if their contribution together is $\geqslant 70\%$. In all other cases those 3 coordinates that contribute strongest to the potential energy are listed. If no assignment is listed, then multiple assignments are given in the original publications. Vibrations dominated by amide group motions are not included. ν, stretching vibration; ν_s, symmetric stretching vibration; ν_{as}, antisymmetric stretching vibration; δ, in-plane bending vibration; δ_{as}, asymmetric in-plane bending vibration; γ_w, wagging vibration; γ_t, twisting vibration; γ_r, rocking vibration.

References: Aliphatic groups (Colthup *et al.* 1975); Arg, Asn (Chirgadze *et al.* 1975; Venyaminov & Kalnin, 1990a; Rahmelow *et al.* 1998; Braiman *et al.* 1999); Asp (Pinchas & Laulicht, 1971; Chirgadze *et al.* 1975; Sengupta & Krimm, 1985; Venyaminov & Kalnin, 1990a; Rahmelow *et al.* 1998); Cys (Susi *et al.* 1983); Gln (Chirgadze *et al.* 1975; Venyaminov & Kalnin, 1990a; Dhamelincourt & Ramirez, 1993; Rahmelow *et al.* 1998); Glu (Pinchas & Laulicht, 1971; Chirgadze *et al.* 1975; Sengupta & Krimm, 1985; Venyaminov & Kalnin, 1990a); His^- (Noguchi *et al.* 1999; Hasegawa *et al.* 2000); HisH (Venyaminov & Kalnin, 1990a; Noguchi *et al.* 1999; Hasegawa *et al.* 2000); $HisH_2^+$ (Chirgadze *et al.* 1975; Hienerwadel *et al.* 1997; Noguchi *et al.* 1999); Lys (Pinchas & Laulicht, 1971; Venyaminov & Kalnin, 1990a; Rahmelow *et al.* 1998); Phe (Venyaminov & Kalnin, 1990a); Pro (Caswell & Spiro, 1987; Rothschild *et al.* 1989; Gerwert *et al.* 1990a); Ser (Pinchas & Laulicht, 1971; Colthup *et al.* 1975; Madec *et al.* 1978; Susi *et al.* 1983); Thr (Pinchas & Laulicht, 1971; Colthup *et al.* 1975); Trp (Lautié *et al.* 1980; Takeuchi & Harada, 1986; Fabian *et al.* 1994; Lagant *et al.* 1998); Tyr (Chirgadze *et al.* 1975; Dollinger *et al.* 1986; Rothschild *et al.* 1986; Takeuchi *et al.* 1988; Venyaminov & Kalnin, 1990a; Gerothanassis *et al.* 1992; Hienerwadel *et al.* 1997; Rahmelow *et al.* 1998).

Krimm & Bandekar, 1986; Venyaminov & Kalnin, 1990a; Goormaghtigh *et al.* 1994a; Wright & Vanderkooi, 1997; Rahmelow *et al.* 1998) and of Raman bands (Lord & Yu, 1970a, b; Rava & Spiro, 1985; Asher *et al.* 1986; Lagant *et al.* 1998; Overman & Thomas, 1999). Only the strongest bands are listed in Table 1, or those in a spectral window free of overlap by bands from other groups.

The absorption of a side-chain in a protein may deviate significantly from its absorption in solution or in a crystal. The special environment provided by a protein is able to modulate the electron density and the polarity of bonds, thus changing the vibrational frequency and the absorption coefficient. Therefore, the band positions given in Table 1 should only be regarded as guidelines for the interpretation of spectra. It may be mentioned here also that the pK_a of acidic residues in proteins may differ significantly from solution values. For example, it has been found that internal aspartate residues of bacteriorhodopsin are protonated at least up to pH 9·5 (Engelhard *et al.* 1985; Metz *et al.* 1992; Zscherp *et al.* 1999).

Particular side-chains. Only two side-chain moieties absorb in spectral regions that are free from overlapping absorption by other groups and thus allow the spectroscopist an unambiguous assignment without further experiments. These are the SH group of Cys (2550–2600 cm^{-1}) and the carbonyl group of protonated carboxyl groups (1710–1790 cm^{-1}) (see Table 1 and references therein). The latter proved to be particularly useful when protonation and deprotonation of carboxyl groups is of interest, for example when proton pathways in proteins are explored (Rothschild, 1992; Gerwert, 1993, 1999; Maeda, 1995; Heberle, 1999).

All other side-chain absorptions overlap with the absorption of other side-chains or of the polypeptide backbone and further experiments are needed to assign an absorption band to a specific side-chain moiety (see below).

Of the many amino-acid side-chain absorption bands, those with strong absorption coefficients are worth mentioning here – they are due to vibrations of polar groups. Protonated Asp and Glu residues have already been described above. When ionized, they absorb strongly at 1550–1580 cm^{-1} and near 1400 cm^{-1}. Both bands shift to higher wavenumbers by 9 and 2 cm^{-1}, respectively, in ^2H_2O medium (Tacket, 1989), with the former increasing in intensity (Chirgadze *et al.* 1975; Venyaminov & Kalnin, 1990a; Barth, 2000b). Upon cation chelation these bands exhibit large shifts depending on the type of coordination, as has been observed in absorbance spectra of several Ca^{2+}-binding proteins (Nara *et al.* 1994, 1995; Mizuguchi *et al.* 1997a, b).

Gln and Asn carbonyl groups in ^1H_2O absorb at 1660–1690 cm^{-1} which overlaps with the amide I absorption of the polypeptide backbone (1610–1700 cm^{-1}). They are, therefore, not readily identified in the absorbance spectrum. In difference spectra of photoreactions of bacteriorhodopsin (Cao *et al.* 1993) and photosystem II mutants (Hienerwadel *et al.* 1997) however, they have been observed at 1659–1704 cm^{-1}. The strong sensitivity to $^1H/^2H$ exchange due to coupling with the $\delta(NH_2)$ vibration distinguishes the Gln and Asn absorption from that of the backbone. While Gln and Asn shift -30 cm^{-1} in ^2H_2O, the backbone amide I band shifts by only up to -15 cm^{-1} (Susi *et al.* 1967; Byler & Susi, 1986; Arrondo *et al.* 1993; Haris & Chapman, 1994; Jackson & Mantsch, 1995). The Asn and Gln $\delta(NH_2)$ vibration absorbs at 1585–1625 cm^{-1} and shifts in ^2H_2O by more than 400 cm^{-1} due to the large contribution of H motion to that normal mode.

Arg absorption near 1635 and 1673 cm^{-1} also overlaps with the amide I absorption but exhibits large shifts upon $^1H/^2H$ exchange of -50 and -70 cm^{-1}, respectively, which distinguishes these bands from the amide I absorption.

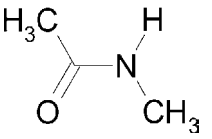

Fig. 1. Structure of *N*-methylacetamide (NMA).

The Tyr ring mode near 1517 cm^{-1} is often readily identified in a spectrum because of its small bandwidth. The slight downshift of only a few wavenumbers in ^2H_2O is also characteristic. Interestingly, this mode is an indicator of the protonation state of the Tyr side-chain since the deprotonated form absorbs near 1500 cm^{-1}. Other Tyr modes with considerable intensity are the ν(C—O$^-$) mode near 1270 cm^{-1} for ionized Tyr, and for protonated Tyr the ν(C—O) mode at 1235–1270 cm^{-1} (small downshift in ^2H_2O) and the δ(COH) mode at 1169–1260 cm^{-1} (strong shift in ^2H_2O) (Dollinger *et al.* 1986; Gerothanassis *et al.* 1992; Hienerwadel *et al.* 1997). Both are sensitive to hydrogen bonding. A ring mode of Phe can be observed as a weak band in protein absorbance spectra at 1498 cm^{-1} (^2H_2O) (Berendzen & Braunstein, 1990; Fabian *et al.* 1996b) and Trp produces bands with considerable intensity near 1334 and 1455 cm^{-1}.

3.2 Normal modes of the amide group

The model compound N-methylacetamide (*NMA*). As shown in Fig. 1, NMA is the smallest molecule that contains a *trans*-peptide group. It has therefore become the starting point for a normal mode analysis of polypeptide backbone vibrations (Krimm & Bandekar, 1986). If the CH_3 groups are regarded as point masses, the number of atoms of NMA is 6 and thus there are 12 normal modes. Of these, the 6 highest frequency ones will be discussed below according to Krimm & Bandekar (1986). The contribution of internal coordinates to these normal modes will generally alter when the amide group is incorporated into a polypeptide.

NH stretching vibrations – amide A and B ($\sim$*3300 and* $\sim$*3170 cm*$^{-1}$). The NH stretching vibration gives rise to the amide A band between 3310 and 3270 cm^{-1}. It is exclusively localized on the NH group and thus insensitive to the conformation of the polypeptide backbone. Its frequency depends on the strength of the hydrogen bond. The amide A band is usually part of a Fermi resonance doublet with the second component absorbing weakly between 3100 and 3030 cm^{-1} (amide B). In NMA and polypeptide helices, the NH stretching vibration is resonant with an overtone of the amide II vibration, in β-sheets with an amide II combination mode.

Amide I ($\sim$*1650 cm*$^{-1}$). The amide I vibration, absorbing near 1650 cm^{-1}, arises mainly from the C═O stretching vibration with minor contributions from the out-of-phase CN stretching vibration, the CCN deformation and the NH in-plane bend. The latter is responsible for the sensitivity of the amide I band to N-deuteration of the backbone. The extent to which the several internal coordinates contribute to the amide I normal mode depends on the backbone structure (Krimm & Bandekar, 1986).

The amide I vibration is hardly affected by the nature of the side-chain. It depends, however, on the secondary structure of the backbone and is therefore the amide vibration that is most commonly used for secondary-structure analysis. The amide I band of proteins will be discussed in more detail in Section 4.

Amide II (*~1550 cm*$^{-1}$). The amide II mode is the out-of-phase combination of the NH in-plane bend and the CN stretching vibration with smaller contributions from the CO in-plane bend and the CC and NC stretching vibrations. As for the amide I vibration, the amide II vibration is hardly affected by side-chain vibrations but the correlation between secondary structure and frequency is less straightforward than for the amide I vibration.

N-deuteration converts the mode to a largely CN stretching vibration at 1490 to 1460 cm^{-1} (named amide II′ mode). The N^2H bending vibration has a considerably lower frequency than the N^1H bending vibration and thus no longer couples with the CN stretching vibration. Instead it mixes with other modes in the 1070 to 900 cm^{-1} region. Because the amide II and amide II′ modes are composed differently from the internal coordinate vibrations, they will be affected differently by the conformation and the environment of the amide group. For example, hydrogen bonding will be sensed predominantly by the NH bending vibration, which contributes to the amide II but not to the amide II′ vibration – the effect of a hydrogen bond will therefore be larger on the amide II vibration than on the amide II′ vibration. The internal coordinate contributions to the amide II vibration depend upon the backbone conformation with a trend to higher frequencies with increasing contribution of the NH bending vibration. The amide II band is weak or absent in the Raman spectrum (Krimm & Bandekar, 1986).

Amide III (*1400 to 1200 cm*$^{-1}$). The amide III mode of NMA is the in-phase combination of the NH bending and the CN stretching vibration with small contributions from the CO in-plane bending and the CC stretching vibration. In polypeptides, the composition of this mode is more complex, since it depends on a side-chain structure and since NH bending contributes to several modes in the 1400 to 1200 cm^{-1} region. Contributions of backbone and side-chain vibrations vary considerably which makes the amide III vibration less suited for secondary-structure analysis. Upon N-deuteration, the N^2H bending vibration separates out and the other coordinates become redistributed into other modes.

Skeletal stretch (*1200 to 880 cm*$^{-1}$). The stretching vibrations of the 3 backbone bonds cause two relatively well defined modes for NMA, a predominantly NC_α stretching mode near 1096 cm^{-1} and a mixed mode near 881 cm^{-1}. Both absorb IR light only weakly. There is no characteristic NC mode in polypeptides. Instead, the skeletal stretching vibrations contribute to a number of modes in the 1180 to 920 cm^{-1} region depending on the side-chain. A skeletal vibration gives rise to a strong Raman band at 960 to 880 cm^{-1}, with minor contributions of side-chain vibrations.

4. Interactions that shape the amide I band

4.1 Overview

The amide I band of polypeptides has long been known to be sensitive to secondary structure and this has caused considerable interest in the understanding of the structure–spectrum relationship. However, the correct description of the large splitting of 60 cm^{-1} of the amide I band of β-sheet structures has presented a challenge for theoreticians. Only with the introduction of the TDC mechanism (Abe & Krimm, 1972) could this splitting in a main band near 1630 cm^{-1} and a side band near 1690 cm^{-1} be explained. Other effects like through-bond coupling and hydrogen bonding also modify the amide I frequency of polypeptides to different degrees. In addition to these effects which are discussed below, changing the dielectric constant of the environment from 1 to 80 (water) reduces the calculated frequency for NMA

by 30 cm^{-1} (Torii *et al.* 1998b), as suggested earlier for protein amide groups (Jackson & Mantsch, 1991).

4.2 Through-bond coupling

The amide I and II vibrations do not involve large displacements of the C_α atom and thus will only interact slightly with the same vibration of the neighbouring peptide group via coupling along the chemical bonds. In consequence, through-bond coupling does not seem to have a major effect on the amide I and II vibrations and cannot explain the large splitting of the amide I band of antiparallel β-sheet structures (Abe & Krimm, 1972). However, there is evidence for some through-bond coupling between nearest neighbours from *ab initio* calculations on NMA (Hamm *et al.* 1999) and di- and tripeptides (Torii & Tasumi, 1998).

4.3 Hydrogen bonding

The effects of hydrogen bonding on the IR spectrum of NMA have been examined theoretically with *ab initio* calculations and experimentally (Torii *et al.* 1998a, b). Each of the two possible hydrogen bonds to the C═O group lowers the amide I frequency by 20–25 cm^{-1} and a hydrogen bond to the NH group by 10–20 cm^{-1}. For polypeptides there is experimental evidence for an effect of hydrogen bonding on the amide I frequency since the different positions of the main absorption band at 1632 cm^{-1} for poly-β-L-Ala and at 1624 cm^{-1} for poly-β-L-Glu were tentatively explained by the stronger hydrogen bonds of the latter (Krimm & Bandekar, 1986). The side band of β-sheets at high wavenumbers, however, seems to be less affected by the strength of hydrogen bonding since it differs by only 1 cm^{-1} for the two polypeptides. For α-helices there is also evidence for an effect of hydrogen bonding on the vibrational frequency since solvated helices (i.e. helices also forming hydrogen bonds to solvent molecules) absorb approximately 20 cm^{-1} lower than non-solvated helices (Parrish & Blout, 1972; Reisdorf & Krimm, 1996; Gilmanshin *et al.* 1997). It is interesting to note that the position of the amide I absorbance maximum of different secondary structures correlates with the strength of hydrogen bonding which decreases in the order: intermolecular extended chains (observed at 1610–1628 cm^{-1}), intramolecular antiparallel β-sheets (1630–1640 cm^{-1}), α-helices (1648–1658 cm^{-1}), 3_{10}-helices (1660–1666 cm^{-1}) and non-hydrogen-bonded amide groups in DMSO (1660–1665 cm^{-1}) (Jackson & Mantsch, 1991). However, hydrogen bonding does not seem to be the dominating effect that causes the low frequency of the main β-sheet band (Abe & Krimm, 1972; Krimm & Abe, 1972; Kubelka & Keiderling, 2001a).

4.4 Transition dipole coupling (TDC)

The effects of TDC. The fundamental mechanism that renders the amide I vibration sensitive to secondary structure is TDC (Abe & Krimm, 1972; Krimm & Abe, 1972; Chirgadze & Nevskaya, 1976a, b; Nevskaya & Chirgadze, 1976). It is a resonance interaction between the oscillating dipoles of neighbouring amide groups and the coupling depends upon the relative orientations of, and the distance between, the dipoles. Coupling is strongest when the coupled oscillators vibrate with the same frequency. TDC has two effects:

(1) *Exciton transfer.* If energy is absorbed by an oscillator it does not remain there, rather it is transferred to a nearby oscillator with a typical time constant of 0·5 ps for an α-helix (Hamm *et al.* 1998) – as a consequence the excited state is delocalized, typically over a

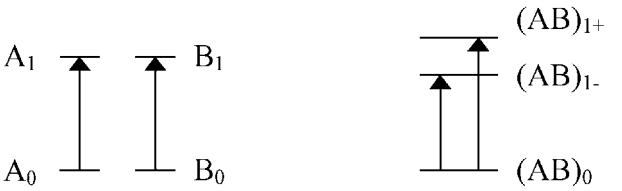

Fig. 2. Energy levels of the two individual oscillators A and B (left) and of the coupled two-oscillator system (right). The interaction results in an exciton splitting of the two excited states $(AB)_{1+}$ and $(AB)_{1-}$ where the excitation energy is no longer localized on one oscillator.

length of 8 Å (Hamm *et al.* 1998). A similar coupling mechanism explains the non-radiative energy transfer according to the Förster mechanism which is observed in fluorescence experiments and which in photosynthesis transfers absorbed light energy to the photosynthetic reaction centres.

(2) *Band splitting or exciton splitting.* TDC leads to a shift of the amide I frequency depending on the orientation, distance and relative phases of the coupled oscillators. If only two coupled oscillators are considered, two different excited energy levels are observed depending on whether the oscillators are in-phase or out-of-phase (see Fig. 2). The result is a splitting of the amide I band which can be as large as 70 cm^{-1} in the case of β-sheet structures – a phenomenon called exciton splitting. Exciton splitting is also observed in UV spectroscopy, for example for the $\pi \rightarrow \pi^*$ transition of the peptide group of α-helices near 200 nm.

A simple example of vibrational coupling. Before explaining TDC in more detail it is illustrative to consider a simple example of vibrational coupling, a linear molecule of three identical atoms which are connected by spring-like bonds (o——o——o) (Colthup *et al.* 1975). The two o——o oscillators are assumed to be identical and will therefore have the same frequency when they are isolated. However, in the molecule their movements are coupled and this coupling leads to two vibrational modes which have different frequencies. One of them is the out-of-phase or antisymmetric mode where the right oscillator contracts when the left expands and vice versa. At a turning point of the vibration (o————o—o, i.e. the left oscillator is expanded and starts to contract, the right is contracted and starts to expand) the left oscillator pulls the middle atom to the left and the right one pushes in the same direction. So the two spring forces act in a concerted way on the middle atom and each spring has to move only half of the middle atom's mass. Thus, we can regard the out-of-phase mode as two separated oscillators with each moving only half of the middle atom's mass. Because of the reduced mass, the frequency of this 'truncated' oscillator, and therefore of the antisymmetric mode, is higher than that of the isolated o——o oscillator.

In the in-phase or symmetric mode both oscillators contract and expand at the same time (o————o————o and later o—o—o). Thus, the two component oscillators exert opposing forces on the middle atom with the result that the middle atom does not move. This is equivalent to two separated oscillators where the atoms corresponding to the middle atom have infinite mass and is the reason for the lower frequency of the symmetric mode.

The above simple example illustrates important effects of coupling two oscillators: (i) coupling is most effective when the isolated oscillators have the same frequency; (ii) instead of observing one frequency, the coupled system exhibits two different frequencies because coupling depends on the relative phase of the movement of the two oscillators; (iii) as the coupling is very strong, the oscillation is no longer localized on one oscillator. In this example

the oscillators are coupled through the bonds between the atoms. In contrast, TDC is not transmitted via bonds but through space because it originates from the Coulomb interactions between the moving partial charges.

Dipole–dipole interaction leads to non-stationary states. The formalism of TDC (Abe & Krimm, 1972; Krimm & Abe, 1972; Chirgadze & Nevskaya, 1976a, b; Nevskaya & Chirgadze, 1976) is probably best described by Cheam & Krimm (1984). It will be briefly outlined here in analogy to the detailed description of chromophore coupling in UV/visible spectroscopy by Cantor & Schimmel (1980). TDC is a resonance interaction that takes place between two oscillators A and B when one of them is in an excited state. The interaction is mediated by the Coulomb interactions between the oscillators. When the distance R is large enough (larger than 3 Å), the interaction $\mathbf{U}_{AB}$ can be expanded in a multipole series with the leading term being the dipole–dipole interaction. However, this does not mean that a permanent dipole moment is required for the interaction, TDC can also occur in the absence of a permanent dipole moment. $\mathbf{U}_{AB}$ in SI units is given by

$$\mathbf{U}_{AB} = (4\pi\varepsilon_r\varepsilon_o)^{-1}(\boldsymbol{\mu}_A\boldsymbol{\mu}_B)/\mathbf{R}^3 - 3(\boldsymbol{\mu}_A\mathbf{R})(\mathbf{R}\boldsymbol{\mu}_B)/\mathbf{R}^5,$$

$\boldsymbol{\mu}_A$ and $\boldsymbol{\mu}_B$ are the dipole moment operators acting on oscillators A and B respectively, $\mathbf{U}_{AB}$ and $\mathbf{R}$ are the operators of the interaction potential and of the distance between A and B, respectively. The dipole–dipole approximation will be used throughout this section but it should be noted that it seems to give too large values for the interaction with the closest neighbours (Lee & Krimm, 1998).

As a consequence of the interaction, the eigenstates of the isolated oscillators are no longer stationary, i.e. if energy is absorbed by one oscillator the excitation will shuttle back and forth between the two oscillators. This can easily be shown using the product state $|A0B0\rangle$ for the ground state and the two states $|A0B1\rangle$ and $|A1B0\rangle$ for the singly excited states. The numbers 0 and 1 indicate the ground and the first excited vibrational states, respectively. For example $|1\rangle$ is a shorthand notation for $|\psi_0\phi_1\rangle$ which represents the first excited vibrational state of the electronic ground state. The dipole–dipole interaction leads to energy transfer from A to B and vice versa, i.e. transitions like $|A1B0\rangle \rightarrow |A0B1\rangle$ will have a non-vanishing probability. According to Fermi's golden rule, the probability of such a transition is proportional to a quantity $|V_{AB}|^2$, where V_{AB} is given by

$$V_{AB} = \langle A0B1|\mathbf{U}_{AB}|A1B0\rangle.$$

When the above expression for $\mathbf{U}_{AB}$ is inserted, V_{AB} can be simplified. (i) The operator $\mathbf{R}$ is replaced by the distance between the geometric centres and is thus a constant quantity when the scalar product is evaluated. (ii) Since the dipole moment operators $\boldsymbol{\mu}_A$ and $\boldsymbol{\mu}_B$ only act on states of 'their' oscillator, the scalar products can be separated. (iii) The complicated dependence on the orientation of and the distance between the two oscillators is summed up in a geometrical factor $X_{AB} = (\cos\alpha - 3\cos\beta\cos\gamma)/R^3$ (Krimm & Abe, 1972) with α being the angle between the two TDMs, β and γ being the angles between the line joining the centres of the TDMs and either the TDM of oscillator A or B, R is the distance between the centres of the TDMs. (iv) As we are considering coupling between the same normal mode on different amide groups, the scalar products $\langle A1|\boldsymbol{\mu}_A|A0\rangle$ and $\langle B1|\boldsymbol{\mu}_B|B0\rangle$ are equal and can be replaced by $\langle 1|\boldsymbol{\mu}|0\rangle$. The final result is:

$$V_{AB} = (4\pi\varepsilon_r\varepsilon_o)^{-1}|\langle 1|\boldsymbol{\mu}|0\rangle|^2 X_{AB}.$$

The scalar product in this expression is the TDM of the isolated oscillators. It is non-zero for an IR-active vibration. When the geometric factor X_{AB} is also non-zero, V_{AB} and therefore the probability of energy transfer $|A1B0\rangle \rightarrow |A0B1\rangle$ are non-zero and in consequence the eigenstates $|A1B0\rangle$ and $|A0B1\rangle$ are non-stationary. The probability of transition depends upon the relative orientation of the oscillators, their distance and on the TDM of the isolated oscillator. The stronger the IR absorbance of the normal mode in question, the more probable will be the transition (exciton transfer).

As the quantity V_{AB} will also appear in the description of the energy levels of the coupled system, the calculation is taken further by evaluating the TDM of the isolated oscillators.

$$\langle 1|\boldsymbol{\mu}|0\rangle = |\langle \boldsymbol{\partial\mu}/\boldsymbol{\partial q}\rangle \langle \phi_1|\mathbf{Q}|\phi_0\rangle| = |\langle \boldsymbol{\partial\mu}/\boldsymbol{\partial q}\rangle|(h/8\pi^2\nu)^{0.5},$$

where $\langle \boldsymbol{\partial\mu}/\boldsymbol{\partial q}\rangle$ stems from the evaluation of the electronic contribution and is the change of dipole moment with the normal coordinate q at equilibrium position and $\langle \phi_1|\mathbf{Q}|\phi_0\rangle$ is the nuclear contribution with the ground state and the first excited state wave function ϕ_0 and ϕ_1, respectively. ν is the frequency of the isolated oscillator. This expression for $\langle 1|\boldsymbol{\mu}|0\rangle$ inserted into the above expression for V_{AB} finally gives

$$V_{AB} = (4\pi\varepsilon_r\varepsilon_o)^{-1}(h/8\pi^2\nu)|\langle \boldsymbol{\partial\mu}/\boldsymbol{\partial q}\rangle|^2 X_{AB},$$

Note that there seems to be an additional factor of $c^{-0.5}$ (c, velocity of light) in Krimm and coworkers' formulation for $\langle 1|\boldsymbol{\mu}|0\rangle$ (Cheam & Krimm, 1984; Krimm & Bandekar, 1986) due to their ν_α being the wavenumber $\tilde{\nu}$. Using $c\tilde{\nu} = \nu$, the same expression is obtained. Also the factor $m_r^{-0.5}$ from the analogous expression in Section 2.3 seems to be missing. This is because the normal coordinates q, used here already contain this factor since $\partial\mu/\partial q = (\partial\mu/\partial R)\ (\partial R/\partial q) = (\partial\mu/\partial R)m_r^{-0.5}$ for the diatomic oscillator.

Stationary states may be obtained by linear combination. Non-stationary states are inadequate to describe the excited states. This dilemma can be avoided by the construction of new states $|1+\rangle$ and $|1-\rangle$ from a linear combination of the states $|A1B0\rangle$ and $|A0B1\rangle$. Doing this we admit that we do not know on which oscillator the energy resides.

$$|1+\rangle = 2^{-0.5}(|A0B1\rangle + |A1B0\rangle),$$

$$|1-\rangle = 2^{-0.5}(|A0B1\rangle - |A1B0\rangle).$$

The ground state is unchanged: $|0\rangle = |A0B0\rangle$. With this set of states, the scalar product $\langle 1-|\mathbf{U}_{AB}|1+\rangle$ is zero and thus transitions like $|1+\rangle \rightarrow |1-\rangle$ and vice versa do not occur. This set of states is therefore stationary and can be used to calculate the energy eigenvalues of the excited states.

The energy eigenvalues of $|1+\rangle$ and $|1-\rangle$. For simplicity it is assumed in the following that we do not have to consider permanent dipole moments, i.e. that $\langle 1|\boldsymbol{\mu}|1\rangle$ and $\langle 0|\boldsymbol{\mu}|0\rangle$ are zero. (If not this would give the same additional energy contribution for the excited and the ground state and therefore has no consequence on the absorption spectrum.) The stationary states $|1+\rangle$ and $|1-\rangle$ have the following energy eigenvalues

$$E_{|1+\rangle} = \langle 1+|\mathbf{H}_A + \mathbf{H}_B + \mathbf{U}_{AB}|1+\rangle = E_1 + E_0 + V_{AB},$$

$$E_{|1-\rangle} = \langle 1-|\mathbf{H}_A + \mathbf{H}_B + \mathbf{U}_{AB}|1-\rangle = E_1 + E_0 - V_{AB}.$$

with $E_0 = \langle 0|\mathbf{H}|0\rangle$ and $E_1 = \langle 1|\mathbf{H}|1\rangle$ being the energy of the ground and the first excited state of the unperturbed isolated oscillator. The perturbation by TDC produces two energy levels $E_1 + E_0 \pm V_{AB}$ for the coupled oscillator system as shown in Fig. 2, instead of only one energy level for the singly excited state $E_1 + E_0$ of two non-interacting oscillators. Because terms like $\langle 0|\boldsymbol{\mu}|0\rangle$ are zero, the energy of the ground state is still

$$E_{|0\rangle} = \langle 0|\mathbf{H}_A + \mathbf{H}_B + \mathbf{U}_{AB}|0\rangle = E_0 + E_0.$$

Thus, the energy difference between ground state and the excited states is

$$\Delta E = \Delta E_{noIA} \pm V_{AB},$$

where ΔE_{noIA} denotes the energy difference $E_1 - E_0$ in the absence of interaction (subscript noIA indicates *no interaction*). Accordingly, the absorbance band of the isolated oscillator splits into two bands for the coupled oscillator system positioned at the wavenumbers

$$\tilde{\boldsymbol{\nu}} = \tilde{\boldsymbol{\nu}}_{noIA} \pm V_{AB}/hc.$$

With the above expression for V_{AB}, the final result for the band splitting is then

$$\tilde{\boldsymbol{\nu}} = \tilde{\boldsymbol{\nu}}_{noIA} \pm (4\pi\varepsilon_r\varepsilon_o)^{-1}(8\pi^2\nu c)^{-1}|\langle \boldsymbol{\partial\mu}/\boldsymbol{\partial q}\rangle|^2 X_{AB}.$$

This equation has several important consequences. First, the absorbance band in the absence of interaction splits into two due to TDC. Secondly, due to the term $\langle \boldsymbol{\partial\mu}/\boldsymbol{\partial q}\rangle$, the splitting is the larger the more the dipole moment changes with the vibration, i.e. the more the isolated oscillator absorbs IR light. Thirdly, the splitting depends on the geometrical factor X_{AB} and thus on the relative orientation of the two oscillators and on their distance.

Energy splitting arises from V_{AB} due to the mixed terms $\langle 1|\boldsymbol{\mu}|0\rangle$, the TDMs, and the interaction is accordingly named TDC. This interaction can be also present when terms like $\langle 1|\boldsymbol{\mu}|1\rangle$ and $\langle 0|\boldsymbol{\mu}|0\rangle$ are zero, i.e. when there is no permanent dipole moment associated with the oscillators.

An approximation for $\langle \boldsymbol{\partial\mu}/\boldsymbol{\partial q}\rangle$ can be obtained from quantum chemical calculations on NMA. X_{AB} is derived from the structure. Thus, the TDC model does not contain free parameters and its physical relevance is easily tested. TDC was found to be essential to explain the split absorbance band of β-sheet structures and is thus considered to be an important, if not the dominant, interaction that determines the shape of the amide I band (Abe & Krimm, 1972; Krimm & Bandekar, 1986). TDC also contributes to the amide II vibration and to a lesser extent to the amide III vibration.

5. The polarization and IR activity of amide I modes

5.1 The coupled oscillator system

When an IR absorbance spectrum is recorded, light is absorbed by the sample. In a coupled oscillator system, transitions like $|0\rangle \rightarrow |1+\rangle$ or $|0\rangle \rightarrow |1-\rangle$ are induced by the absorption of photons. The transition probability for the coupled system is given here in analogy to the treatment for UV/visible spectroscopy given by Cantor & Schimmel (1980). The interaction potential, $\mathbf{U}_{em}$, between oscillator system and light is analogous to Section 2.3 given by

$$\mathbf{U}_{em} = \boldsymbol{\mu}_A E + \boldsymbol{\mu}_B E,$$

with E the vector of the electric field, $\mathbf{U}_{em}$, $\boldsymbol{\mu}_A$, and $\boldsymbol{\mu}_B$ being operators indicated by bold face. Because the electric field E does not act on the oscillator states and can thus be separated from the scalar product, the probability of a transition $|0\rangle \rightarrow |1+\rangle$ is proportional to $|\langle 1+|\boldsymbol{\mu}_A+\boldsymbol{\mu}_B|0\rangle|^2$ according to Fermi's golden rule. The calculation will be performed at the same time for $|1+\rangle$ and $|1-\rangle$ which will be denoted by the symbol $|1\pm\rangle$. This gives

$$|\langle 1\pm|\boldsymbol{\mu}_A+\boldsymbol{\mu}_B|0\rangle|^2 = \tfrac{1}{2}|\langle B1|\boldsymbol{\mu}_B|B0\rangle \pm \langle A1|\boldsymbol{\mu}_A|A0\rangle|^2 = |\langle 1|\boldsymbol{\mu}|0\rangle|^2(1\pm\cos\Theta).$$

In the calculation it has been assumed that operator $\boldsymbol{\mu}_A$ only acts on states of oscillator A and $\boldsymbol{\mu}_B$ only on states of operator B, terms like $\langle A1B0|\boldsymbol{\mu}_A|A0B0\rangle$ are therefore equal to $\langle A1|\boldsymbol{\mu}_A|A0\rangle$. Terms like $\langle A0|\boldsymbol{\mu}_A|A0\rangle$ are zero as mentioned in Section 2.3. The last step assumes that $|\langle A1|\boldsymbol{\mu}_A|A0\rangle| = |\langle B1|\boldsymbol{\mu}_B|B0\rangle|$ because the same oscillation (for example the amide I mode) is considered for both oscillators, Θ is the angle between the two TDMs of A and B. This calculation shows that the polarization of a coupled-system transition is no longer identical to the polarization of the isolated oscillator transition. Instead the overall polarization can be calculated by adding (or subtracting) the TDMs of the isolated oscillators when the oscillators oscillate in-phase (or out-of-phase).

The above equation also has consequences for the interpretation of amide I difference bands that are observed for protein reactions. Conformational changes will alter the relative orientation of the amide I TDMs. As the overall probability of absorption depends upon the relative orientation of the TDMs, a conformational change will, in general, also alter the amide I extinction coefficient of the respective structural unit.

5.2 Optically allowed transitions

The amide I and II modes are localized on the peptide group and cause only small movements of the C_α atoms. Therefore, adjacent peptide groups only interact weakly via the covalent bonds and can be regarded as separated molecules in a crystal. In crystals, the IR and Raman active modes are only those where corresponding groups in every unit cell move in phase. These are the optically allowed transitions. The constraint means that the allowed phase differences between the oscillators within the unit cell (repeat unit) are limited. The phase differences are denoted with δ for intrachain neighbours and, for β-sheets, with δ' for the hydrogen-bonded groups in adjacent chains. Some of the optically allowed transitions will turn out to be IR inactive because the TDMs of the unit cell amide groups add up to zero.

5.3 The infinite parallel β-sheet

The unit cell of an infinite parallel β-sheet contains only one chain and two adjacent peptide groups (see Fig. 3). Therefore, adjacent chains move in-phase for optically active vibrations ($\delta' = 0$). Within a chain the phase difference has to be 0 or 2π between two adjacent unit cells. This ensures that the motions in all unit cells are in-phase. Thus, the phase difference between two adjacent groups within one chain can be 0 or π ($\delta = 0, \pi$) (Miyazawa, 1960). This gives two vibrational modes $\pi(\delta, \delta')$ that are optically active: A(0,0) and B(π, 0) which are named A or B according to their symmetry properties.

The overall TDM of the unit cell determines the polarization of the transition and the extinction coefficient of the vibrational mode. It can be calculated according to Section 5.1 by adding the contributions of the individual oscillators. For the in-phase combination A(0,0) the

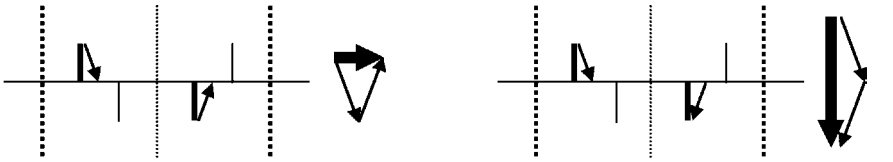

Fig. 3. Scheme of the 2 amide I normal modes of the parallel β-sheet (modified from Miyazawa, 1960). The unit cell consists of 2 peptide groups. The long, horizontal lines represent the peptide backbone, the short lines the C═O and N—H bonds, C═O bonds are bold, N—H bonds normal weight. Kinks in the β-sheet are indicated by dashed lines, with the bold line above the paper plane, the thin line below. The arrows represent the contributions of the respective amide groups to the overall TDM. For a phase difference of 0 this contribution equals the TDM of the respective group. For a phase difference of π the contribution points in the direction opposite to the TDM. The TDM is a vector whose centre is located close to the oxygen and close to the C═O bond. It points away from the C═O bond towards the C—N bond by 20° (Torii & Tasumi, 1992b). For a clearer presentation, the approximate location and orientation of the TDM contributions are shown as found for non-α and non-β structures, for α and β structures they are parallel shifted towards the C═O bond (Torii & Tasumi, 1992b). The arrows on the right-hand side of every unit cell show the addition of the individual contributions to the overall TDM (bold arrow) on an enlarged scale.

contributions are identical to the TDMs, for the out-of-phase combination $B(\pi,0)$ the TDMs have to be multiplied with the phase factor -1 for those groups with a phase difference of π. Fig. 3 shows these contributions for the two optically active vibrations.

In the $A(0,0)$ mode, the TDM contributions perpendicular to the paper plane cancel and the transition is polarized parallel to the chains. The overall TDM is small.

For the $B(\pi,0)$ mode, the TDM contributions parallel to the chain cancel. This transition is thus polarized perpendicular to the chains and gives rise to the main IR absorption band because of its large overall TDM.

5.4 The infinite antiparallel β-sheet

The unit cell of an antiparallel β-sheet is shown in Fig. 4. It contains 4 peptide groups, 2 in one chain and 2 in the adjacent chain. Therefore the intrachain phase difference, δ, between two adjacent amide groups is either 0 or π for optically active modes, as for the infinite parallel β-sheet. A similar argument gives the same phase differences δ' between two adjacent chains. Thus, a maximum number of 4 modes $\nu(\delta,\delta')$ will be optically active (Miyazawa, 1960) with the phase differences $\delta=0,\pi$ and $\delta'=0,\pi$ which are named according to their symmetry properties $A(0,0)$, $B_1(0,\pi)$, $B_2(\pi,0)$ and $B_3(\pi,\pi)$. Figure 4 shows the contributions of the individual groups in the unit cell to the overall TDM. These contributions cancel for the $A(0,0)$ mode which is therefore IR inactive. It is however Raman active (Krimm & Bandekar, 1986).

For the $B_1(0,\pi)$ mode, adjacent chains vibrate with a phase difference of π and thus the contributions of the top chain in Fig. 4 point in the opposite direction to those of the bottom chain. The contributions add in the paper plane but cancel perpendicular to it: the overall TDM lies in the paper plane and parallel to the chains but is relatively small. This vibration gives rise to the weak IR band near 1695 cm^{-1}. It is also Raman active (Krimm & Bandekar, 1986).

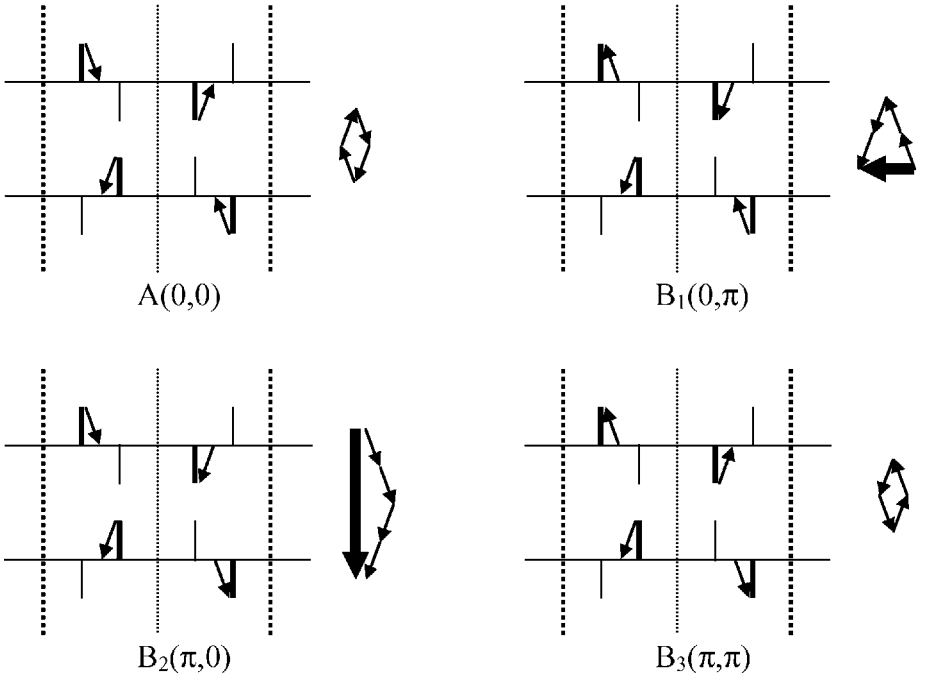

Fig. 4. Scheme of the 4 normal modes of the antiparallel β-sheet (modified from Miyazawa, 1960; Chirgadze & Nevskaya, 1976a). The unit cell consists of 4 peptide groups. C═O groups are bold, N—H groups normal weight. The arrows represent the contributions of the respective amide groups to the overall TDM. See legend of Fig. 3 for further explanation.

For the $B_2(\pi, 0)$ mode, groups adjacent in the chain vibrate with a phase difference of π. The TDM contributions add in the paper plane but cancel perpendicular to it. This mode gives rise to the main band of β-sheet IR absorption near 1630 cm^{-1} because the overall TDM is very large. The transition is polarized perpendicular to the chain direction and is also Raman active (Krimm & Bandekar, 1986).

For the $B_3(\pi, \pi)$ vibration, the contributions in the paper plane cancel, but add perpendicular to it. The overall TDM is oriented perpendicular to the paper plane. It is very small and therefore this transition is hardly observed in the IR spectrum. This mode is Raman active (Krimm & Bandekar, 1986).

5.5 The infinite α-helix

For the infinite α-helix there are two values for the phase difference between two adjacent peptide groups that lead to IR-active vibrational modes: $\delta_1 = 0$ (overall TDM parallel to the helix axis) and $\delta_2 = 2\pi/3{\cdot}6$. The latter value corresponds to the angle between two adjacent groups if the helix is viewed along the helix axis. Since the unit cell consists of 5 helix turns with 18 amino acids, and $18 \times \delta_2 = 10\pi$, this selection of δ_2 ensures that motions in adjacent unit cells are in-phase as required. The corresponding vibration is degenerate and the overall TDM is perpendicular to the helix axis.

A species ($\delta_1 = 0$). For the A mode with a phase difference of 0, the contributions parallel to the helix axis add but cancel perpendicular to it. The latter can be easily visualized for a

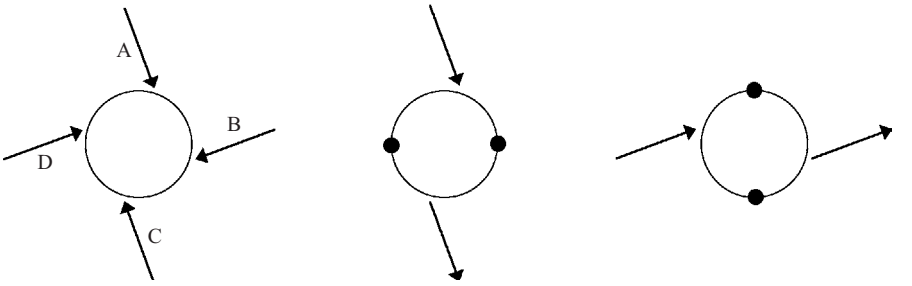

Fig. 5. Scheme of the vibrational modes of the hypothetical helix with 4 peptide groups per turn. The view is along the helix axis. The arrows indicate the contributions perpendicular to the helix axis of the individual amide groups to the overall TDM. Left: phase difference $\delta_1 = 0$. The contributions cancel perpendicular to the helix axis, but add parallel to it. Middle and right: phase difference $\delta_2 = 2\pi/4$. Contributions are shown for the two degenerate vibrations which are polarized perpendicular to each other and perpendicular to the helix axis.

hypothetical helix with 4 peptide groups per turn, as shown in Fig. 5, for which one turn would constitute the unit cell. The mode is both Raman and IR active.

E_1 species ($\delta_2 = 2\pi/3{\cdot}6$). The properties of this vibration are discussed by the analogous vibration of the hypothetical helix model with 4 residues per turn. This would give a phase difference of $2\pi/4$ between the vibrations of two adjacent residues which therefore do not couple. Instead, the second next neighbours couple, having a phase difference of π. Two pairs of coupled residues are possible for the hypothetical helix and thus, two degenerate vibrations are possible. In the quantum mechanical description this corresponds to the linear combinations $|A0C1\rangle - |A1C0\rangle$ and $|B0D1\rangle - |B1D0\rangle$ for the two degenerate excited states if consecutive groups in the helix are named A–D. For both transitions, the contributions parallel to the helix axis cancel and thus they are both polarized perpendicular to the helix axis and perpendicular to each other.

E_2 species ($\delta_2 = 4\pi/3{\cdot}6$). This mode is only Raman active. In our simple helix model with 4 peptide residues per turn, the phase difference between adjacent groups is π and the 4 contributions to the overall TDM cancel showing that this mode is IR inactive.

6. Calculation of the amide I band

6.1 Overview

There are several ways of calculating the amide I band of a protein:

(1) For infinite secondary structures, their symmetry considerably reduces the number of observable vibrational modes (see above) and the effect of TDC is easily calculated. The strength of TDC between every pair of oscillators can be calculated from the equations above and the frequency shift for the coupled system evaluated according to the perturbation theory by Miyazawa (see below). This simple approach can explain the general features of amide I absorbance of secondary structures.

(2) For calculating the amide I band of proteins, a 'floating oscillator model' has been developed (Torii & Tasumi, 1992b, 1996). Here, the amide groups of a protein are regarded as isolated oscillators that only interact via TDC. The unperturbed oscillators vibrate with

the frequency ν_0. By adjusting the unperturbed frequency, effects of hydrogen bonding, non-planarity of the peptide group and through-bond interactions may be accounted for. A calculation analogous to a normal mode calculation is then carried out with a matrix of force constants that contains only the diagonal force constants (which determine ν_0) and interaction force constants f_{AB} due to TDC between amide group A and group B (which shift the oscillator frequency). These interaction force constants are calculated classically from the dipole–dipole interaction potential U_{AB} of Section 4.4 using $f_{AB} = \partial^2 U_{AB}/\delta q_A \delta q_B$. Here, q_A and q_B are the normal coordinates of the amide I vibration of groups A and B, respectively. In the calculation, terms like $\partial \mu_A/\partial q_A$ occur which are equated with the TDM of oscillator A. This model gave a good agreement with experimental protein spectra (Torii & Tasumi, 1992b) and leads to interesting insights which are discussed below. Brauner *et al.* (2000) extended this approach: they included interactions like through-H-bond and through-valence-bond coupling in the non-diagonal force constants and considered higher multipoles than the dipole approximation, which is advantageous for the agreement between simulated and experimental spectra of isotopically labelled peptides in β-sheet structures.

(3) A normal mode analysis can be carried out using a simplified general-valence force field for the polypeptide with that of NMA serving as a starting point (Krimm & Bandekar, 1986). The force field is then refined for a given polypeptide structure in order to match the calculated frequencies with the experiment. Hydrogen bonds can be included in the force field by assigning force constants to the H···O stretching and the N—H···O and C═O···H bending vibrations. TDC is also accounted for using interaction force constants calculated classically from the interaction potential U_{AB}, similar to the floating oscillator approach. However, instead of normal coordinates, internal coordinates are used. For example, for the interaction due to the vibration of the internal coordinate i on oscillator A (s_{Ai}) and j on B (s_{Bj}), the interaction force constant is calculated according to $f_{AiBj} = \partial^2 U_{AB}/\partial s_{Ai} \partial s_{Bj}$. These calculations were able to reproduce the observed vibrational spectra of regular polypeptides with an average error of 5 cm^{-1} (Krimm & Bandekar, 1986). Recently it was suggested (Lee & Krimm, 1998) that the weak coupling approximation is not sufficient to describe the degenerate modes of the α-helix, in particular the Raman-active E_2 species. In this approximation, the TDM of a reference group is thought to be an intrinsic property of that group. Thus, only terms like $\partial \mu_A/\partial s_{Ai}$ appear in the interaction force constants which contain only internal coordinates of the reference group A. However, terms like $\partial \mu_A/\partial s_{Bi}$ may also be important, where the TDM of group A depends on coordinates of group B. As these are presently not available for polypeptides from *ab initio* calculations, optimized interaction force constants were used instead that were based on *ab initio* calculations of (L-Ala)$_2$ (Lee & Krimm, 1998). This improved the calculated frequency of the E_2 mode considerably.

(4) For small peptides with a defined structure, density functional calculations can be carried out that include TDC, through-bond coupling and the effects of hydrogen bonds (Kubelka & Keiderling, 2001a). The calculated force field can then be transferred to larger peptides.

In the following, the approach used for infinite secondary structures is discussed in more detail, it is then applied to various secondary structures and the results are augmented by those of the other methods.

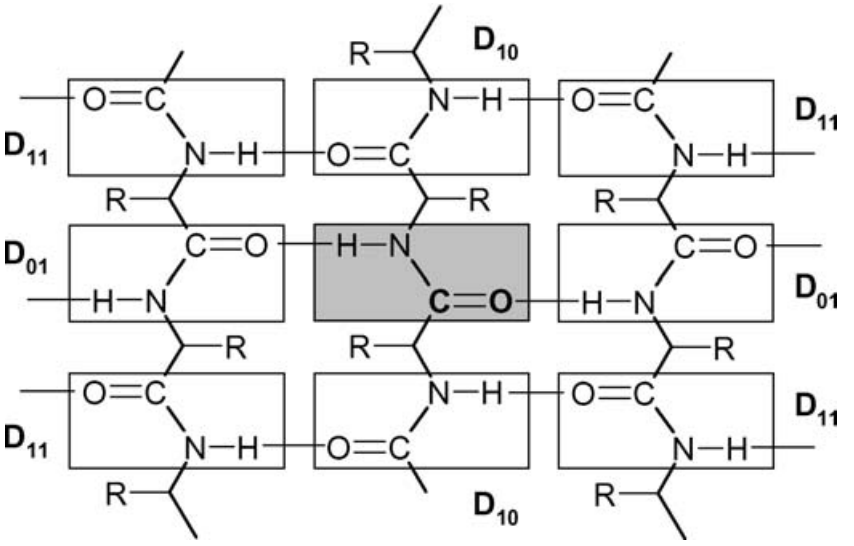

Fig. 6. Terminology for Miyazawa's perturbation treatment. The numbering of the groups that interact with the centre group is shown. The effects of groups with the same intra- and interchain distance are summed up in one term. For example four amide groups contribute to D_{11}.

6.2 Perturbation treatment by Miyazawa

As the amide I and II vibrations are highly localized in the peptide group, interactions between different peptide groups can be treated by a 'weakly coupled oscillator model' according to Miyazawa (1960). An amide oscillator with the unperturbed frequency, ν_0, will experience a frequency shift when it is incorporated in a polypeptide due to interactions with adjacent oscillators. The interactions are strongest when the interacting amide groups vibrate with the same frequency. The interaction, and thus the frequency shift of the amide oscillator, will depend on the phase difference of the vibrations between the interacting groups, being strongest for phase differences of 0 and π and 0 for a phase difference of $\pi/2$. In a α-helix only intrachain interactions are considered and for the frequency, ν, of the coupled oscillator system the following expression is found.

$$\nu(\delta) = \nu_0 + \sum D_s \cos(s\delta) \quad \text{(summed over } s\text{)},$$

where ν_0 is the unperturbed frequency of the isolated oscillator, ν its frequency in the coupled oscillator system. D_s is the interaction constant between peptide groups that are separated by s groups. For example, for two adjacent groups $s=1$ and the effects of the right and the left neighbour are summed in D_1. δ is the phase difference between the vibrations of two adjacent groups, $s\delta$ the phase difference of two groups separated by s groups.

For β-sheets interchain interactions also have to be considered and the above expression has to be generalized according to Moore & Krimm (1975) to

$$\nu(\delta, \delta) = \nu_0 + \sum\sum D_{st} \cos(s\delta) \cos(t\delta') \quad \text{(summed over } s \text{ and } t\text{)}.$$

Here, D_{st} is the interaction constant between peptide groups that are separated by t chains and s groups as shown in Fig. 6. δ' is the phase difference between two adjacent chains.

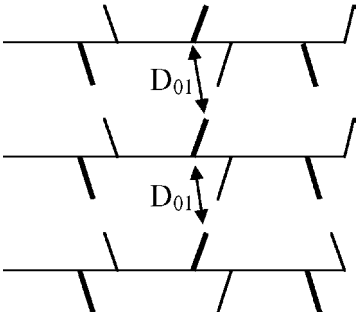

Fig. 7. The most important TDC interactions for the parallel β-sheet. C═O groups are bold, N—H groups normal weight.

To calculate the vibrational frequencies one needs the phase differences δ and δ' and a physical model for the interactions D_{st}. As we have seen above, for infinite secondary structures only a few phase differences give rise to IR-active vibrational modes. In early work only the D_{10} and D_{01} terms were considered for β-sheets. However, no reasonable force field could account for the large D_{10} term that in this approximation was required to explain the observed amide I band splitting. Therefore, the D_{11} term was introduced and the physical origin of this interaction was ascribed to TDC (Abe & Krimm, 1972; Krimm & Bandekar, 1986). This interaction leads to the following interaction constants:

$$D_{st} = \sum V_{\mathrm{AB}st}/b,$$

Here, the interactions V_{AB} of oscillator A with all oscillators B_{st} from Section 4.4 are summed up for the intra- and the interchain distance specified by s and t.

6.3 The parallel β-sheet

The most important TDC interactions. Chirgadze & Nevskaya (1976b) investigated the influence of the TDC interactions on the amide I frequency and found that the strongest TDC interaction in a parallel β-sheet is D_{01}, the interaction between the hydrogen-bonded peptide groups. This interaction is shown in Fig. 7. Intrachain interactions are considerably smaller (Chirgadze & Nevskaya, 1976b; Torii & Tasumi, 1992b) and interactions over a distance of more than 10 Å are negligible (Chirgadze & Nevskaya, 1976b) ($D_{01} \gg D_{11} > D_{10}$).

The infinite parallel β-sheet. The frequencies for the infinite parallel β-sheet can be calculated according to Miyazawa's perturbation treatment (Miyazawa, 1960) and the TDC model (Krimm & Abe, 1972; Chirgadze & Nevskaya, 1976b):

$$\mathrm{A}(0,0) = \nu_0 + D_{01}(+D_{11} + D_{10}) \quad \text{(band predicted near 1651 cm}^{-1}\text{)},$$
$$\mathrm{B}(\pi,0) = \nu_0 + D_{01}(-D_{11} - D_{10}) \quad \text{(main band predicted near 1637 cm}^{-1}\text{)}.$$

Both vibrations are IR active. The leading TDC term D_{01} causes a frequency shift of $-27\ \mathrm{cm}^{-1}$ (Chirgadze & Nevskaya, 1976b) for both of them and this is the main effect of TDC. Since D_{01} has the same sign for both vibrations, only the minor contributions D_{11} and D_{10} lead to a small amide I splitting of $14\ \mathrm{cm}^{-1}$.

The finite parallel β-sheet. For finite parallel β-sheets, the position of the main band is insensitive to the number of groups per chain in the sheet, but shifts to lower wavenumbers with an

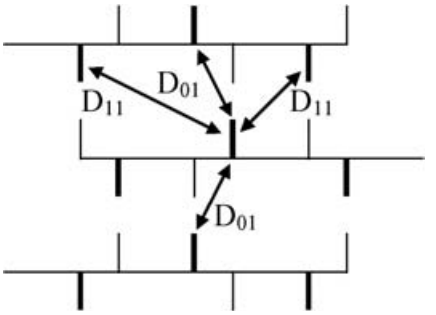

Fig. 8. Antiparallel β-sheet with the most important TDCs. C═O groups are bold, N—H groups normal weight. Only two of the four D_{11} interactions are shown: those to the nearest C═O oscillators.

increasing number of chains. This is because the intrachain interaction D_{10} is negligible compared to the interchain interaction D_{01}. A high-frequency band is predicted in the calculations which is shifted by at most 40 cm^{-1} with respect to the main band (Chirgadze & Nevskaya, 1976b). Thus, the spectra of finite parallel β-sheets are predicted to be similar to those of finite antiparallel β-sheets (discussed below) and to mixed sheets. These predictions are supported by the calculations of protein amide I bands by Tori & Tasumi (1992b) where parallel β-sheets exhibit their main absorption near 1630 cm^{-1} but show smaller bands between 1650 and 1680 cm^{-1} (calculated for ^2H_2O).

6.4 The antiparallel β-sheet

The most important TDC interactions. The most important TDC interactions in the antiparallel β-sheet (Chirgadze & Nevskaya, 1976a) are shown in Fig. 8. Eighty per cent of the observed amide I band splitting can be accounted for by a nearest-neighbour approximation.

The strongest TDC interactions are between peptide groups that are hydrogen-bonded (D_{01}) and to the nearest C═O group (D_{11}, arrow to the right in Fig. 8). A smaller but significant contribution with opposite sign stems from a second diagonal term (D_{11}, arrow to the left in Fig. 8). Coupling between adjacent groups within one chain is negligible (Chirgadze & Nevskaya, 1976a; Torii & Tasumi, 1992b). Thus, $D_{01} > D_{11} \gg D_{10}$. Long-range TDC interactions do not seem to have a large effect (Kubelka & Keiderling, 2001a).

The infinite antiparallel β-sheet. Using only the two leading contributions, the frequencies of the infinite antiparallel β-sheet amide I modes can be calculated according to Miyazawa (1960) and the TDC model (Krimm & Abe, 1972; Chirgadze & Nevskaya, 1976a):

$$
\begin{aligned}
&A(0,0) && \nu = \nu_0 + D_{01} + D_{11} && \text{(IR inactive)},\\
&B_1(0,\pi) && \nu = \nu_0 - D_{01} - D_{11} && \text{(band near 1690 cm}^{-1}\text{)},\\
&B_2(\pi,0) && \nu = \nu_0 + D_{01} - D_{11} && \text{(main band near 1630 cm}^{-1}\text{)},\\
&B_3(\pi,\pi) && \nu = \nu_0 - D_{01} + D_{11} && \text{(very weak)}.
\end{aligned}
$$

The vibrations that contribute most to the amide I IR spectrum are $B_1(0,\pi)$ and $B_2(\pi,0)$. For these, the leading interaction term D_{01} has a different sign. This leads to the large-frequency splitting that is observed for the amide I vibration of antiparallel β-sheets.

The finite antiparallel β-sheet. For finite β-sheets, more than two vibrations are calculated to give rise to IR absorption, in most cases 3–5. The frequency splitting increases with the number of

chains in the sheet which is a consequence of the strong coupling between groups in adjacent chains. It is close to the splitting for the infinite sheet already for 6 chains. In contrast, the number of groups in a chain has only a minor influence on the frequencies because of the weak intrachain coupling (Chirgadze & Nevskaya, 1976a; Kubelka & Keiderling, 2001a). Splitting is largest in planar antiparallel β-sheets but reduced in twisted sheets (Kubelka & Keiderling, 2001b). The main maximum arises from vibrations of the same type as for the infinite antiparallel β-sheet, i.e. neighbours in a chain are out-of-phase and hydrogen-bonded groups of adjacent chains are in-phase. The most intense of these modes are localized more on the inner strands of antiparallel β-sheets with 3–5 strands. The outer strands contribute more to modes at higher frequencies (Kubelka & Keiderling, 2001a).

Comparison with experimental spectra. TDC accounts well for the observed splitting of the amide I band of proteins with a high antiparallel β-sheet content (Abe & Krimm, 1972; Krimm & Abe, 1972; Chirgadze & Nevskaya, 1976a). For the main band, a correlation has been proposed (Kleffel *et al.* 1985) between the chain length of β-sheets and the position of the amide I band using the proteins ribonuclease A (1640 cm^{-1}), α-chymotrypsin (1638 cm^{-1}) and concanavalin A (1633 cm^{-1}). Such a correlation would be in contrast to the theoretical considerations above which predict only a minor effect of the chain length. However, these 3 proteins also differ in the number of chains that constitute the β-sheets and the wavenumber of the amide I maximum decreases with the number of chains as predicted by the theory. The wavenumber is lowest for concanavalin A, which has two antiparallel sheets with 7 strands each that are well aligned.

It is often claimed that parallel and antiparallel sheets can be distinguished because parallel β-sheets only absorb at low wavenumbers and lack the high wavenumber component of the antiparallel β-sheet – this is true for *infinite* sheets. However, Susi & Byler (1987) assigned absorption near 1675 cm^{-1} (in ^2H_2O) to parallel β-sheets which is consistent with the predictions from theory for *finite* parallel sheets. Also a recently discovered parallel β-helix fold shows a high-frequency component near 1690 cm^{-1} (in ^1H_2O) (Khurana & Fink, 2000). The main component in both studies is observed near 1630–1640 cm^{-1}. A distinction between parallel and antiparallel β-sheets therefore seems to be difficult for finite sheets (Susi & Byler, 1987; Khurana & Fink, 2000; Kubelka & Keiderling, 2001b).

6.5 The α-helix

The most important TDC interactions. In the infinite α-helix, the strongest TDC interactions are with the direct neighbours in the chain (D_{10}) and with the groups that are hydrogen-bonded (D_{30}): $D_{10}>D_{30}>D_{20}$ (Nevskaya & Chirgadze, 1976). These interactions are shown in Fig. 9. No interchain interactions have to be considered for the α-helix. Interactions over a distance of more than 15 Å have only minor effects.

The infinite α-helix. These interactions give rise to the following vibrational frequencies for the infinite α-helix (Miyazawa, 1960; Nevskaya & Chirgadze, 1976):

$$A(0) = \nu_0 + D_{10} + D_{20} + D_{30} \quad \text{(main band)},$$

$$E_1(2\pi/3{\cdot}6) = \nu_0 + D_{10}\cos(2\pi/3{\cdot}6) + D_{20}\cos(4\pi/3{\cdot}6) + D_{30}\cos(6\pi/3{\cdot}6).$$

D_{10} is positive, D_{30} and D_{20} are negative and their contributions nearly cancel for A(0). Thus, the shift due to TDC is only 5–10 cm^{-1} for the infinite α-helix. For $E_1(2\pi/3{\cdot}6)$, $\cos(2\pi/3{\cdot}6)$ is

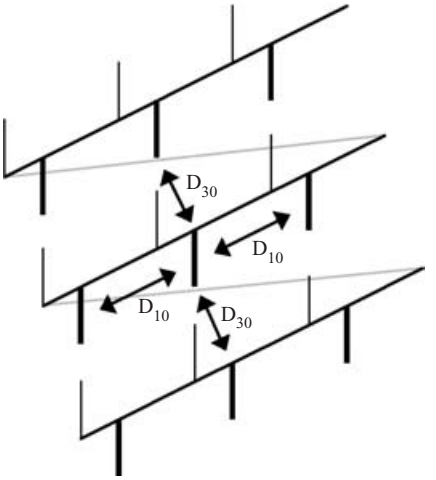

Fig. 9. The most important TDC interactions of an α-helix. C═O groups are bold, N—H groups normal weight.

close to zero which makes the frequency shift due to the largest interaction constant D_{10} small, $\cos(4\pi/3{\cdot}6)$ is close to -1 which relatively enhances the frequency shift caused by the smallest interaction constant D_{20} and $\cos(6\pi/3{\cdot}6)$ is close to 0·5 with the result that the frequency shifts due to D_{20} and D_{30} nearly cancel. This leaves the small negative contribution of D_{10} $\cos(2\pi/3{\cdot}6)$ and the shift from ν_0 is therefore small also for $E_1(2\pi/3{\cdot}6)$. Because both IR-active vibrations of the helix experience only a small TDC-induced frequency shift, the calculated splitting between the frequencies of A(0) and $E_1(2\pi/3{\cdot}6)$ is also very small, 2 cm^{-1} (Krimm & Bandekar, 1986) to 4 cm^{-1} (Nevskaya & Chirgadze, 1976). Good agreement with the experimental spectra is obtained for $\nu_0 = 1663$ cm^{-1} (Nevskaya & Chirgadze, 1976).

The finite α-helix. A finite α-helix of up to 3 turns results in a complicated spectrum (Nevskaya & Chirgadze, 1976). For most short helices, 3 bands are calculated which occur in a spectral range of 40 cm^{-1}. The frequency of the most prominent side band of symmetry type E_1 is usually smaller than that of the main band (symmetry type A). As the helix elongates, the main band dominates the spectrum and its frequency decreases by 20 cm^{-1}.

These results are confirmed by calculations of α-helix contributions to protein spectra (Torii & Tasumi, 1992b). Here, side bands below 1640 cm^{-1} with a lower frequency than the main band are also found and assigned to the E_1 symmetry species. Splitting for a long helix is calculated to be smaller than for a short helix. Particularly interesting is the contribution of an α-helix to the spectra of lysozyme and α-lactalbumin. The secondary structure is very similar for the two proteins with the exception of an α-helix that has only 2 turns in α-lactalbumin but 3 turns in lysozyme. Only the longer helix gives a calculated spectrum with the 'typical' main band near 1650 cm^{-1}. The shorter helix shows the main band near 1640 cm^{-1}, two bands with slightly lower intensity at 1660 and 1670 cm^{-1} and a minor band near 1680 cm^{-1}. Thus, theory seems to predict that short helices do not produce the 'typical' α-helix spectrum with a main band near 1650 cm^{-1}.

Comparison with experimental spectra. Experiments confirm that splitting of the α-helix modes is very small. Also the dependence of band position on the helix length seems to be correctly predicted by theory (Nevskaya & Chirgadze, 1976; Torii & Tasumi, 1992a) since myoglobin absorbs near 1655 cm^{-1} and tropomyosin with longer helices near 1646 cm^{-1} (Torii & Tasumi,

1992a). The fact that the TDC interactions nearly cancel for the α-helix may explain the spectral changes observed upon isotopic substitution in a single C═O group of α-helical peptides. The frequency shift is as expected for an isolated C═O oscillator. In contrast, for β-sheet structures, where the TDC effect is large, a more complicated behaviour is observed (Brauner *et al.* 2000).

6.6 Other secondary structures

α_{II}-*helix*. Because of weaker hydrogen bonds and an altered TDC interaction, the amide I frequency of the α_{II}-helix approximately absorbs 10 cm^{-1} higher than that of the α-helix and the splitting slightly increases to 7 cm^{-1} (Krimm & Bandekar, 1986).

Turns. Turn structures are expected to absorb between 1700 and 1630 cm^{-1}, depending on the type of turn and on the dihedral angles (Krimm & Bandekar, 1980, 1986; Lagant *et al.* 1984). In proteins, non-α and non-β structures seem to absorb in the entire spectral region of the amide I band, making it difficult to distinguish between turn and other structures (Torii & Tasumi, 1992b).

7. Experimental analysis of protein secondary structure

Analysing the secondary structure of proteins in their native aqueous environment with IR spectroscopy has a long tradition (Susi *et al.* 1967; Timasheff *et al.* 1967). While NMR and X-ray crystallography are of course superior for a full structure determination, the advantage of the IR approach is that it is fast and inexpensive. The relevance of this IR spectroscopic application might even increase in the proteomics age where vast numbers of proteins await characterization. An aspect that may become of particular importance is that it is possible to distinguish between native and aggregated protein. IR spectroscopy, therefore, increasingly becomes a valuable biotechnological and biomedical tool.

In the preceding sections we have described the theoretical background for the analysis of the secondary structure of proteins. Here, the experimental techniques and results are briefly summarized. For detailed reviews see, for example, Goormaghtigh *et al.* (1994a) and Arrondo *et al.* (1993). Essentially, there are two different approaches to determine the secondary-structure composition of proteins. The first is based on band narrowing and curve-fitting of the amide I band (Byler & Susi, 1986). The second method uses a calibration set of spectra from proteins with known structure to perform pattern-recognition calculations (Dousseau & Pezolet, 1990; Lee *et al.* 1990; Rahmelow & Hübner, 1996; Baumruk *et al.* 1996). Both predominantly use the amide I band (1610–1700 cm^{-1}) of the protein IR spectrum. Protein spectra in ^1H_2O and ^2H_2O in the spectral region between 4000 and 1000 cm^{-1} are shown in Fig. 10.

7.1 Band fitting

The various secondary-structure components of a protein absorb at different positions in the amide I region of the IR spectrum. However, the components largely overlap and a more or less broad and featureless amide I band is observed. The goal in the curve-fitting approach to secondary-structure analysis is to decompose the amide I band into the various component bands which can then be assigned to the different types of secondary structure. First the component bands have to be resolved by mathematical procedures of band-narrowing to obtain the band positions, then the amide I band is fitted with bands placed at the positions found and

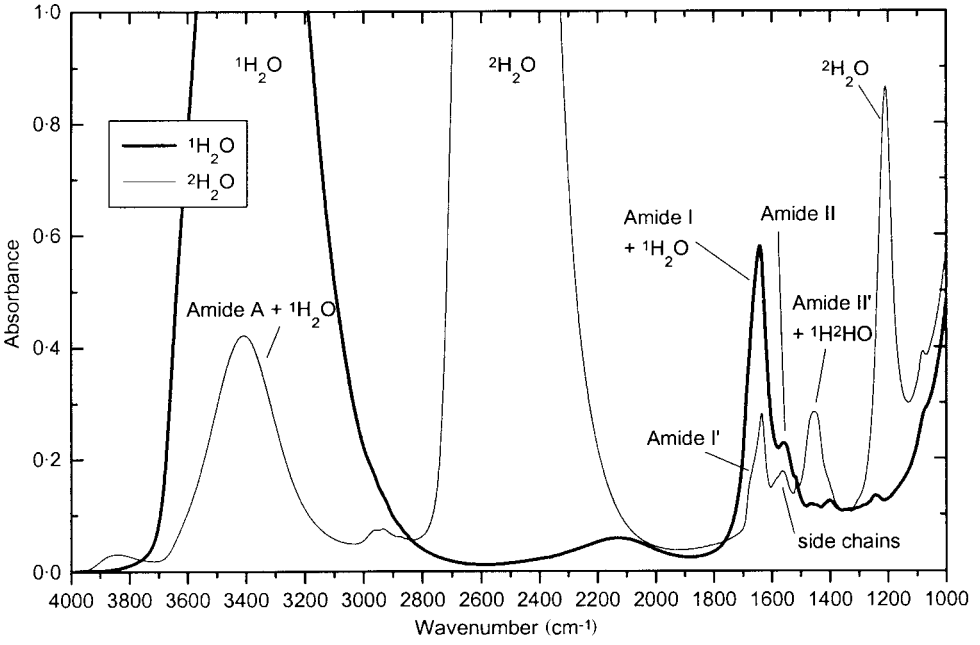

Fig. 10. Room temperature IR spectra of the all-β-sheet protein tendamistat in ^1H_2O (bold line) and ^2H_2O (thin line). Sample thickness was approximately 6 and 20 μm for ^1H_2O and ^2H_2O, respectively. Complete $^1H/^2H$ exchange was ensured by incubation of the sample in ^2H_2O at 80 °C for 10 min before data recording. At 80 °C tendamistat unfolds and opens the hydrogen bonds of the β-sheets which allows $^1H/^2H$ exchange (cf. Fig. 13). Before spectra recording, the temperature was reduced to room temperature which allows tendamistat to refold into its native structure.

the integrated absorbance of the component bands is calculated. Finally, the component bands are assigned to secondary structures, using the data presented in Table 2. To resolve the various components of the amide I band, several methods of band-narrowing can be applied which are compared in Fig. 11. The first possibility is to calculate the second derivative of the spectrum (Fig. 11*b*). The linewidth of the second derivative of a band is smaller than that of the original band. Thus, the second derivative can be used to resolve overlapping bands. The minima of the second derivative give the positions of the overlapping components (note that the second derivative is multiplied by −1 in Fig. 11). Secondly, the so-called Fourier deconvolution can be applied (Fig. 11*c*, dotted line) (Kauppinen *et al.* 1981). The line-narrowing principle of Fourier self-deconvolution is the multiplication of the Fourier transform of the original spectrum by a line-shape-dependent function that increases with increasing distance from the centre peak. In the case of deconvoluting Lorentzian lines, an exponential function is used. In this way those regions of the Fourier transform that encode for the fine structure in the original spectrum are weighted more strongly. After back-transformation into a spectrum, those components of the spectrum that change strongly with wavenumber (or wavelength or frequency) are amplified: the component bands appear to be 'sharper'.

A third approach is fine-structure enhancement (Barth, 2000a); here a smoothed version of the original spectrum is multiplied with a factor slightly smaller than 1 and subsequently subtracted from the original spectrum, enhancing the fine structure of the spectrum similarly to Fourier self-deconvolution (Fig. 11*c*, solid line).

Table 2. *Assignment of amide I band positions to secondary structure based on experimental data and assignments of various authors collected and evaluated by Goormaghtigh et al. (1994b)*

	Band position in ^1H_2O/cm^{-1}		Band position in ^2H_2O/cm^{-1}	
Secondary structure	Average	Extremes	Average	Extremes
α-helix	1654	1648–1657	1652	1642–1660
β-sheet	1633	1623–1641	1630	1615–1638
β-sheet	1684	1674–1695	1679	1672–1694
Turns	1672	1662–1686	1671	1653–1691
Disordered	1654	1642–1657	1645	1639–1654

In similar tables sometimes a discrimination between parallel and antiparallel β-sheet can be found, because theory predicts no high wavenumber component for infinite parallel β-sheets (Chirgadze & Nevskaya, 1976b). However, as discussed above, similar spectra are expected for finite β-sheets (Chirgadze & Nevskaya, 1976b; Torii & Tasumi, 1992b) and there is no experimental evidence for a difference between the frequencies of parallel and antiparallel β-sheets (Susi & Byler, 1987; Khurana & Fink, 2000).

Although the derivative spectra or the deconvoluted spectra are sometimes used for the fitting procedure, it is recommended that data fitting is performed with the unprocessed absorbance spectra since derivatization does not preserve the areas of the components and the results have been shown to be influenced by the deconvolution parameters (Goormaghtigh *et al.* 1994b). Comparison of the resulting curve with the original curve both treated with the same resolution-enhancing method can be used to check the quality of the result as shown in Fig. 12.

A possible source of error, for the inexperienced investigator, of the methods based on curve-fitting is a certain subjectivity of the approach which is due to the number of parameters involved in the band-narrowing and -fitting procedure. The quality of the result may be enhanced by analysing the amide I band using both ^1H_2O and ^2H_2O as solvents. The result should be independent of the solvent which gives an extra criterion for the quality of secondary structure prediction.

A fundamental problem is that the assignment of a given component band to a secondary-structure type is not unique or straightforward (Surewicz *et al.* 1993). Examples are the overlap of α-helix and random structures in ^1H_2O, side bands of α-helices below 1650 cm^{-1} which are commonly assigned to β-sheets and give rise to errors for proteins with a large α-helical content, the absorption of bent helices below 1650 cm^{-1} (Heimburg *et al.* 1999) and the assignment of bands in only the 1660–1690 cm^{-1} region to turn structures although they are predicted to absorb in the entire amide I region (see previous section). Again, hydrogen/deuterium exchange partly resolves this problem: for example the overlap of α-helix and random structure bands in ^1H_2O is greatly reduced in ^2H_2O.

Hydrogen/deuterium exchange leads to small band shifts of the amide I components. This is caused by the small contribution of the N—H bending vibration to the amide I mode. For proteins the amount of the shift is dependent on the type of secondary structure. Often, a shift of 15 cm^{-1} is observed for the weak high-frequency component of β-sheets and of turns. Bands assigned to disordered structures are shifted by 10 cm^{-1} whereas for all other bands the shift is only a few wavenumbers. Several factors may contribute to this phenomenon: (i) The N—H contribution to the amide I mode may differ for the various secondary structures, since the composition of the amide I mode generally depends on the structure of the polypeptide (Krimm & Bandekar, 1986). The size of the band shift in turn will depend on the extent of the

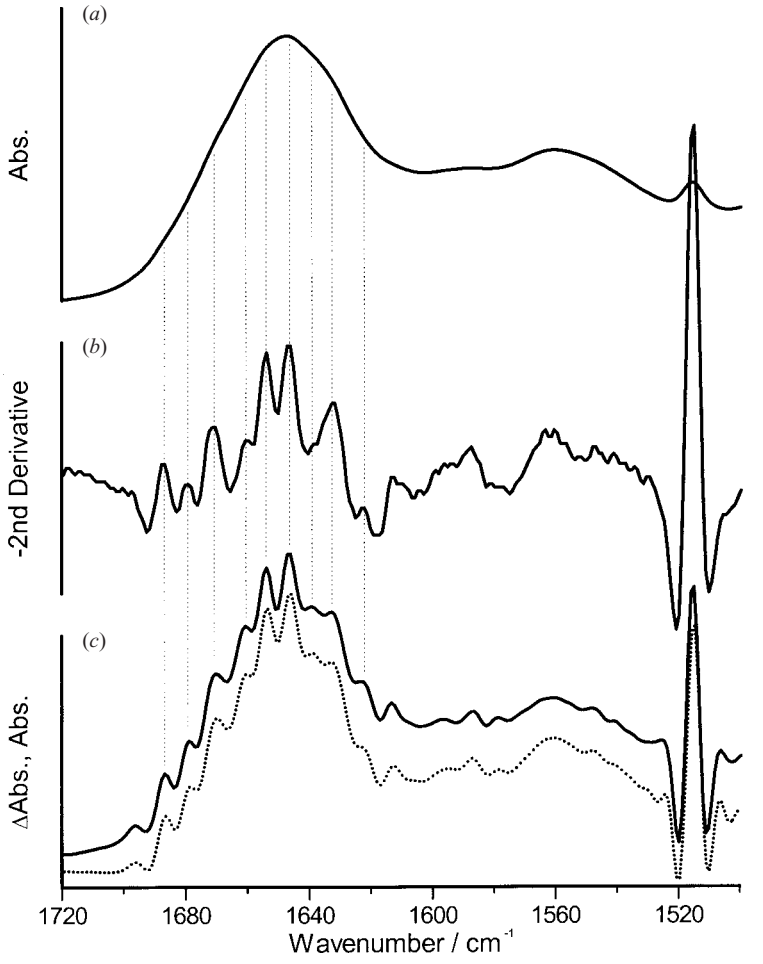

Fig. 11. Comparison of the band-narrowing techniques' second derivative, Fourier self-deconvolution (Kauppinen *et al.* 1981) and fine-structure enhancement (Barth, 2000a). (*a*) IR absorbance spectrum of the protein papain in ^2H_2O recorded at 2 cm^{-1} resolution. (*b*) Second derivative of the papain spectrum multiplied by −1. The positive peaks identify the position of several component bands that together constitute the amide I band (1700 to 1610 cm^{-1}). The large peak near 1515 cm^{-1} is the sharp band of the Tyr side-chains. (*c*) Fine-structure enhancement (solid line, smoothing range 12 cm^{-1}, weighting factor 0·985) and Fourier self-deconvolution (dotted line, resolution enhancement factor 2·6, Lorentzian line shape with full width at half maximum of 17 cm^{-1}) of the papain spectrum. These two methods give very similar results, the same component bands are identified as with the second derivative.

N—H contribution to the amide I mode. (ii) $^1H/^2H$ exchange is often incomplete for proteins and this may hold particularly for those ordered secondary structures that show only a small shift. The latter assumption is supported by a study of polypeptides where a similar shift between 5 and 10 cm^{-1} has been found for all secondary structures (Chirgadze *et al.* 1973; Chirgadze & Brazhnikov, 1974; Venyaminov & Kalnin, 1990b).

7.2 Methods using calibration sets

The second group of methods for secondary-structure analysis, working with factor analysis, partial least squares, or singular value decomposition, avoids some of the problems of the

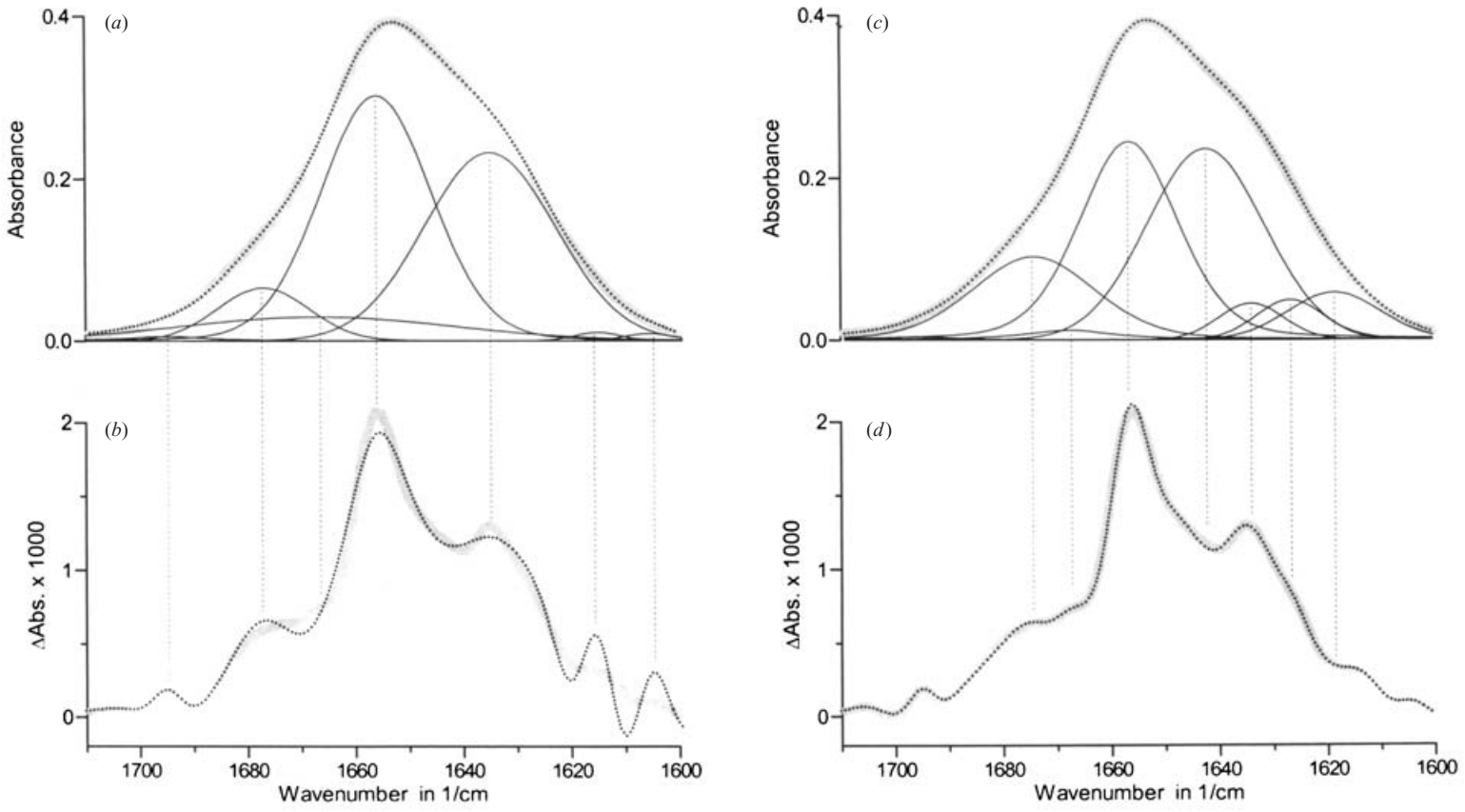

Fig. 12. For legend see opposite page.

band-fitting approach: the large number of free parameters and the assignment of component bands to specific secondary structures. A set of proteins with known structure is used as the calibration set which correlates the IR spectra with the secondary structures of the proteins. The large number of IR spectra of the calibration set of proteins is reduced to a few linearly independent basis spectra. The spectrum of a protein with unknown secondary structure can then be constructed from the basis spectra which reveals the secondary-structure content of that protein. This approach is similar to the decomposition of an arbitrary vector in 3D space into its components along the basis vectors in *x*-, *y*- and *z*-direction. For the method to be universally applicable, the calibration set should be diverse and large in order to cover as many different structures as possible. Since there are only a few structures of membrane proteins solved at present, it is difficult to assess the accuracy of the secondary-structure prediction of membrane proteins.

7.3 Prediction quality

There are several problems connected with the prediction of secondary structure by IR spectroscopy regardless of the particular method applied (Surewicz *et al.* 1993). As already discussed above, there is no unique spectrum for a given secondary structure, rather the spectrum also depends on structural details like helix bending or the number of adjacent strands in a β-sheet.

Another problem is the presence of side-chain absorption in the amide I region. It is estimated that 10–30% of the total absorption in that region derives from side-chains (Chirgadze

---

Fig. 12. A consistency check of fit models used for secondary-structure analysis. Fine-structure enhancement and two fits to the amide I band of a putative potassium channel (Ungar *et al* . 2001). (*a*) Amide I band of a putative potassium channel in ^2H_2O (full, grey line) and first fit (dotted line) with component bands (thin lines). The fit model was set up using the fine-structure enhanced spectrum shown in (*b*). Component bands were placed at the positions determined from the peaks in the fine-structure enhanced spectrum. The position of component bands was held fixed in the fit, while the intensity, bandwidth and line shape were allowed to vary. The resulting fit model exhibits two unusual features: (i) a very broad band at 1667 cm^{-1}, broader than expected for a typical secondary-structure element and (ii) the lack of a band near 1645 cm^{-1} characteristic of irregular structure. This fit model was checked by fine-structure enhancement of the fit [see (*b*)]. (*b*) Check of the first fit model: fine-structure enhancement of the measured absorbance spectrum (full, grey line) and of the first fit (dotted line) of (*a*). There are clear deviations between the two fine-structure enhanced spectra, showing that the first fit model does not represent the 'true' composition of the amide I band, although absorbance spectrum and fit superimpose very well in (*a*). Band narrowing of the fit is therefore a very sensitive check of the fit model. In this case the fit model needed improvement and the resulting improved fit is shown in (*c*). (*c*) Improved fit model: amide I band of a putative potassium channel in ^2H_2O [full, grey line, from (*a*)] and improved fit (dotted line) with component bands (thin lines). The fit model was improved in an iterative manual procedure, where component band position and line width were held fixed in the fit, the resulting fit model was then checked by fine-structure enhancement and, in the next step of the iteration, band positions and line widths adjusted to improve the agreement between the fine-structure enhanced fit and the fine-structure enhanced absorbance spectrum. Two new component bands had to be introduced, at 1627 and 1642 cm^{-1}. The consistency of the improved fit model was again checked by comparing the fine-structure enhanced spectrum and fit in (*d*). (*d*) Check of the improved fit model: fine-structure enhancement of the measured absorbance spectrum (full, grey line) and of the improved fit (dotted line) of (*c*). The fine-structure enhanced spectra of fit and spectrum superimpose very well, proving that the fit model is consistent with the experimental data. The choice of the fit model has a strong impact on the interpretation of the spectrum: the fit model in (*a*) contains no component band near 1645 cm^{-1} that is characteristic of irregular structures but a strong β-sheet band at 1635 cm^{-1}, the improved fit model shows a strong band at 1642 cm^{-1} assigned to irregular structures and considerably smaller β-sheet bands at 1619, 1627 and 1634 cm^{-1}.

et al. 1975; Venyaminov & Kalnin, 1990a; Rahmelow *et al.* 1998) and attempts have been made to subtract the side-chain contribution (Chirgadze *et al.* 1975; Venyaminov & Kalnin, 1990a; Rahmelow *et al.* 1998) using spectra of model compounds in aqueous solution. However, this may be problematic for side-chains not exposed to the surrounding water since the influence of the protein on the spectral parameters of these side-chain bands is unknown. Both methods are also based on the assumption that the integrated absorbance of the different types of structure are the same. However, evidence has been presented that this is not always so (De Jongh *et al.* 1996).

In spite of the potential shortcomings listed above, secondary-structure analysis by IR spectroscopy seems to work quite well in practice. According to the numbers given in the review by Goormaghtigh *et al.* (1994b) the average deviation of the prediction from the secondary-structure analysis of X-ray structures is in the range of 4–10%.

A comparison of the prediction quality of IR spectroscopy with the corresponding accuracy of electronic CD and vibrational CD using the same set of proteins revealed that the three methods give similar results (Baumruk *et al.* 1996). However, there seems to be a tendency that IR spectroscopy is weaker in the prediction of α-helical structure but superior in the estimation of the β-sheet content of proteins (Sarver & Krueger, 1991; Pribic *et al.* 1993). The prediction accuracy can be enhanced by combining electronic CD with IR spectroscopy (Sarver & Krueger, 1991; Pribic *et al.* 1993; Baumruk *et al.* 1996) and by analysing IR data measured at 6 different $^1H_2O/^2H_2O$ ratios (Baello *et al.* 2000).

When the quality of secondary-structure determination of different methods is compared, it is important to realize that the results of the various methods are judged in relation to secondary-structure assignments to X-ray structures of proteins. However, if the same X-ray data are analysed by different assignment criteria, a considerable variation of the secondary-structure content is often observed. Unfortunately, not only the application of different methods with different criteria but also the use of the same method by different authors can lead to a distinct variation of the results. For example, the analysis of myoglobin yielded between 77% (Dousseau & Pezolet, 1990) and 88% (Lee *et al.* 1990) α-helix, although the same method (Levitt & Greer, 1977) was applied.

8. Protein stability

8.1 Thermal stability

An unfolded protein with a random backbone structure exhibits a broad amide I band centred at approximately 1654 cm^{-1} (in ^1H_2O, room temperature) or 1645 cm^{-1} (in ^2H_2O, room temperature). The amide I band of an aggregated protein is dominated by a large component at 1620 to 1615 cm^{-1} (Jackson & Mantsch, 1991) and a minor component at the high-frequency edge of the amide I region due to the formation of intermolecular β-sheets. Thus, the amide I band of unfolded or aggregated proteins can be distinguished easily from the amide I band of a native protein. Therefore, IR spectroscopy is well suited for protein-stability studies.

Folding and unfolding of proteins can be initiated in various ways: chemically, thermally, and by changing the pressure. Unfortunately, IR spectroscopy of proteins treated with the denaturants urea or guanidinium hydrochloride is hampered by the overlap of their absorption bands with the amide I band of proteins. This overlap can largely be avoided by using [^{13}C]urea (Fabian & Mantsch, 1995).

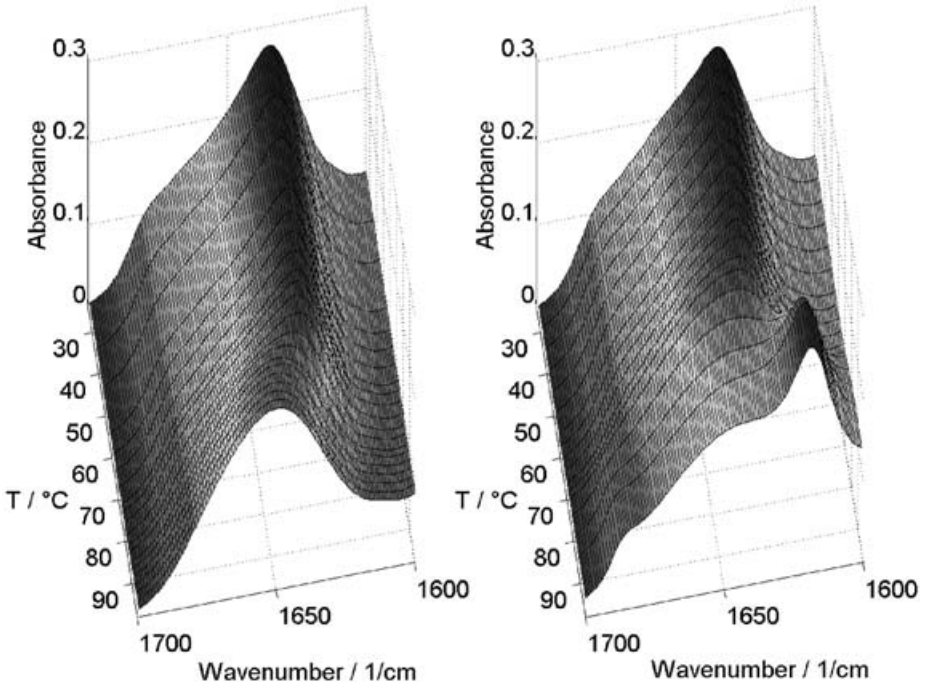

Fig. 13. Temperature-dependent IR spectra of the α-amylase inhibitor tendamistat, a small β-sheet protein. With a midpoint temperature of 82 °C, the wild-type protein unfolds and adopts an irregular structure. This leads to a broad amide I band centred at 1650 cm^{-1} (left). Mutation of the three Pro residues to Ala does not significantly alter the amide I band at room temperature (right). However, heating the Pro-free protein results in a downshift of the amide I maximum indicating aggregation of the sample. Moreover, the transition is already observed at 67 °C (C. Zscherp, H. Aygün, J. W. Engels & W. Mäntele, unpublished observations).

In contrast, recording temperature-dependent IR spectra is straightforward. Although small linear shifts of amide I bands can be observed upon a change in temperature, a transition between the native state of the protein and the unfolded or aggregated state induces much greater changes in the IR spectrum of a protein. As an example, the temperature-dependent IR absorbance in the amide I region of the small all-β-sheet protein tendamistat is shown in Fig. 13. The midpoint unfolding temperature is 82 °C for the wild type. In the case of a mutant protein where all three Pro residues have been exchanged for Ala residues, the transition temperature is strongly reduced. In addition, for the wild-type protein temperature-induced unfolding is reversible, whereas the Pro-free tendamistat aggregates irreversibly upon heating. It is recommended to perform the experiments in ^2H_2O solution since the strong band of the ^1H_2O bending vibration is temperature dependent also (Venyaminov & Prendergast, 1997, and references therein). The temperature dependency of the amide I bandwidth, of the wavenumber of maximum absorption, or of the absorbance at appropriate wavenumbers can be used for determination of the transition temperature. In some cases, the shift of the strong and sharp band of the Tyr aromatic ring-stretching vibration at approximately 1515 cm^{-1} can be analysed (Fabian *et al.* 1993, 1994). Whereas the amide I band is related to the secondary structure of the protein, the Tyr band shifts due to altered hydrogen bonding or changes in π–π interaction and thus indicates alterations of the local environment of the Tyr side-chains. In this way, changes

of the secondary structure and local conformational changes as a consequence of unfolding or aggregation can be probed simultaneously. In addition to the transition temperature, the van't Hoff enthalpy for the transition can be derived from the temperature-dependent IR data provided that a two-state transition between the folded and the unfolded state can be assumed (Fabian *et al.* 1993, 1994). IR spectroscopy is not restricted to equilibrium studies. Laser-induced temperature jump experiments with ps or μs time-resolution (Dyer *et al.* 1998) as well as stopped-flow studies with denaturant or temperature-induced protein unfolding have been reported (Backmann *et al.* 1995; Reinstädler *et al.* 1996).

Unfortunately, many proteins aggregate upon thermally induced unfolding. Therefore, it is a clear advantage of IR spectroscopy in comparison with CD or fluorescence that aggregation can be recognized easily. On the other hand, the relatively high protein concentrations needed for IR experiments may promote aggregation.

8.2 $^{1}H/^{2}H$ exchange

Another way of probing the stability and flexibility of proteins is to follow hydrogen to deuterium exchange (Englander & Kallenbach, 1984; Raschke & Marqusee, 1998; Goormaghtigh *et al.* 1999). Amide and side-chain hydrogen exchange rates depend on pH, temperature, and protein environment. Groups exposed to the solvent exchange fastest. The hydrogens of a structured region of a protein exchange more slowly compared to the hydrogens of an unstructured part. This is due to hydrogen bonding, low solvent accessibility, and steric blocking. A protected amide hydrogen can be regarded as 'closed' to exchange. A transition to an 'open' state is required to enable exchange with the solvent at the pH-dependent intrinsic rate for an unstructured peptide, k_{in}. With k_{op} and k_{cl} being the rates for the opening and closing reactions, respectively, this leads to the following scheme (Raschke & Marqusee, 1998):

$$\text{close} \underset{k_{cl}}{\overset{k_{op}}{\rightleftharpoons}} \text{open} \xrightarrow{k_{in}} \text{exchanged}.$$

In this model there are two limiting cases called EX1 ($k_{in} \gg k_{cl}$) and EX2 ($k_{in} \ll k_{cl}$) which can be adopted by a given system depending on the experimental conditions. In the EX1 case, the observed exchange rate k_{obs} equals k_{op}. Under EX2 conditions, k_{obs} is proportional to k_{in} and to the fraction of time the segment is open k_{op}/k_{cl} ($k_{obs} = k_{in}k_{op}/k_{cl} = k_{in}K_{op}$, with K_{op} the opening equilibrium constant). Therefore, the experimental conditions determine whether the observed exchange rate reports on the kinetics or on the thermodynamics of the opening reaction.

There are two possibilities of how the time-course of the isotope exchange can be followed. Either lyophilized protein dissolved in $^{2}H_2O$ can be observed in transmission experiments, or attenuated total reflection (ATR) techniques can be used. In the latter case a thin protein film is deposited on an internal reflection element. After moderately drying the protein film, $^{2}H_2O$-saturated nitrogen is flushed into a chamber surrounding the internal reflection element with the protein film. The two methods reveal comparable results, provided that approximately 0·5 g water per g protein is present in the ATR experiments (Goormaghtigh *et al.* 1999). It is important to control temperature and pH because both parameters influence the exchange rate. The $^{1}H/^{2}H$ exchange can be followed using the amide II band of proteins, a mode that couples NH bending and CN stretching contributions. After $^{1}H/^{2}H$ exchange the N–^{2}H in-plane bending mode no longer couples with the CN stretching vibration resulting in an amide II′ mode which

is largely a CN stretching vibration. This mode has an approximately 100 cm^{-1} lower frequency compared to the amide II mode. Due to the large downshift, the two bands are clearly separated in the spectrum. Determination of the amide II′ area is hampered by overlap with the $^1H^2HO$ mode and is therefore not used to determine the fraction of exchanged amide groups. Instead the amide II band area is monitored. However, some side-chain vibrations contribute to the absorption in the spectral region of the amide II band, making it difficult to determine the amide II area before, during and after the exchange. In the case of a protein which unfolds reversibly, the spectrum of the fully exchanged protein can be measured after short incubation of the sample at a temperature close to the transition temperature of the protein. However, in the general case this treatment will not lead to refolding to the native structure when the temperature is lowered and, therefore, is not universally applicable. The exchange at room temperature may take a very long time: even after months it is unclear whether all buried hydrogens have been exchanged or not. Therefore, the suggestion has been made to correct for the contributions of the side-chains as a function of the deuteration level (Goormaghtigh *et al.* 1996). For this purpose, spectra of the side-chains alone in ^1H_2O (Venyaminov & Kalnin, 1990a) and ^2H_2O (Chirgadeze *et al.* 1975) can be used. The fraction of deuterated side-chains can be estimated from the intensity decay at 1673 cm^{-1}, which monitors mainly Arg and Asn deuteration (Goormaghtigh *et al.* 1996), or from the depletion of the ^1H_2O band at 3408 cm^{-1} (De Jongh *et al.* 1997b). The first approach assumes that all side-chains exchange at the same rate. The second approach for the ATR technique assumes that the remaining fraction of unexchanged side-chains rapidly adjusts to the decreasing ^1H_2O content in the protein film. The result from these ATR experiments is that hydrogens of side-chains exchange rapidly, for example, completely within 2 min in the case of lysozyme (Goormaghtigh *et al.* 1996). This is faster than the time-resolution of a transmission experiment. Correction of protein spectra for side-chain contributions is only an approximation for some buried residues since the different environments of the side-chains in proteins may significantly alter the absorption spectra of the side-chains in respect to water. This problem is concerned with the determination of the amount of exchange only. The determination of the exchange kinetics is not disturbed.

A disadvantage of IR spectroscopy compared to the nuclear magnetic resonance (NMR) technique is that site-specific information is not available. However, it has been demonstrated recently that a detailed and careful analysis of the absorbance changes of the amide I band caused by $^1H/^2H$ exchange allows the assignment of exchange rates to different types of secondary structure (De Jongh *et al.* 1997a, b). In contrast to NMR experiments, the IR studies require relatively small amounts of protein and can be applied to membrane proteins in a lipid environment.

$^1H/^2H$ exchange experiments can be used to compare the flexibility of different proteins. For example, a mesophilic and a thermophilic α-amylase have been examined with the unexpected result that the thermophilic protein is more flexible (Fitter & Heberle, 2000). Several membrane proteins have been investigated. The amount of exchangeable amide protons can vary with a broad range. For bacteriorhodopsin, less than 30% of the amides exchange upon a 2-day exposure to ^2H_2O (Earnest *et al.* 1990), whereas 45% of the protons exchange within 3 h in the case of *Streptomyces lividans* K^+ channel, and approximately 90% of the amide protons of lactose permease within 3 h (le Coutre *et al.* 1998). In the same way, the flexibility of a given protein can be investigated using different solvent conditions. By this means, the effect of ligands or membranes on the protein structure can be determined (Muga *et al.* 1991; Scheirlinckx *et al.* 2001).

9. Molecular reaction mechanisms of proteins

9.1 Reaction-induced IR difference spectroscopy

Elucidating the molecular mechanism of proteins is a major challenge for the life-science community. IR spectroscopy continues to provide important contributions in this field and combines several of its advantages in these studies: high time resolution (<1 μs), universal applicability from small soluble proteins to large membrane proteins and the high molecular information content combined with a sensitivity high enough to detect a change in the environment around a single atom of a large protein.

In favourable cases, effects of a protein reaction on the IR spectrum can already be observed in the absorbance spectrum (Trewhalla *et al.* 1989; Jackson *et al.* 1991; Nara *et al.* 1994; Fabian *et al.* 1996b). In other cases, the associated IR absorbance changes have to be monitored; or in other words: the associated IR difference spectrum has to be recorded. This has been done by carefully subtracting the spectrum of a sample where the protein is in state B from a spectrum where it is in state A (Alben & Caughey, 1968; Riepe & Wang, 1968; Belasco & Knowles, 1980; Tonge *et al.* 1989, 1991; Trewhalla *et al.* 1989). However, the absorbance changes usually observed for protein reactions are very small, in the order of 0·1% of the maximum absorbance. In consequence, the approach described above does not generally allow the sensitive detection of the small absorbance changes between the two protein states. Instead, the protein reaction of interest has to be initiated directly in the cuvette. Figure 14 illustrates how a typical reaction-induced difference spectrum is created. The protein is prepared in the stable state A and the absorbance of this state is measured. Then the reaction is triggered, the protein proceeds to state B and again the absorbance is recorded. State B may also be a sequence of transient states. In that case the interconversion between the product states B_1, B_2, etc. can be followed by time-resolved methods (Siebert *et al.* 1980; Mäntele *et al.* 1982; reviewed by Siebert, 1995; Mäntele, 1996; Slayton & Anfinrud, 1997).

From the spectrum recorded before the start of the reaction (state A) and the spectra recorded during and after the reaction (state B) difference spectra are calculated. They only originate from those molecular groups that are affected by the reaction. All 'passive' groups are invisible in the difference spectrum which, therefore, exhibits details of the reaction mechanism on the molecular level despite a large background absorption. As indicated in the idealized difference spectrum in Fig. 14, negative bands in difference spectra are characteristic of the initial state A, while positive bands reflect state B during or after the reaction.

The reaction between the two protein states can be induced by methods like stopped and continuous flow, ATR with buffer exchange, photolytic release of effector substances from caged compounds, light-induced difference spectroscopy, temperature and pressure jump, equilibrium electrochemistry, and photoreduction. This enables investigation of molecule–protein interactions, light-induced reactions, protein folding, and redox reactions. A description of these methods, examples of applications, and a discussion of the advantages and drawbacks can be found in recent reviews (Mäntele, 1993b, 1996; Gerwert, 1993, 1999; Siebert, 1995; Heberle, 1999; Jung, 2000; Vogel & Siebert, 2000; Wharton, 2000; Kim & Barry, 2001; Zscherp & Barth, 2001). There are a number of reviews focusing on Raman spectroscopy of enzyme reactions of ligand–protein interactions (Callender & Deng, 1994; Carey & Tonge, 1995; Carey, 1998, 1999; Deng & Callender, 1999, 2001) that are well worth reading, also for the IR spectroscopist. As these reviews excellently cover the field, we do not attempt here to give an overview of IR difference spectroscopy. Instead we focus on general aspects of spectra

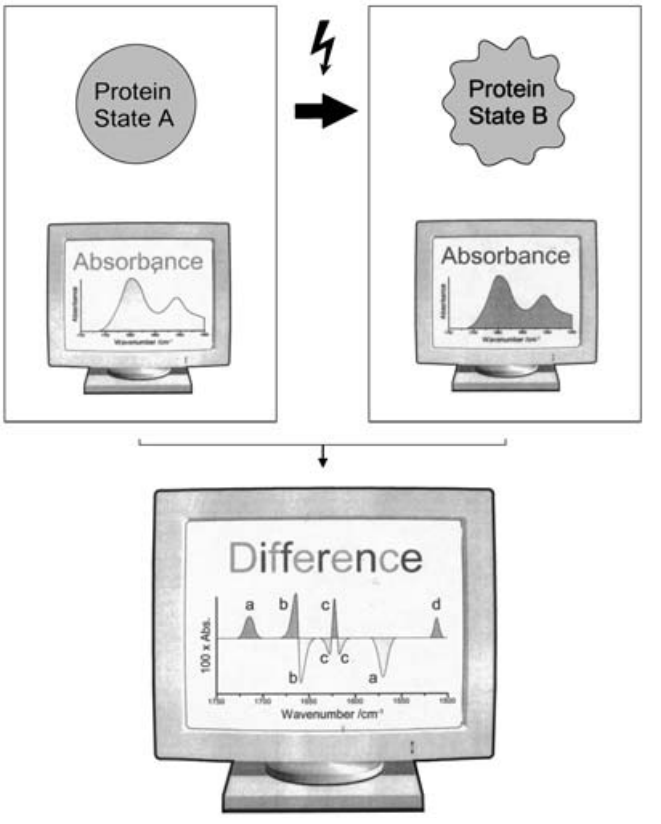

Fig. 14. Principle of reaction-induced IR difference spectroscopy. The protein is prepared in state A and the IR absorbance of this state is characterized. Then the reaction from state A to state B is triggered in the IR cuvette and the absorbance of state B measured. From the two absorbance spectra, a difference spectrum is calculated which shows the absorbance changes due to the reaction. Negative bands are characteristic of the initial state A (in light grey) and positive bands of the final state B (in dark grey). Several causes for absorbance changes are discussed in the text.

interpretation and on interpretation tools. The work cited is merely to illustrate some selected examples.

9.2 The origin of difference bands

Difference bands arise from several sources and four examples are given in Fig. 14. Chemical reactions transform molecular groups from the educt group to the product group which usually have different IR absorbance spectra. An example is the protonation of an Asp or Glu residue. In the difference spectrum of the reaction, the absorbance of the disappearing educt group shows as negative bands, while the absorbance of the product group gives rise to positive bands. The bands of the appearing and disappearing groups may be widely separated in the spectrum. In Fig. 14 this is illustrated with the two difference bands marked 'a' for the protonation of a carboxylate group. The negative band marked 'a' in Fig. 14 is due to the antisymmetric stretching vibration of the COO^- group that disappears in the course of the reaction and the positive band marked 'a' is due to the stretching vibration of the C═O bond of the

appearing COOH group (an additional band due to the symmetric stretching vibration of the COO^- group is located near 1400 cm^{-1}, but not shown in Fig. 14).

Alternatively, a vibration may experience a shift in frequency, due to a conformational or environmental change that alters the electron density of the vibrating bonds or the coupling with other vibrations. This band shift leads to a pair of signals, composed of a negative and a positive band which are close together. An example is shown in Fig. 14 for the two bands marked 'b' in the amide I region of polypeptide backbone absorption. Here, the amide I vibration absorbs at lower wavenumber (i.e. has lower vibrational frequency) in the initial state A than in the product state B. In the case of the amide I vibration of proteins, band shifts can be ascribed to an altered coupling with neighbouring amide oscillators due to a change in backbone structure or to a different degree of hydrogen bonding which changes the electron density in the C═O bond.

A difference band with side lobes of opposite sign is produced when the width of a band changes in the reaction from state A to B. If a decrease in bandwidth is considered, the intensity will decrease on the sides of the band but will increase at the centre (if the extinction coefficient remains constant) leading to a positive band with negative side lobes. This case is shown in Fig. 14 for the bands marked 'c'. As the bandwidth is a measure of conformational flexibility, the decrease of bandwidth shown indicates a more rigid structure in the product state B.

Only one band is observed when the reaction results in a change of the extinction coefficient of a vibrational mode, for example because of a polarity change of the vibrating bond(s). A minimum (or maximum) in the difference spectrum then indicates a reduced (or increased) absorption of the product state B compared to the initial state A. This case is illustrated with the band marked 'd' at a spectral position that is characteristic of Tyr absorption. In the case shown, the increased extinction coefficient of Tyr in state B may be due to an environmental change that leads to an increased polarity in the Tyr ring.

9.3 The difference spectrum seen as a fingerprint of conformational change

Although a difference spectrum contains a wealth of relevant information on the catalytic mechanism of proteins, it is often difficult to make use of it. This is because an assignment of the difference bands to individual molecular groups is not straightforward and requires additional experiments. However, a very simple but nevertheless powerful approach is to regard the spectra as a characteristic fingerprint of the conformational change without attempting a molecular interpretation at that stage. The signature of a conformational change in the spectrum can then be used to detect and define transient conformational states of a protein. Similar approaches have a long history in fluorescence and absorption spectroscopy. IR spectroscopy has the advantage that it looks in a single experiment at backbone conformation and hydrogen bonding, at side-chain structure and environment and at ligand or cofactor interactions.

The underlying idea may be illustrated with a visit to a modern arts museum as shown in Fig. 15. Often the art lover is puzzled by the meaning of a specific painting. However, even the uneducated spectator is able to draw some very simple conclusions. It is obvious in Fig. 15 that two of the three paintings have a similar size, whereas the third is considerably smaller. In addition, two of the paintings are similar in style, whereas the third is not. If the observer is very patient, then he may observe that some of the paintings are removed and exchanged for

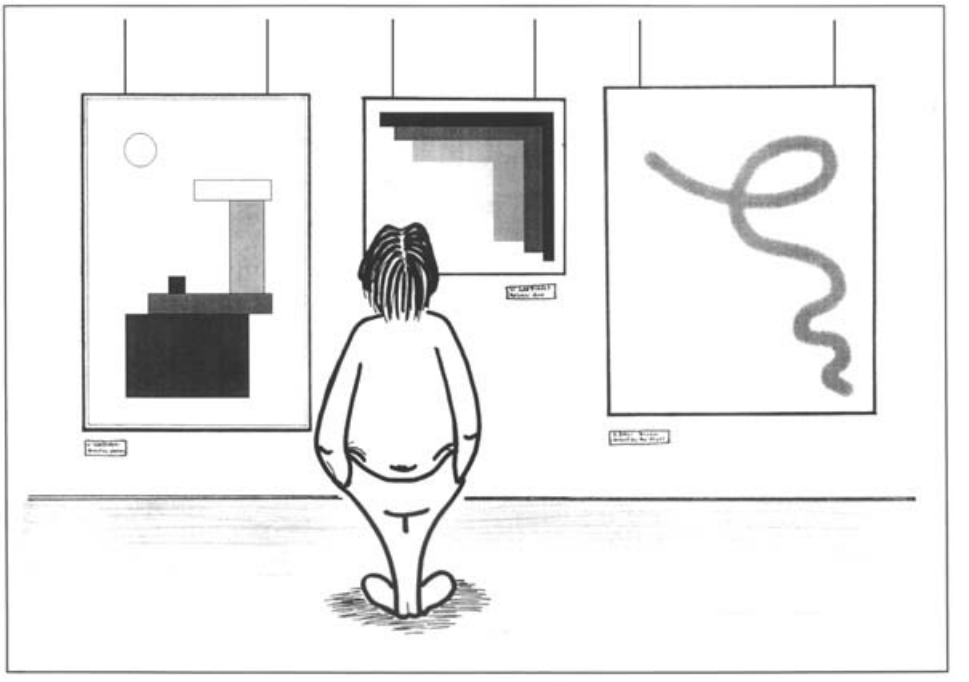

Fig. 15. The art of spectra interpretation. Without arts background the three paintings may be analysed according to their size, style and the time at which they are exchanged for other paintings. These simple comparisons can be also applied to the interpretation of IR difference spectra when they are regarded as a characteristic fingerprint of the conformational change of a protein.

others. Translated into our problem of interpreting difference spectra this means that the difference signals can be analysed according to their magnitude, shape, and time-course.

Intermediates. From the time-course it is possible to evaluate the number of intermediates in the reaction. Here, time-resolved vibrational spectroscopy has the advantage that the observation is not restricted to a limited number of chromophores (i.e. Trp residues) or to an extrinsic fluorescence label which will largely reflect local changes in the vicinity of the chromophore(s) and may miss conformational changes occurring in distant regions of the protein. Instead, in vibrational spectroscopy all carbonyl 'chromophores' of the backbone amide groups are monitored, and this will reveal any change in backbone conformation even if very small. In the same experiment it is possible to additionally follow the fate of individual catalytically active groups. Thus, IR spectroscopy simultaneously looks, on the one hand locally at the catalytic site, and on the other at the protein as a whole.

This property has, for example, been exploited in studies of the Ca^{2+}-ATPase pump mechanism (Barth *et al.* 1996) where one of the postulated intermediates in the reaction cycle was sought for but not detected. It was therefore concluded that it is either short-lived or does not exist. For Ca^{2+}-ATPase it was found that the overall backbone conformational changes proceed at the same time as the local perturbations of side-chains (Barth *et al.* 1996). Similarly, synchronized absorbance changes of protein backbone, side-chains, and chromophore were found for bacteriorhodopsin (Gerwert *et al.* 1990b) and the photoactive yellow protein (Brudler *et al.* 2001), a blue-light receptor from purple bacteria. IR spectroscopy detected here two new intermediates in the photocycle. In contrast to the above examples, backbone and side-chain

signals proceed with different rates in the complex refolding of ribonuclease T1 (Reinstädler *et al.* 1999); the very late events due to the *trans*→*cis* isomerization of a prolyl peptide bond lead to an increased compactness of the protein structure but not to an environmental change of Asp, Glu and Tyr residues. Thus, they have adopted their native environment already in the preceding processes.

The latter example illustrates that IR spectroscopy is particularly valuable in protein-folding studies for the detection and characterization of folding intermediates. Other examples are the pH-induced refolding of α-lactalbumin, where an intermediate with non-native β-sheet structure was identified (Troullier *et al.* 2000). For α-lactoglobulin a compact β-sheet intermediate with a life-time of 7 ms was detected for the β-sheet to α-helix transition induced by the addition of trifluoroethanol (Kauffmann *et al.* 2001). As a final example, time-resolved IR spectroscopy with ns time resolution was essential to obtain a detailed picture of the folding of apomyoglobulin involving two intermediates in the folding process (reviewed by Dyer *et al.* 1998).

Similar conformational changes. From the shape of the spectra, conformational changes can be classified according to their similarity. This can be used to compare different preparations of a protein or related partial reactions. For example, it has been shown that the subunits III and IV of cytochrome *c* oxidase do not participate in electron and proton transfer, since the spectra obtained with the essential subunits I and II are virtually identical to those obtained with four subunits (Hellwig *et al.* 1998). Similarly, a comparison between monomeric and trimeric photosystem I has revealed that protein–protein interaction has little impact on the conformational changes associated with oxidation of the primary electron donor P700 (Hamacher *et al.* 1996).

Related partial reactions have been compared for Ca^{2+}-ATPase. Difference spectra of the two Ca^{2+}-release reactions from the phosphorylated and the unphosphorylated enzyme show a striking similarity (Barth *et al.* 1997) (see Fig. 16), and very similar conformational changes are inferred from this observation. Since difference spectra of a reaction contain information on the initial and the final state, the observed similarity suggests that the occupied and unoccupied Ca^{2+}-binding sites are most likely the same in the two reactions. Thus, a model with only one pair of binding sites for Ca^{2+} is favoured from the IR spectra.

For the nicotinic acetylcholine receptor it was found that the two agonists acetylcholine and carbamylcholine induce similar conformational changes (Baenziger *et al.* 1993). Interestingly, they resemble those of bleaching the photoreceptor rhodopsin, which indicates that the structural changes in both receptors are related.

The extent of conformational change. From the magnitude of the difference signals, the extent of conformational change in a protein reaction may be estimated using the amide I region of the spectrum. As already mentioned, the amide I mode of the polypeptide backbone is predominantly a C═O vibration and absorbs in the region from 1700 to 1610 cm^{-1}. The peak position of the amide I mode of a peptide group depends upon the secondary structure into which it is inserted due to TDC. On this basis, the amplitude of the IR difference signals in the amide I region can be used to estimate the change of the secondary structure.

Proceeding along this line, one has to consider the following:

(1) Signals of conformational changes may overlap in such a way that they cancel each other leading to an underestimation of the extent of structural change. Therefore, the IR difference spectrum reveals only the *net* change of secondary structure. A worst-case scenario is

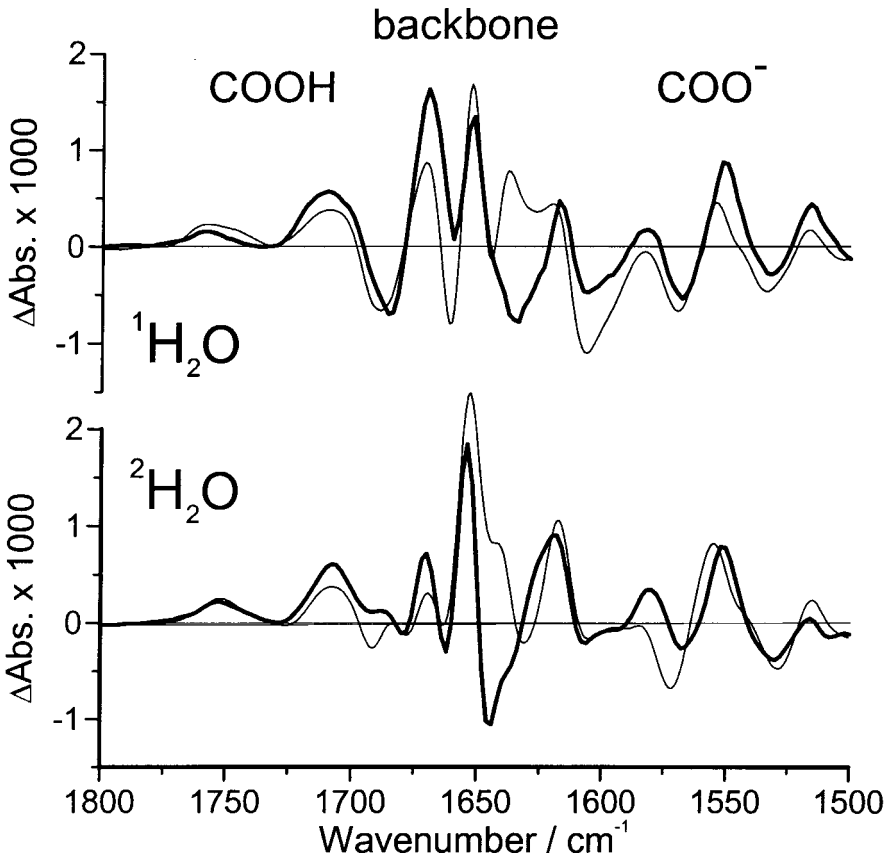

Fig. 16. Similar conformational changes in the reaction cycle of Ca^{2+}-ATPase detected by IR spectroscopy (Barth *et al.* 1997). Shown are the difference spectra of the two Ca^{2+}-release reactions from the phosphorylated (thin lines) and the unphosphorylated ATPase (bold lines) in ^1H_2O (top panel) and ^2H_2O (bottom panel). Positive bands are characteristic of the Ca^{2+}-free states, negative bands of the Ca^{2+}-loaded states. The spectral range shown provides information on structural changes of the protein backbone in the amide I region (1700 to 1610 cm^{-1}), on the Ca^{2+} chelation mode of carboxylate groups (near 1550 cm^{-1}) and on the protonation state and strength of hydrogen bonding of protonated carboxyl groups (1700–1760 cm^{-1}). It is known that Ca^{2+} release leads to the protonation of some of the former Ca^{2+} ligands. The similarity of the spectra indicates similar binding sites on the phosphorylated and the unphosphorylated ATPase, in particular similar elements of backbone conformation, a similar Ca^{2+}-binding mode and a similar protonation state and hydrogen bonding of at least two carboxyl groups – most likely Ca^{2+} ligands – that become protonated when Ca^{2+} leaves. The simplest conclusion from this agreement is that the pair of binding sites on the phosphorylated ATPase is the same as that on the unphosphorylated ATPase.

shown in Fig. 17*a*, where nearly all residues change their secondary structure, but the net change is zero.

(2) Movements of rigid domains are not visible, only the working portion that changes its backbone geometry is represented in the difference spectra. Thus, it may be misleading to use terms such as 'large' and 'small' conformational change since considerable movements of rigid domains may originate from very small flexible parts of a protein like hinge regions that comprise only a few residues. An example is shown in Fig. 17*b*. Movement of the rigid domains (shown in grey) does not lead to signals in the IR difference spectrum. Only the

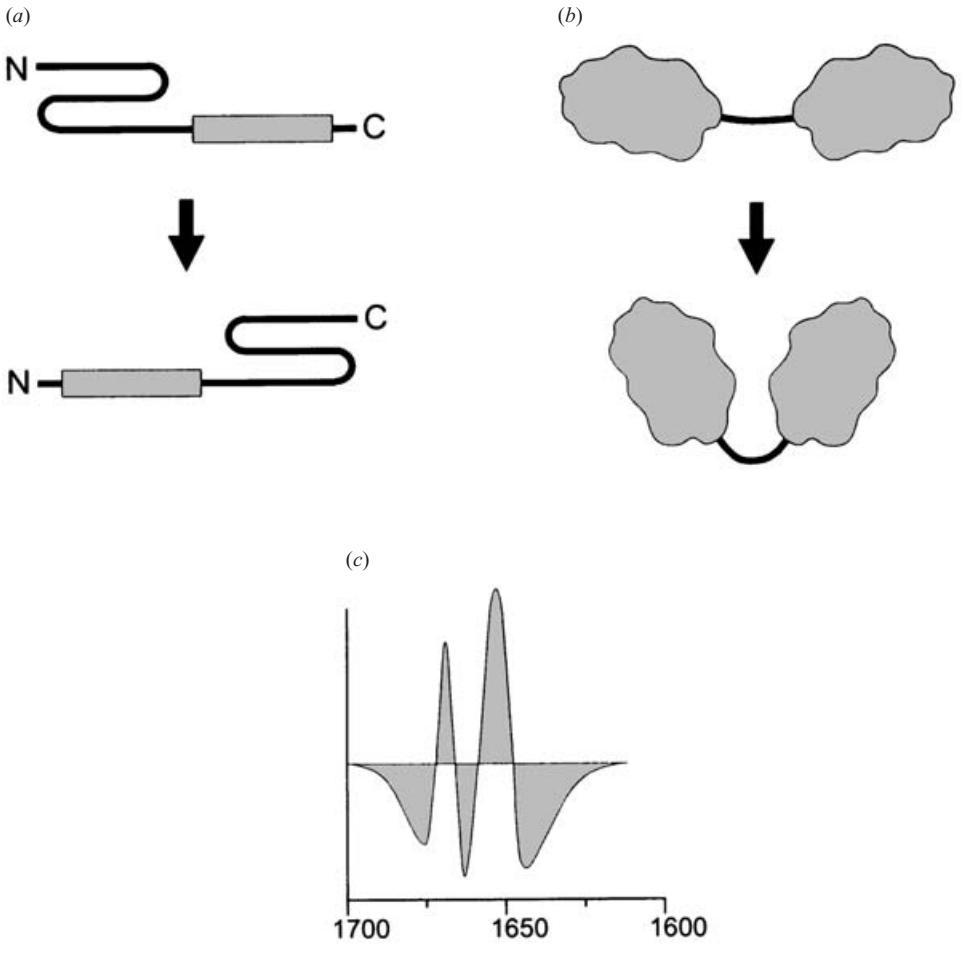

Fig. 17. Quantifying the extent of conformational change with IR difference spectroscopy. (*a*) Worst-case scenario: the protein undergoes a large conformational change, but the net change of secondary structure is zero since the N-terminal β-sheet converts into an α-helix and the C-terminal α-helix into a β-sheet. IR difference spectroscopy would not detect that conformational change – only the net change is detected. (*b*) Rigid domains are invisible for IR difference spectroscopy. When they move relative to each other, only the working part of the protein that causes the movement (shown in black) shows up in the spectrum. A large change in shape of a protein may, therefore, be accompanied only by small IR absorbance changes. (*c*) Calculation of the COBSI index. The index relates the absorbance changes in the amide I region to the total absorbance. Shown here are the absorbance changes. The integral of the absolute value of the absorbance changes is used in the calculation, i.e. the sum of the shaded areas.

flexible part (shown in black), where the conformational change alters the relative orientation of neighbouring amide groups, gives rise to IR difference signals.

(3) Since TDC leads to delocalized amide I modes, a simple linear relationship between signal magnitude and secondary-structure change is not expected when individual residues change their secondary structure. The sensitivity towards conformational changes, however, seems to be very high. For example, if an α-helix shortens, this affects not only the amide modes of the backbone portion that unwinds, but also those of the remaining helix (Nevskaya & Chirgadze, 1976).

(4) In addition to a secondary-structure change, more subtle changes such as changes of hydrogen bonding to the C═O oxygen within a persisting secondary structure will also be manifest in the spectrum.
(5) Signals due to amino-acid side-chains may overlap although the amide I mode has a strong extinction coefficient (Chirgadze *et al.* 1973; Venyaminov & Kalnin, 1990b) which is generally larger than that of amino-acid side-chains in the amide I region (Chirgadze *et al.* 1975; Venyaminov & Kalnin, 1990a).

Usually, signals of protein backbone perturbations are found to be rather small, as shown for ligand binding to creatine kinase (Raimbault *et al.* 1996), annexin VI (Bandorowicz-Pikula *et al.* 1999), and GroEL (Von Germar *et al.* 1999); partial reactions of P-type ATPases (Chetverin *et al.* 1980; Arrondo *et al.* 1987; Goormaghtigh *et al.* 1994d; Barth *et al.* 1996; Troullier *et al.* 1996; Scheirlinckx *et al.* 2001; Vander Stricht *et al.* 2001); and the electron transfer reactions of the photosynthetic reaction centre (Mäntele, 1993a, 1996), cytochrome *c* oxidase (Hellwig *et al.* 1996), cytochrome *c* (Moss *et al.* 1990; Schlereth & Mäntele, 1993), bacterial cytochrome c_3 (Schlereth *et al.* 1993), cytochrome bc_1 (Baymann *et al.* 1999) and myoglobin (Schlereth & Mäntele, 1992). This indicates that in many cases the protein provides an 'optimized solvent' (Mäntele, 1996) rather than acting via a considerable reorganisation of secondary structure.

In order to quantify the structural changes of the protein backbone from the difference signals, several strategies have been employed based on amplitude and band area of the difference spectra (Barth *et al.* 1996; Troullier *et al.* 1996; Chittock *et al.* 1999; Scheirlinckx *et al.* 2001). One approach that takes into account spectral overlap between the structures before and after the protein reaction uses the *change of backbone structure and interaction* (COBSI) index (Barth *et al.* 1996). The COBSI index is calculated from a difference spectrum of a protein reaction using the amide I region from 1700 to 1610 cm^{-1} according to the following formula:

$$\text{COBSI index} = \frac{\int_{1610}^{1700} \frac{1}{2}|\Delta\text{Abs}|\, d\tilde{\nu}}{\int_{1610}^{1700} \text{Abs}\, d\tilde{\nu}}.$$

The COBSI index relates the integrated absorbance change $|\Delta\text{Abs}|$ (see Fig. 17*c*) to the integrated total protein absorbance. The COBSI index is 1 if the total absorbance in the amide I region of a protein is shifted strongly in going from state A to state B so that there is no overlap between the absorbance spectra of states A and B. If 20% of the backbone C═O groups in a protein experience such a shift in absorbance, the COBSI index will be 0·2. However, in most cases there will be significant overlap of the absorption spectra of the two states, the overlap being most pronounced, for example, for subtle changes of hydrogen bonding and being less for a change in secondary structure. Therefore, in order to calibrate COBSI indices with changes of structure, COBSI indices for 100% secondary-structure changes were calculated from absorbance spectra in the literature (Barth *et al.* 1996). COBSI indices for 100% secondary-structure changes, for example from an ordered to an irregular structure are typically in the range 0·2–0·6, indicating that 20–60% of the integrated absorbance is redistributed upon such a transition. As expected, a lower value of 0·09 is obtained when antiparallel and parallel β-sheets are compared because the backbone is in an extended conformation in both cases and the main band absorbs at a similar spectral position for both conformations.

Taking the Ca^{2+}-ATPase as an example (Barth *et al.* 1996), the small COBSI indices of its partial reactions (in the order of 0·001) suggest that only a few flexible residues form the working part of the enzyme whereas most other residues belong to rigid structures. Only 1% of all peptide groups (corresponding to 10 residues) are seen by IR spectroscopy to be involved in a net change of secondary structure which is surprising since the protein couples events at sites that are separated by 50 Å. A comparison of two Ca^{2+}-ATPase structures (Toyoshima *et al.* 2000; Toyoshima & Nomura, 2002) shows that much of the conformational change can be explained by rigid domain movements, kinking of helices or movements of helices relative to others. However, it is clear that this results in a considerable change of protein conformation and shape. If the secondary structure of the two states is analysed by the method of Kabsch & Sander (1983), there is a net gain of 10 residues in coil structure, of 7 in helical structures and a net loss of 17 residues in β-sheet and β-bridge structure on going from the Ca_2E_1 state to the E_2 state of the ATPase. The net change of secondary structure therefore corresponds to 17 residues being involved. Nevertheless, the total number of residues that experience a secondary-structure change is 121 and this large number is not revealed in the IR spectra because opposing changes in different regions of the protein largely compensate in the spectra. The spectra therefore reflect only the *net* change of secondary structure. The number of 17 residues involved in the net secondary-structure change is still larger than expected from the IR results and one explanation might be that the secondary-structure assignment algorithm by Kabsch & Sander (1983) is based on hydrogen-bonding pattern, whereas the frequencies of amide I vibrations are determined by backbone geometry. Also the two crystal structures might not represent the average structures for the two states in solution since crystal contacts and the use of the inhibitor thapsigargin lock the ATPase in one defined conformation for each state whereas an ensemble of structures will be adopted in solution (Toyoshima & Nomura, 2002).

9.4 Molecular interpretation: strategies of band assignment

IR difference spectra usually contain many different bands which indicate the wealth of information that is encoded in the spectrum. However, to extract this information is often difficult and ideally requires the assignment of the difference signals to individual molecular groups of the protein. Assignment of IR bands to specific chemical bonds is possible by studying model compounds, by chemical modifications of cofactors or ligands, by site-directed mutagenesis and by isotopic labelling of ligands, cofactors and amino acids. We will first discuss these interpretation tools and finally show how they can be used in combination to study the proton-pump mechanism of bacteriorhodopsin.

Model spectra contributions of cofactors or substrate molecules to the IR spectrum can be identified by normal mode calculations or by comparison with the spectra of the isolated molecules or model compounds in an appropriate environment. An example is chlorophyll studies (reviewed by Katz *et al.* 1966, 1978; Lutz & Mäntele, 1991). Resonance Raman spectra are helpful for the assignment of chromophore bands. Yet, the intensities of the bands can be very different from those of IR bands, since the Raman effect depends on a change in polarizability whereas IR absorption depends on the change of the dipole moment of the vibration.

Site-directed mutagenesis is a very powerful approach. Ideally, an IR signal due to a specific amino acid is missing when this amino acid has been selectively replaced. However, mutagenesis may not be applicable in all cases since substitution of critical amino acids usually results in serious perturbation of protein function. In addition, a mutation may lead to more severe

conformational effects than just the replacement of one amino-acid side-chain by another and therefore may result in complicated alterations to the spectrum. For this reason, the spectra of mutant proteins have to be evaluated very carefully.

Isotopic labelling avoids the introduction of perturbations into the protein which may be reflected in the IR spectra. Because of the mass effect (see Section 2.1) on the vibrational frequencies, labelling introduces band shifts in the IR spectra which help identify the absorption of the labelled groups. Ligands, cofactors and protein side-chains as well as backbone groups can be labelled.

Labelling ligands is very powerful when the interaction between ligands and proteins is investigated (Alben & Caughey, 1968; Belasco & Knowles, 1980; Potter *et al.* 1987). This is very well illustrated by a number of studies on GTP and GDP binding to the regulatory protein Ras (Cepus *et al.* 1998; Du *et al.* 2000; Allin & Gerwert, 2001; Cheng *et al.* 2001). Using ^{18}O labelling of individual nucleotide phosphate groups, it was possible from the isotopic shifts in the IR difference spectra to nearly completely assign the phosphate vibrations. As a result, a detailed picture has been obtained of the interactions between Ras and the three phosphate groups, of which β-phosphate is particularly strongly bound (Cepus *et al.* 1998; Allin & Gerwert, 2001) and is restricted in mobility (Cepus *et al.* 1998; Cheng *et al.* 2001). This points towards a dissociative mechanism of hydrolysis (Cepus *et al.* 1998; Du *et al.* 2000). When the educt GTP binds to Ras, its charge distribution on the phosphates approaches that of the product GDP (Allin & Gerwert, 2001) and there is also evidence that the transition state is GDP-like (Du *et al.* 2000). The bridging P—O bond between β- and γ-phosphate is weakened (Cepus *et al.* 1998; Cheng *et al.* 2001), which accounts for an 140-fold increase in hydrolysis rate compared to solution (Cheng *et al.* 2001).

In favourable cases the substrate can transfer a labelled group to the protein which can then be studied in its protein environment. This approach has been used to study the acyl enzyme of Ser proteases (Tonge *et al.* 1991; White *et al.* 1992; reviewed by Wharton, 2000) and the phosphate group of the phosphoenzyme intermediates of Ca^{2+}-ATPase (Barth & Mäntele, 1998; Barth, 1999). In the latter example, the γ-phosphate of the substrate ATP is labelled, phosphorylates the protein and produces labelled phosphoenzyme. In this way a phosphate band has been identified that appears when the second phosphoenzyme intermediate is formed. This shows that there is a conformational change that directly affects the geometry and/or the electron density of the phosphate group and indicates very different interactions between phosphate group and protein in the two phosphoenzyme intermediates. The band position for the second phosphoenzyme intermediate is unusual for phosphate groups in water and may be explained by a very hydrophobic environment in line with other findings (Dupont & Pougeois, 1983; Nakamoto & Inesi, 1984; Highsmith, 1986).

Protein cofactors have also been labelled and this is discussed for bacteriorhodopsin below. Another example is isotope-edited studies on the photosynthetic reaction centres which have been reviewed by Mäntele (1995), Nabedryk (1996) and Breton (2001).

Protein groups can be labelled in various ways. $^1H/^2H$ exchange is simply done by replacing ^1H_2O by ^2H_2O which exchanges the protons of accessible acidic groups, like OH, NH and SH, by deuteriums. The observed characteristic band shifts often allow the assignment of these bands to peptide groups or to specific amino-acid side-chains. An additional advantage is the shift of the strong water absorbance away from the amide I region (1610–1700 cm^{-1}) which is sensitive to protein structure. Regrettably, $^1H/^2H$ exchange does not always help because there may be too many changes to the spectrum or because amino acids deeply buried in the protein core do not exchange.

In a more selective approach, recombinant proteins can be labelled uniformly with, for example, ^{13}C or ^{15}N, all amino acids of one type can be labelled or a label can be placed specifically on one particular amino acid. This site-directed labelling is the most powerful interpretation tool, but unfortunately requires great effort and is usually not feasible.

The labelling of backbone carbonyls with ^{13}C shifts the amide I band by 36–38 cm^{-1} to lower wavenumbers (Haris *et al.* 1992; reviewed by Fabian *et al.* 1996a). This can be used to separate the amide I bands of two proteins or a protein and a peptide for binding studies. The influence of binding the proteins γ- and β_L-crystallin to the chaperone α-crystallin was investigated by this approach (Das *et al.* 1999). Another example is a study of the binding of peptides to calmodulin (Zhang *et al.* 1994). The isotope-induced frequency shift of the amide I mode can also be utilized to probe the local secondary structure of peptides at the level of individual residues (Lansbury *et al.* 1995; Ludlam *et al.* 1995, 1996; Decatur & Antonic, 1999; Brauner *et al.* 2000; Gordon *et al.* 2000; Silva *et al.* 2000; Kubelka & Keiderling, 2001a).

Isotopic labelling and mutagenesis can even be combined. An example is the study of haem propionate involvement in proton-transfer reactions of cytochrome *c* oxidase. First, the very small signals of the haem propionate groups were identified in the spectrum with specific isotopic labelling of the four propionate carboxyl groups (Behr *et al.* 1998). While this approach detected the involvement of the haem propionate groups in the reaction, it did not allow the assignment of a signal to a specific group. This was achieved by removing hydrogen bonds to an individual haem propionate group using site-directed mutagenesis (Behr *et al.* 2000). Since the position of the propionate signals is sensitive to hydrogen bonding, shifts of the formerly identified propionate signals are expected and were observed for the mutated enzymes. In this way it was found that only one of the four propionate groups seems to act as a proton acceptor upon reduction of cytochrome *c* oxidase (Behr *et al.* 2000).

The small membrane protein, bacteriorhodopsin, which functions as a light-driven proton pump has been used for a large number of IR studies (reviewed by Rothschild, 1992; Gerwert, 1993, 1999; Maeda, 1995; Heberle, 1999). All the band-assignment strategies listed above have been used to enable the detailed interpretation of the difference spectra. As an example the difference spectrum between the spectra of the photointermediate M and of the unphotolysed state of bacteriorhodopsin is shown in Fig. 18.

Fortunately, it is possible to remove the chromophore retinal and replace it by an isotopically labelled analogue. This enabled determination of the contributions of the chromophore to the spectra (Gerwert & Siebert, 1986). Distinction between aspartic and glutamic acids was accomplished by [4-^{13}C]labelling of all aspartic acids (Engelhard *et al.* 1985). In order to label a single aspartic acid, the labelled and the unlabelled protein were each cut into two parts with the help of a protease. In the next step the labelled fragment V-1 was reconstituted with the unlabelled fragment V-2 and vice versa. Since Asp212 is the only aspartic acid in the V-2 fragment, the bands due to this side-chain could be separated from the contributions of other Asp residues (Fahmy *et al.* 1993). In another approach, which involves cell-free expression of bacteriorhodopsin, site-directed isotopic labelling of single Tyr residues was successful (Ludlam *et al.* 1995). Recently, site-directed isotopic labelling of bacteriorhodopsin was realized by the exchange of specific residues for Cys (Hauser *et al.* 2002). Since wild-type bacteriorhodopsin lacks this amino acid, incorporation of labelled Cys enabled site-directed isotopic labelling of this protein. As in the case of the Tyr experiment, the ^{13}C isotope was inserted at the position of the carbonyl carbon in order to permit a molecular interpretation of amide I difference bands.

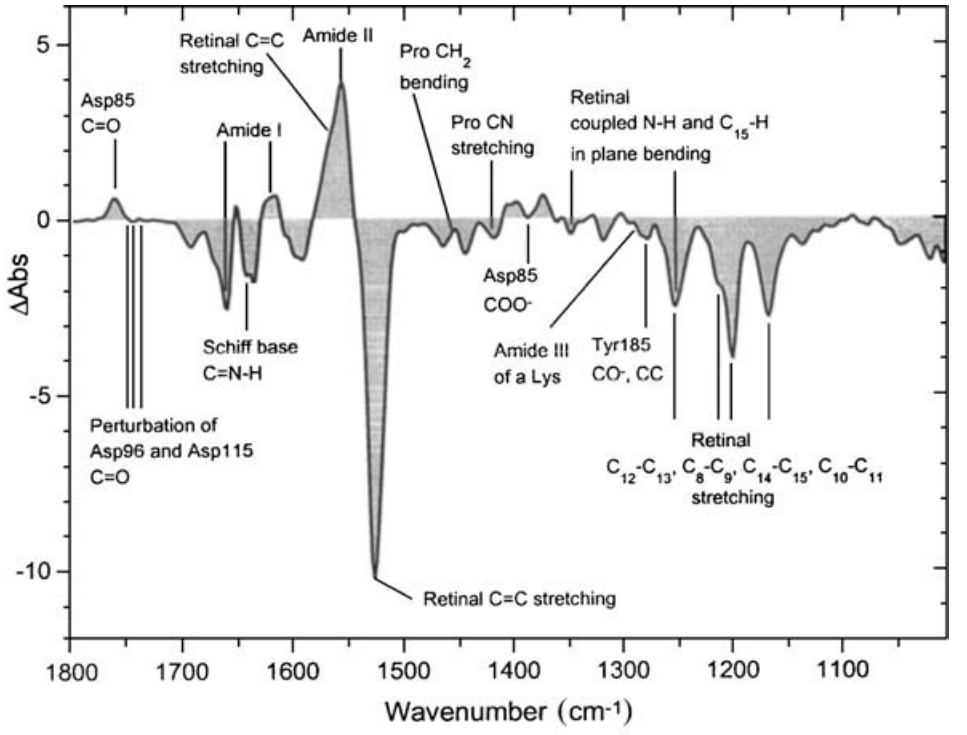

Fig. 18. Light-induced IR difference spectrum between the spectrum of the photointermediate M and that of the unphotolysed state of bacteriorhodopsin (BR). Positive bands correspond to the M state and negative bands to the ground state. Assignments are indicated as reviewed by Maeda (1995). The details of the C—C assignments are taken from Raman work (Smith *et al.* 1987). The chromophore retinal is all-*trans* in BR and 13-*cis* isomerized in M. Retinal is covalently linked to Lys216 by a Schiff base. The Schiff base is protonated in the unphotolysed state and deprotonates upon M formation. The internal acceptor of this proton is Asp85. This proton transfer as well as isomerization of retinal and changes in the protein backbone conformation are clearly reflected in the difference spectra (see the respective labels). Time-resolved spectra recorded between 0·3 and 0·4 ms were averaged. Measurements were performed at 20 °C and pH 8·4 using the ATR technique. For experimental details see Zscherp & Heberle (1997).

Also without isotopic labelling site-directed mutagenesis is a powerful tool for band assignments of amino-acid side-chains. Early work on mutants of Asp96 and Asp85 (Braiman *et al.* 1988a; Gerwert *et al.* 1989) allowed these side-chains to be identified as key residues in the mechanism of proton transport. The comparison of wild-type and mutant difference spectra led to the assignment of difference bands at 1277 and 833 cm^{-1} to Tyr185 (Braiman *et al.* 1988b). The elegant work of Sasaki and co-workers who analysed the tiny bands due to C═O stretching vibrations of aspartic-acid residues in the late part of the photoreaction of bacteriorhodopsin may serve as an additional example (Sasaki *et al.* 1994).

10. Outlook

As the discussion above has shown, the vibrational spectrum of proteins contains a wealth of information that can be exploited to learn about the structure and function of proteins. This makes it an attractive method in combination with other advantages like the universal application range

from small soluble proteins to large membrane protein complexes, the high time-resolution (< μs with moderate effort) and the relatively low costs [<100 000 (euros or dollars) for a top-class IR spectrometer]. Furthermore, exciting developments promise new ways of investigation:

(1) New methods to perturb proteins or to initiate protein reactions will expand the number of systems that can be investigated with reaction-induced IR difference spectroscopy and will also pave the way for biotechnology applications. Of particular interest here are a number of mixing devices that have recently been developed (White *et al.* 1995; Fahmy, 1998, 2001; Masuch & Moss, 1999; Hinsmann *et al.* 2001; Kauffmann *et al.* 2001) and which aim at making IR spectroscopy as universally applicable as UV/visible spectroscopy.
(2) New applications of IR spectroscopy and IR imaging in biomedicine (reviewed by Jackson & Mantsch, 1996; Jackson *et al.* 1997; Naumann, 2001).
(3) The combination of experiments with quantum chemical calculations promising highly detailed insight into the catalytic mechanism of enzymes (Deng *et al.* 1998a; Wang *et al.* 1998; Cheng *et al.* 2001).
(4) An increasing number of studies on ligand–protein interactions (Alben & Caughey, 1968; Riepe & Wang, 1968; Belasco & Knowles, 1980; reviewed by Wharton, 2000; Barth & Zscherp, 2000) and protein–protein interactions (Haris *et al.* 1992; Zhang *et al.* 1994; Liang & Chakrabarti, 1998; Das *et al.* 1999; Fahmy *et al.* 2000b; Krueger *et al.* 2000; Allin *et al.* 2001).
(5) Generalized 2D correlation spectroscopy as proposed by Noda (1993) enables an informative presentation of spectral variations as a function of physical variables like time, temperature, pressure or concentrations. The high sensitivity of this method has been used for example to study the sequence of unfolding events of the λ Cro-V55C repressor protein (Fabian *et al.* 1999).
(6) The advent of ultrafast multi-pulse IR experiments that are directly analogous to multi-dimensional NMR and have the ultimate goal of deducing the structure from the coupling between vibrations like the amide I modes located on different amide groups (Hamm *et al.* 1999; Asplund *et al.* 2000).

Thus, vibrational spectroscopy will continue to provide important contributions to the understanding of proteins.

11. Acknowledgements

The authors gratefully acknowledge continuous support by W. Mäntele. We are grateful to J. Corrie (NIMR, London) for helpful comments on the manuscript. The current work of A.B. is supported by grants Ba 1887/1-1, 2-1 and 4-1 of the Deutsche Forschungsgemeinschaft.

12. References

Abe, Y. & Krimm, S. (1972). Normal vibrations of crystalline polyglycine I. *Biopolymers* **11**, 1817–1839.

Alben, J. O. & Caughey, W. S. (1968). An infrared study of bound carbon monoxide in the human red blood cell, isolated hemoglobin, and heme carbonyls. *Biochemistry* **7**, 175–183.

Allin, C., Ahmadian, M. R., Wittinghofer, A. & Gerwert, K. (2001). Monitoring the GAP catalysed H-Ras GTPase reaction at atomic resolution in real time. *Proc. natn. Acad. Sci. USA* **98**, 7754–7759.

Allin, C. & Gerwert, K. (2001). Ras catalyzes GTP hydrolysis by shifting negative charges from γ- to β-phosphate as revealed by time-resolved FTIR difference spectroscopy. *Biochemistry* **40**, 3037–3046.

Arrondo, J. L. R. & Goñi, F. M. (1999). Structure and dynamics of membrane proteins as studied by infrared spectroscopy. *Prog. Biophys. molec. Biol.* **72**, 367–405.

Arrondo, J. L. R., Goñi, F. M. & Macarulla, J. M. (1984). Infrared spectroscopy of phosphatidylcholines

in aqueous suspension. A study of the phosphate group vibrations. *Biochim. Biophys. Acta* **794**, 165–168.

ARRONDO, J. L. R., MANTSCH, H. H., MULLNER, N., PIKULA, S. & MARTONOSI, A. (1987). Infrared spectroscopic characterization of the structural changes connected with the E1–E2 transition in the Ca–ATPase of SR. *J. Biol. Chem.* **262**, 9037–9043.

ARRONDO, J. L. R., MUGA, A., CASTRESANA, J. & GOÑI, F. M. (1993). Quantitative studies of the structure of proteins in solution by Fourier-transform infrared-spectroscopy. *Prog. Biophys. molec. Biol.* **59**, 23–56.

ASHER, S. A., LUDWIG, M. & JOHNSON, C. R. (1986). UV resonance Raman excitation profiles of the aromatic amino acids. *J. Am. chem. Soc.* **108**, 3186–3197.

ASPLUND, M. C., ZANNI, M. T. & HOCHSTRASSER, R. M. (2000). Two-dimensional infrared spectroscopy of peptides by phase-controlled femtosecond vibrational photon echos. *Proc. natn. Acad. Sci. USA* **97**, 8219–8224.

BACKMANN, J., FABIAN, H. & NAUMANN, D. (1995). Temperature-jump-induced refolding of ribonuclease A: a time-resolved FTIR spectroscopic study. *FEBS Lett.* **364**, 175–178.

BADGER, R. M. & BAUER, S. H. (1937). Spectroscopic studies of the hydrogen bond. II. The shift of the O–H vibrational frequency in the formation of the hydrogen bond. *J. chem. Phys.* **5**, 839–851.

BAELLO, B. I., PANCOSKA, P. & KEIDERLING, T. A. (2000). Enhanced prediction accuracy of protein secondary structure using hydrogen exchange Fourier transform infrared spectroscopy. *Analyt. Biochem.* **280**, 46–57.

BAENZIGER, J. E., MILLER, K. W. & ROTHSCHILD, K. J. (1993). Fourier transform infrared difference spectroscopy of the nicotinic acetylcholine receptor: evidence for specific protein structural changes upon desensitization. *Biochemistry* **32**, 5448.

BANDOROWICZ-PIKULA, J., WRZOSEK, A., DANIELUK, M., PIKULA, S. & BUCHET, R. (1999). ATP-binding site of annexin VI characterized by photochemical release of nucleotide and infrared difference spectroscopy. *Biochem. biophys. Res. Commun.* **263**, 775–779.

BARTH, A. (1999). Phosphoenzyme conversion of the sarcoplasmic reticulum Ca^{2+} ATPase. Molecular interpretation of infrared difference spectra. *J. biol. Chem.* **274**, 22170–22175.

BARTH, A. (2000a). Fine-structure enhancement – assessment of a simple method to resolve overlapping bands in spectra. *Spectrochim. Acta* (*A*) **56**, 1223–1232.

BARTH, A. (2000b). The infrared absorption of amino acid side chains. *Prog. Biophys. molec. Biol.* **74**, 141–173.

BARTH, A. & MÄNTELE, W. (1998). ATP-induced phosphorylation of the sarcoplasmic reticulum Ca^{2+} ATPase – molecular interpretation of infrared difference spectra. *Biophys. J.* **75**, 538–544.

BARTH, A., MÄNTELE, W. & KREUTZ, W. (1991). Infrared spectroscopic signals arising from ligand binding and conformational changes in the catalytic cycle of sarcoplasmic reticulum Ca^{2+} ATPase. *Biochim. Biophys. Acta* **1057**, 115–123.

BARTH, A., MÄNTELE, W. & KREUTZ, W. (1997). Ca^{2+} release from the phosphorylated and the unphosphorylated sarcoplasmic reticulum calicum ATPase results in parallel structural changes. An infrared spectroscopic study. *J. biol. Chem.* **272**, 25507–25510.

BARTH, A., VON GERMAR, F., KREUTZ, W. & MÄNTELE, W. (1996). Time-resolved infrared spectroscopy of the Ca^{2+} ATPase. The enzyme at work. *J. biol. Chem.* **271**, 30637–30646.

BARTH, A. & ZSCHERP, C. (2000). Substrate binding and enzyme function investigated by infrared spectroscopy. *FEBS Lett.* **477**, 151–156.

BAUMRUK, V., PANCOSKA, P. & KEIDERLING, T. A. (1996). Predictions of secondary structure using statistical analyses of electronic and vibrational circular dichroism and Fourier transform infrared spectra of proteins in H_2O. *J. molec. Biol.* **259**, 774–791.

BAUSCHER, M. & MÄNTELE, W. (1992). Electrochemical and infrared-spectroscopic characterization of redox reactions of *p*-quinones. *J. phys. Chem.* **96**, 11101–11108.

BAUSCHER, M., NABEDRYK, E., BAGLEY, K., BRETON, J. & MÄNTELE, W. (1990). Investigation of models for photosynthetic electron acceptors. Infrared spectroelectrochemistry of ubiquinone and its anions. *FEBS Lett.* **261**, 191–195.

BAYMANN, F., ROBERTSON, D. E., DUTTON, P. L. & MÄNTELE, W. (1999). Electrochemical and spectroscopic investigations of the cytochrome bc(1) complex from *Rhodobacter capsulatus*. *Biochemistry* **38**, 13188–13199.

BEHR, J., HELLWIG, P., MÄNTELE, W. & MICHEL, H. (1998). Redox dependent changes at the heme propionates in cytochrome *c* oxidase from *Paracoccus denitrificans*: direct evidence from FTIR difference spectroscopy in combination with heme propionate ^{13}C labelling. *Biochemistry* **37**, 7400–7406.

BEHR, J., MICHEL, H., MÄNTELE, W. & HELLWIG, P. (2000). Functional properties of the heme propionates in cytochrome *c* oxidase from *Paracoccus denitrificans*. Evidence from FTIR difference spectroscopy and site-directed mutagenesis. *Biochemistry* **39**, 1356–1363.

BELASCO, J. G. & KNOWLES, J. R. (1980). Direct observation of substrate distortion by triosephosphate isomerase using Fourier transform infrared spectroscopy. *Biochemistry* **19**, 472–477.

BERENDZEN, J. & BRAUNSTEIN, D. (1990). Temperature-derivative spectroscopy: A tool for protein dynamics. *Proc. natn. Acad. Sci. USA* **87**, 1–5.

BRAIMAN, M. S., MOGI, T., MARTI, T., STERN, L. J., KHORANA, H. G. & ROTHSCHILD, K. J. (1988a). Vibrational spectroscopy of bacteriorhodopsin mutants: light-driven proton transport involves protonation changes of aspartic acid residues 85, 96, and 212. *Biochemistry* **27**, 8516–8520.

Braiman, M. S., Mogi, T., Stern, L. J., Hackett, N. R., Chao, B. H., Khorana, H. G. & Rothschild, K. J. (1988b). Vibrational spectroscopy of bacteriorhodopsin mutants: I. Tyrosine-185 protonates and deprotonates during the photocycle. *Proteins* **3**, 219–229.

Braiman, M. S., Briercheck, D. M. & Kriger, K. M. (1999). Modeling vibrational spectra of amino acid side chains in proteins: effects of protonation state, counterion, and solvent on arginine C–N stretch frequencies. *J. phys. Chem.* (*B*) **103**, 4744–4750.

Brauner, J. W., Dugan, C. & Mendelsohn, R. (2000). ^{13}C isotope labelling of hydrophobic peptides. Origin of the anomalous intensity distribution in the infrared amide I spectral region of β-sheet structures. *J. Am. chem. Soc.* **122**, 677–683.

Breton, J. (2001). Fourier transform infrared spectroscopy of primary electron donors in type I photosynthetic reaction centers. *Biochim. Biophys. Acta* **1507**, 180–193.

Brown, E. B. & Peticolas, W. L. (1975). Conformational geometry and vibrational frequencies of nucleic acid chains. *Biopolymers* **14**, 1259–1271.

Brudler, R., Rammelsberg, R., Woo, T. T., Getzoff, E. D. & Gerwert, K. (2001). Structure of the I_1 early intermediate of photoactive yellow protein by FTIR spectroscopy. *Nature Struct. Biol.* **8**, 265–270.

Bürgi, H.-B. & Dunitz, J. C. (1987). Fractional bonds: relations among their lengths, strengths, and stretching force constants. *J. Am. chem. Soc.* **109**, 2924–2926.

Byler, D. M. & Susi, H. (1986). Examination of the secondary structure of proteins by deconvolved FTIR spectra. *Biopolymers* **25**, 469–487.

Callender, R. & Deng, H. (1994). Nonresonance Raman difference spectroscopy: a general probe of protein structure, ligand binding, enzymatic catalysis, and the structures of other biomacromolecules. *Annu. Rev. Biophys. biomol. Struct.* **23**, 215–245.

Cantor, C. R. & Schimmel, P. R. (1980). *Biophysical Chemistry, Part II. Techniques for the Study of Biological Structure and Function*. San Francisco: W. H. Freeman and Company.

Cao, Y., Varo, G., Klinger, A. L., Czajkowsky, D. M., Braiman, M. S. & Needleman, R. (1993). Proton transfer from Asp-96 to the bacteriorhodopsin Schiff base is caused by a decrease of the pK_a of Asp-96 which follows a protein conformational change. *Biochemistry* **32**, 1981–1990.

Carey, P. R. (1998). Raman spectroscopy in enzymology: the first 25 years. *J. Raman Spectrosc.* **29**, 7–14.

Carey, P. R. (1999). Raman spectroscopy, the sleeping giant in structural biology, awakes. *J. biol. Chem.* **274**, 26625–26628.

Carey, P. R. & Tonge, P. J. (1995). Unlocking the secrets of enzyme power using Raman spectroscopy. *Acc. chem. Res.* **28**, 8–13.

Caswell, D. S. & Spiro, T. G. (1987). Proline signals in ultraviolett resonance Raman spectra of proteins: *Cis-trans* isomerism in polyproline and ribonuclease A. *J. Am. chem. Soc.* **109**, 2796–2800.

Cepus, V., Scheidig, A. J., Goody, R. S. & Gerwert, K. (1998). Time-resolved FTIR studies of the GTPase reaction of H-*ras* p21 reveal a key role for the β-phosphate. *Biochemistry* **37**, 10263–10271.

Cheam, T. C. & Krimm, S. (1984). Transition dipole interaction in polypeptides: *ab initio* calculation of transition dipole parameters. *Chem. Phys. Lett.* **107**, 613–616.

Cheng, H., Sukal, S., Deng, H., Leyh, T. S. & Callender, R. (2001). Vibrational structure of GDP and GTP bound to RAS: an isotope-edited FTIR study. *Biochemistry* **40**, 4035–4043.

Chetverin, A. B., Venyaminov, S. Y., Emelyanenko, V. I. & Burstein, E. A. (1980). Lack of gross protein structure changes in the working cycle of (Na^+, K^+)-dependent adenosinetriphosphatase. *Eur. J. Biochem.* **108**, 149–156.

Chirgadze, Y. N. & Brazhnikov, E. V. (1974). Intensities and other spectral parameters of infrared amide bands of polypeptides in the α-helical form. *Biopolymers* **13**, 1701–1712.

Chirgadze, Y. N., Fedorov, O. V. & Trushina, N. P. (1975). Estimation of amino acid residue side chain absorption in the infrared spectra of protein solutions in heavy water. *Biopolymers* **14**, 679–694.

Chirgadze, Y. N. & Nevskaya, N. A. (1976a). Infrared spectra and resonance interaction of amide-I vibration of the antiparallel-chain pleated sheet. *Biopolymers* **15**, 607–625.

Chirgadze, Y. N. & Nevskaya, N. A. (1976b). Infrared spectra and resonance interaction of amide-I vibration of the parallel-chain pleated sheet. *Biopolymers* **15**, 627–636.

Chirgadze, Y. N., Shestopalov, B. V. & Venyaminov, S. Y. (1973). Intensities and other spectral parameters of infrared amide bands of polypeptides in the β- and random forms. *Biopolymers* **12**, 1337–1351.

Chittock, R. S., Ward, S., Wilkinson, A.-S., Caspers, P., Mensch, B., Page, M. G. P. & Wharton, C. W. (1999). Hydrogen bonding and protein perturbation in α-lactam acyl-enzymes of streptococcus pneumoniae penicillin-binding protein PBP2x. *Biochem. J.* **338**, 153–159.

Colthup, N. B., Daly, L. H. & Wiberley, S. E. (1975). *Introduction to Infrared and Raman Spectroscopy*, 2nd edn. New York: Academic Press.

Das, K. P., Choo-Smith, L. P., Petrash, J. M. & Surewicz, W. K. (1999). Insight into the secondary structure of non-native proteins bound to a molecular chaperone α-crystallin. An isotope-edited infrared spectroscopic study. *J. biol. Chem.* **274**, 33209–33212.

De Jongh, H. H. J., Goormaghtigh, E. & Ruysschaert, J.-M. (1996). The different molar absorptivities of the secondary structure types in the amide I region: an

attenuated total reflection infrared study on globular proteins. *Analyt. Biochem.* **242**, 95–103.

De Jongh, H. H., Goormaghtigh, E. & Ruysschaert, J. M. (1997a). Amide-proton exchange of water-soluble proteins of different structural classes studied at the submolecular level by infrared spectroscopy. *Biochemistry* **36**, 13603–13610.

De Jongh, H. H., Goormaghtigh, E. & Ruysschaert, J. M. (1997b). Monitoring structural stability of trypsin inhibitor at the submolecular level by amide-proton exchange using Fourier transform infrared spectroscopy: a test case for more general application. *Biochemistry* **36**, 13593–13602.

Deacon, G. B. & Phillips, R. J. (1980). Relationships between the carbon-oxygen stretching frequencies of carboxylate complexes and the type of carboxylate coordination. *Coord. Chem. Rev.* **33**, 227–250.

Decatur, S. M. & Antonic, J. (1999). Isotope-edited infrared spectroscopy of helical peptides. *J. Am. chem. Soc.* **121**, 11914–11915.

Deng, H. & Callender, R. (1999). Raman spectroscopic studies of the structures, energetics, and bond distortions of substrates bound to enzymes. *Methods Enzymol.* **308**, 176–201.

Deng, H. & Callender, R. (2001). Vibrational studies of enzymatic catalysis. In *Infrared and Raman Spectroscopy of Biological Materials* (eds. H. U. Gremlich & B. Yan), pp. 477–515. New York: Marcel Dekker Inc.

Deng, H., Wang, J., Callender, R. H., Grammer, J. C. & Yount, R. G. (1998a). Raman difference spectroscopic studies of the myosin S1·MgADP·vanadate complex. *Biochemistry* **37**, 10972–10979.

Deng, H., Wang, J., Callender, R. & Ray, W. J. (1998b). Relationship between bond stretching frequencies and internal bonding for [$^{16}O_4$]- and [$^{18}O_4$]phosphates in aqueous solution. *J. phys. Chem.* (*B*) **1022**, 3617–3623.

Dhamelincourt, P. & Ramirez, F. J. (1993). Polarized micro-Raman and FT-IR spectra of L-glutamine. *Appl. Spectrosc.* **47**, 446–451.

Dioumaev, A. K. & Braiman, M. S. (1995). Modeling vibrational spectra of amino acid side chains in proteins: the carbonyl stretch frequency of buried carboxylic residues. *J. Am. chem. Soc.* **117**, 10572–10574.

Dollinger, G., Eisenstein, L., Shuo-Liang, L., Nakanishi, K. & Termini, J. (1986). Fourier transform infrared difference spectroscopy of bacteriorhodopsin and its photoproducts regenerated with deuterated tyrosine. *Biochemistry* **25**, 6524–6533.

Dousseau, F. & Pezolet, M. (1990). Determination of the secondary structure content of proteins in aqueous solutions from their amide I and amide II infrared bands. Comparison between classical and partial least-squares methods. *Biochemistry* **29**, 8771–8779.

Du, X., Frei, H. & Kim, S.-H. (2000). The mechanism of GTP hydrolysis by Ras probed by Fourier transform infrared spectroscopy. *J. biol. Chem.* **275**, 8492–8500.

Dupont, Y. & Pougeois, R. (1983). Evaluation of H_2O activity in the free or phosphorylated catalytic site of Ca-ATPase. *FEBS Lett.* **156**, 93–98.

Dyer, R. B., Gai, F., Woodruff, W. H., Gilmanshin, R. & Callender, R. H. (1998). Infrared studies of fast events in protein folding. *Acc. chem. Res.* **31**, 709–716.

Earnest, T. N., Herzfeld, J. & Rothschild, K. J. (1990). Polarized Fourier transform infrared spectroscopy of bacteriorhodopsin. Transmembrane α-helices are resistant to hydrogen/deuterium exchange. *Biophys. J.* **58**, 1539–1546.

Engelhard, M., Gerwert, K., Hess, B., Kreutz, W. & Siebert, F. (1985). Light-driven protonation changes of internal aspartic acids of bacteriorhodopsin: an investigation by static and time-resolved infrared difference spectroscopy using [4-^{13}C]aspartic acid labeled purple membrane. *Biochemistry* **24**, 400–407.

Englander, S. W. & Kallenbach, N. R. (1984). Hydrogen exchange and structural dynamics of proteins and nucleic acids. *Q. Rev. Biophys.* **16**, 521–655.

Fabian, H., Chapman, D. & Mantsch, H. H. (1996a). New trends in isotope-edited infrared spectroscopy. In *Infrared Spectroscopy of Biomolecules* (eds. H. H. Mantsch & D. Chapman), pp. 341–352. New York: Wiley-Liss.

Fabian, H. & Mantsch, H. H. (1995). Ribonuclease A revisited: infrared spectroscopic evidence for lack of native-like secondary structures in the thermally denatured state. *Biochemistry* **34**, 13651–13655.

Fabian, H., Mantsch, H. H. & Schultz, C. P. (1999). Two-dimensional IR correlation spectroscopy: sequential events in the unfolding process of the lambda Cro-V55C repressor protein. *Proc. natn. Acad. Sci. USA* **96**, 13153–13158.

Fabian, H., Schultz, C., Backmann, J., Hahn, U., Saenger, W., Mantsch, H. H. & Naumann, D. (1994). Impact of point mutations on the structure and thermal stability of ribonuclease T1 in aqueous solution probed by Fourier transform infrared spectroscopy. *Biochemistry* **33**, 10725–10730.

Fabian, H., Schultz, C., Naumann, D., Landt, O., Hahn, U. & Saenger, W. (1993). Secondary structure and temperature-induced unfolding and refolding of ribonuclease T1 in aqueous solution. *J. molec. Biol.* **232**, 967–981.

Fabian, H., Yuan, T., Vogel, H. J. & Mantsch, H. H. (1996b). Comparative analysis of the amino- and carboxy-terminal domains of calmodulin by Fourier transform infrared spectroscopy. *Eur. Biophys. J.* **24**, 195–201.

Fahmy, K. (1998). Binding of transducin and transducin-derived peptides to rhodopsin studied by attenuated total reflection-Fourier transform infrared difference spectroscopy. *Biophys. J.* **75**, 1306–1318.

FAHMY, K. (2001). Application of ATR-FTIR spectroscopy for studies of biomolecular interactions. *Recent Res. devel. Chem.* **2**, 1–17.

FAHMY, K., SAKMAR, T. P. & SIEBERT, F. (2000a). Structural determinants of active state conformation of rhodopsin: molecular biophysics approaches. *Methods Enzymol.* **315**, 178–196.

FAHMY, K., SAKMAR, T. P. & SIEBERT, F. (2000b). Transducin-dependent protonation of glutamic acid 134 in rhodopsin. *Biochemistry* **39**, 10607–10612.

FAHMY, K., WEIDLICH, O., ENGELHARD, M., SIGRIST, H. & SIEBERT, F. (1993). Aspartic acid-212 of bacteriorhodopsin is ionized in the M and N photocycle intermediates: an FTIR study on specifically ^{13}C-labelled reconstituted purple membranes. *Biochemistry* **32**, 5862–5869.

FISHER, J., BELASCO, J. G., KHOSLA, S. & KNOWLES, J. R. (1980). β-Lactamase proceeds via an acyl-enzyme intermediate. Interaction of the *Escherichia coli* RTEM enzyme with cefoxitin. *Biochemistry* **19**, 2895–2901.

FITTER, J. & HEBERLE, J. (2000). Structural equilibrium fluctuations in mesophilic and thermophilic α-amylase. *Biophys. J.* **79**, 1629–1636.

GEORGE, L., SANKARAN, K., VISWANATHAN, K. S. & MATHEWS, C. K. (1994). Matrix-isolation infrared spectroscopy of hydrogen-bonded complexes of triethyl phosphate with H_2O, D_2O, and methanol. *Appl. Spectrosc.* **48**, 801–807.

GEROTHANASSIS, I. P., BIRLIRAKIS, N., SAKARELLOS, C. & MARRAUD, M. (1992). Solvation state of the Tyr side chain in peptides – an FT-IR and O-17 NMR approach. *J. Am. chem. Soc.* **114**, 9043–9047.

GERWERT, K. (1993). Molecular reaction mechanisms of proteins as monitored by time-resolved FTIR spectroscopy. *Curr. Opin. struct. Biol.* **3**, 769–773.

GERWERT, K. (1999). Molecular reaction mechanisms of proteins monitored by time-resolved FTIR-spectroscopy. *Biol. Chem.* **380**, 931–935.

GERWERT, K., HESS, B. & ENGELHARD, M. (1990a). Proline residues undergo structural changes during proton pumping in bacteriorhodopsin. *FEBS Lett.* **261**, 449–454.

GERWERT, K., HESS, B., SOPPA, J. & OESTERHELT, D. (1989). Role of aspartate-96 in proton translocation by bacteriorhodopsin. *Proc. natn. Acad. Sci. USA* **86**, 4943–4947.

GERWERT, K. & SIEBERT, F. (1986). Evidence for light-induced 13-cis,14-s-cis isomerization in bacteriorhodopsin obtained by FTIR difference spectroscopy using isotopically labelled retinals. *EMBO J.* **5**, 805–811.

GERWERT, K., SOUVIGNIER, G. & HESS, B. (1990b). Simultaneous monitoring of light-induced changes in protein side-group protonation, chromophore isomerization, and backbone motion of bacteriorhodopsin by time-resolved Fourier-transform infrared spectroscopy. *Proc. natn. Acad. Sci. USA* **87**, 9774–9778.

GILMANSHIN, R., WILLIAMS, S., CALLENDER, R. H., WOODRUFF, W. H. & DYER, R. B. (1997). Fast events in protein folding: relaxation dynamics and structure of the I form of apomyoglobin. *Biochemistry* **36**, 15006–15012.

GOORMAGHTIGH, E., CABIAUX, V. & RUYSSCHAERT, J.-M. (1994a). Determination of soluble and membrane protein structure by Fourier transform infrared spectroscopy. I. Assignments and mode compounds. *Subcell. Biochem.* **23**, 329–362.

GOORMAGHTIGH, E., CABIAUX, V. & RUYSSCHAERT, J.-M. (1994b). Determination of soluble and membrane protein structure by Fourier transform infrared spectroscopy. III. Secondary structures. *Subcell. Biochem.* **23**, 405–450.

GOORMAGHTIGH, E., CABIAUX, V. & RUYSSCHAERT, J.-M. (1994c). Determination of soluble and membrane protein structure by Fourier transform infrared spectroscopy. II. Experimental aspects, side chain structure, and H/D exchange. *Subcell. Biochem.* **23**, 363–403.

GOORMAGHTIGH, E., DE JONGH, H. H. J. & RUYSSCHAERT, J.-M. (1996). Relevance of protein thin films prepared for attenuated total reflection Fourier transform infrared spectroscopy: significance of the pH. *Appl. Spectrosc.* **50**, 1519–1527.

GOORMAGHTIGH, E., RAUSSENS, V. & RUYSSCHAERT, J.-M. (1999). Attenuated total reflection infrared spectroscopy of proteins and lipids in biological membranes. *Biochim. Biophys. Acta* **1422**, 105–185.

GOORMAGHTIGH, E., VIGNERON, L., SCARBOROUGH, G. A. & RUYSSCHAERT, J.-M. (1994d). Tertiary conformational changes of the *Neurospora crassa* plasma membrane H^+-ATPase monitored by hydrogen/deuterium exchange kinetics. *J. biol. Chem.* **269**, 27409–27413.

GORDON, L. M., LEE, K. Y. C., LIPP, M. M., ZASADZINSKI, J. A., WALTHER, F. J., SHERMAN, M. A. & WARING, A. J. (2000). Conformational mapping of the N-terminal segment of surfactant protein B in lipid using ^{13}C-enhanced Fourier transform infrared spectroscopy. *J. Peptide Res.* **55**, 330–347.

HAMACHER, E., KRUIP, J., RÖGNER, M. & MÄNTELE, W. (1996). Characterization of the primary electron donor of photosystem I, P700, by electrochemistry and Fourier transform infrared (FTIR) difference spectroscopy. *Spectrochim. Acta* (*A*) **52**, 107–121.

HAMM, P., LIM, M., DEGRADO, W. F. & HOCHSTRASSER, R. M. (1999). The two-dimensional IR nonlinear spectroscopy of a cyclic penta-peptide in relation to its three-dimensional structure. *Proc. natn. Acad. Sci. USA* **96**, 2036–2041.

HAMM, P., LIM, M. & HOCHSTRASSER, R. M. (1998). Structure of the amide I band of peptides measured by femtosecond nonlinear-infrared spectroscopy. *J. phys. Chem.* (*B*) **102**, 6123–6138.

HARIS, P. I. & CHAPMAN, D. (1994). Analysis of polypeptide and protein structures using Fourier transform infrared spectroscopy. In *Methods in Molecular Biology,*

Microscopy, Optical Spectroscopy, and Macroscopic Techniques, vol. 22 (eds. C. Jones, B. Mulloy & A. H. Thomas), pp. 183–202. Totowa, NJ: Humana Press Inc.

Haris, P. I., Robillard, G. T., Van Dijk, A. A. & Chapman, D. (1992). Potential of ^{13}C and ^{15}N labelling for studying protein-protein interactions using Fourier transform infrared spectroscopy. *Biochemistry* **31**, 6279–6284.

Hasegawa, K., Ono, T.-A. & Noguchi, T. (2000). Vibrational spectra and ab initio DFT calculations of 4-methylimidazole and its different protonation forms: infrared and Raman markers of the protonation state of a histidine side chain. *J. phys. Chem.* (*B*) **104**, 4253–4265.

Hauser, K., Engelhard, M., Friedman, N., Sheves, M. & Siebert, F. (2002). Interpretation of amide I difference bands observed during protein reactions using site-directed isotopically labeled bacteriorhodopsin as a model system. *J. phys. Chem.* (*A*) **106**, 3553–3559.

Heberle, J. (1999). Time-resolved ATR/FT-IR spectroscopy of membrane proteins. *Recent Res. devel. Appl. Spectr.* **2**, 147–159.

Heimburg, T., Schünemann, J., Weber, K. & Geisler, N. (1999). FTIR-spectroscopy of multistranded coiled coil proteins. *Biochemistry* **38**, 12727–12734.

Hellwig, P., Mogi, T., Tomson, F. L., Gennis, R. B., Iwata, J., Miyoshi, H. & Mäntele, W. (1999). Vibrational modes of ubiquinone in cytochrome bo_3 from *Escherichia coli* identified by Fourier transform infrared difference spectroscopy and specific ^{13}C labelling. *Biochemistry* **38**, 14683–14689.

Hellwig, P., Ostermeier, C., Michel, H., Ludwig, B. & Mäntele, W. (1998). Electrochemically induced FT-IR difference spectra of the two- and four-subunit cytochrome *c* oxidase from *P. denitrificans* reveal identical conformational changes upon redox transitions. *Biochim. Biophys. Acta* **1409**, 107–112.

Hellwig, P., Rost, B., Kaiser, U., Ostermeier, C., Michel, H. & Mäntele, W. (1996). Carboxyl group protonation upon reduction of the *Paracoccus denitrificans* cytochrome *c* oxidase: direct evidence by FTIR spectroscopy. *FEBS Lett.* **385**, 53–57.

Hienerwadel, R., Boussac, A., Breton, J., Diner, B. & Berthomieu, C. (1997). Fourier transform infrared difference spectroscopy of photosystem II tyrosine D using site-directed mutagenesis and specific isotope labelling. *Biochemistry* **36**, 14712–14723.

Highsmith, S. (1986). Solvent accessibility of the ATP catalytic site of SR Ca-ATPase. *Biochemistry* **25**, 1049–1054.

Hinsmann, P., Haberkorn, M., Frank, J., Svasek, P., Harasek, M. & Lendl, B. (2001). Time-resolved FT-IR spectroscopy of chemical reactions in solution by fast diffusion-based mixing in a micromachined flow cell. *Appl. Spectrosc.* **55**, 241–251.

Jackson, M., Haris, P. I. & Chapman, D. (1991). Fourier transform infrared spectroscopic studies of Ca^{2+}-binding proteins. *Biochemistry* **30**, 9681–9686.

Jackson, M. & Mantsch, H. H. (1991). Protein secondary structure from FT-IR spectroscopy: correlation with dihedral angles from three-dimensional Ramachandran plots. *Can. J. Chem.* **69**, 1639–1642.

Jackson, M. & Mantsch, H. H. (1995). The use and misuse of FTIR spectroscopy in the determination of protein structure. *Crit. Rev. Biochem. molec. Biol.* **30**, 95–120.

Jackson, M. & Mantsch, H. H. (1996). Biomedical infrared spectroscopy. In *Infrared Spectroscopy of Biomolecules* (eds. H. H. Mantsch & D. Chapman), pp. 311–340. New York: Wiley-Liss.

Jackson, M., Sowa, M. G. & Mantsch, H. H. (1997). Infrared spectroscopy: a new frontier in medicine. *Biophys. Chem.* **68**, 109–125.

Johnston, N. & Krimm, S. (1971). An infrared study of unordered poly-L-proline in $CaCl_2$ solutions. *Biopolymers* **10**, 2597–2605.

Jung, C. (2000). Insight into protein struture and protein-ligand recognition by Fourier transform infrared spectroscopy. *J. molec. Recognit.* **13**, 325–351.

Kabsch, W. & Sander, C. (1983). Dictionary of protein secondary structure: pattern recognition of hydrogen-bonded and geometrical features. *Biopolymers* **22**, 2577–2637.

Katz, J. J., Dougherty, R. C. & Boucher, L. J. (1966). Infrared and nuclear magnetic resonance spectroscopy of chlorophyll. In *The Chlorophylls* (eds. L. P. Vernon & G. R. Seely), pp. 185–251. New York: Academic Press.

Katz, J. J., Shipman, L. L., Cotton, T. M. & Janson, T. R. (1978). Chlorophyll aggregation: coordination interactions in chlorophyll monomers, dimers, and oligomers. In *The Porphins*, vol. 5 (ed. D. Dolphin), pp. 401–458. New York: Academic Press.

Kauffmann, E., Darnton, N. C., Austin, R. H., Batt, C. & Gerwert, K. (2001). Lifetimes of intermediates in the β-sheet to α-helix transitions of β-lactoglobulin by using a diffusional IR mixer. *Proc. natn. Acad. Sci. USA* **98**, 6646–6649.

Kauppinen, J. K., Moffatt, D. J., Mantsch, H. H. & Cameron, D. G. (1981). Fourier self-deconvolution: a method for resolving intrinsically overlapped bands. *Appl. Spectrosc.* **35**, 271–276.

Khurana, R. & Fink, A. L. (2000). Do parallel β-helix proteins have a unique Fourier transform infrared spectrum? *Biophys. J.* **78**, 994–1000.

Kim, S. & Barry, B. A. (2001). Reaction-induced FT-IR spectroscopic studies of biological energy conversion in oxygenic photosynthesis and transport. *J. phys. Chem.* **105**, 4072–4083.

Kleffel, B., Garavito, R. M., Baumeister, W. & Rosenbusch, J. P. (1985). Secondary structure of a channel-forming protein: porin from *E. coli* outer membranes. *EMBO J.* **4**, 1589–1592.

Krimm, S. & Abe, Y. (1972). Intermolecular interaction effects in the amide I vibrations of β polypeptides. *Proc. natn. Acad. Sci. USA* **69**, 2788–2792.

KRIMM, S. & BANDEKAR, J. (1980). Vibrational analysis of peptides, polypeptides, and proteins. V. Normal vibrations of β-turns. *Biopolymers* **19**, 1–29.

KRIMM, S. & BANDEKAR, J. (1986). Vibrational spectroscopy and conformation of peptides, polypeptides, and proteins. *Adv. Prot. Chem.* **38**, 181–367.

KRUEGER, J. K., GALLAGHER, S. C., WANG, C. L. A. & TREWHELLA, J. (2000). Calmodulin remains extended upon binding to smooth muscle caldesmon: a combined small-angle scattering and Fourier transform infrared spectroscopy study. *Biochemistry* **39**, 3979–3987.

KUBELKA, J. & KEIDERLING, T. A. (2001a). The anomalous infrared amide I intensity distribution in ^{13}C isotopically labelled peptide β-sheets comes from extended multiple-stranded structures. An *ab initio* study. *J. Am. chem. Soc.* **123**, 6142–6150.

KUBELKA, J. & KEIDERLING, T. A. (2001b). Differentiation of β-sheet forming structures: *ab initio*-based simulations of IR absorbtion and vibrational CD for model peptide and protein β-sheets. *J. Am. chem. Soc.* **123**, 12048–12058.

LAGANT, P., VERGOTEN, G., FLEURY, G. & LOUCHEUX-LEFEBVRE, M.-H. (1984). Vibrational normal modes of folded prolyl-containing peptides. Application to β turns. *Eur. J. Biochem.* **139**, 149–154.

LAGANT, P., VERGOTEN, G. & PETICOLAS, W. L. (1998). On the use of ultraviolet resonance Raman intensities to elaborate molecular force fields: application to nucleic acid bases and aromatic amino acid residues models. *Biospectroscopy* **4**, 379–393.

LANSBURY, P. T., COSTA, P. R., GRIFFITHS, J. M., SIMON, E. J., AUGER, M., HALVERSON, K. J., KOCISKO, D. A., HENDSCH, Z. S., ASHBURN, T. T., SPENCER, R. G. S., TIDOR, B. & GRIFFIN, R. G. (1995). Structural model for the beta-amyloid fibril based on interstrand alignment of an antiparallel-sheet comprising a C-terminal peptide. *Nature Struct. Biol.* **2**, 990–998.

LAUTIÉ, A., LAUTIÉ, M. F., GRUGER, A. & FAKHRI, S. A. (1980). Etude par spectrométrie i.r. et Raman de l'indole et de l'indolizine. Liaison hydrogène NH$\cdots\pi$*. *Spectrochim. Acta* (*A*) **36**, 85–94.

LE COUTRE, J., KABACK, H. R., PATEL, C. K., HEGINBOTHAM, L. & MILLER, C. (1998). Fourier transform infrared spectroscopy reveals a rigid α-helical assembly for the tetrameric *Streptomyces lividans* K^+ channel. *Proc. natn. Acad. Sci. USA* **95**, 6114–6117.

LEE, D. C., HARIS, P. I., CHAPMAN, D. & MITCHELL, D. C. (1990). Determination of protein secondary structure using factor analysis of infrared spectra. *Biochemistry* **29**, 9185–9193.

LEE, S.-H. & KRIMM, S. (1998). General treatment of vibrations of helical molecules and application to transition dipole coupling in amide I and amide II modes of α-helical poly(L-alanine). *Chem. Phys.* **230**, 277–295.

LEHNINGER, A. L. (1987). *Biochemie*, 2nd German edn. Weinheim: VCH Verlagsgesellschaft.

LEWIS, R. N. A. H. & MCELHANEY, R. N. (1996). Fourier transform infrared spectroscopy in the study of hydrated lipids and lipid bilayer membranes. In *Infrared Spectroscopy of Biomolecules* (eds. H. H. Mantsch & D. Chapman), pp. 159–202. New York: John Wiley & Sons.

LEVITT, M. & GREER, J. (1977). Automatic identification of secondary structure in globular proteins. *J. molec. Biol.* **114**, 181–239.

LIANG, J. J. & CHAKRABARTI, B. (1998). Intermolecular interaction of lens crystallins: from rotationally mobile to immobile states at high protein concentrations. *Biochem. biophys. Res. Commun.* **246**, 441–445.

LORD, R. C. & YU, N.-T. (1970a). Laser-excited Raman spectroscopy of biomolecules. I. Native lysozyme and its constituent amino acids. *J. molec. Biol.* **50**, 509–524.

LORD, R. C. & YU, N.-T. (1970b). Laser-excited Raman spectroscopy of biomolecules. II. Native ribonuclease and α -chymotrypsin. *J. molec. Biol.* **51**, 203–213.

LUDLAM, C. F., SONAR, S., LEE, C. P., COLEM, M., HERZFELD, X., RAJBHANDARY, U. & ROTHSCHILD, K. (1995). Site-directed isotope labelling and ATR-FTIR difference spectroscopy of bacteriorhodopsin: the peptide carbonyl group of Tyr 185 is structurally active during the bR$\rightarrow$N transition. *Biochemistry* **34**, 2–6.

LUDLAM, C. F. C., ARKIN, I. T., LIU, X. M., ROTHMAN, M. S., RATH, P., AIMOTO, S., SMITH, S. O., ENGELMAN, D. M. & ROTHSCHILD, K. J. (1996). Fourier transform infrared spectroscopy and site-directed isotope labelling as a probe of local secondary structure in the transmembrane domain of phospholamban. *Biophys. J.* **70**, 1728–1736.

LUTZ, M. & MÄNTELE, W. (1991). Vibrational spectroscopy of chlorophylls. In *Chlorophylls* (ed. H. Scheer), pp. 855–902. Boca Raton, FL: CRC Press.

MADEC, C., LAURANSAN, J. & GARRIGOU-LAGRANGE, C. (1978). Etude du spectre de vibration de la DL-serine et des ses dérivés deuteries. *Can. J. Spectr.* **23**, 166–172.

MAEDA, A. (1995). Application of FTIR spectroscopy to the structural study on the function of bacteriorhodopsin. *Israel J. Chem.* **35**, 387–400.

MÄNTELE, W. (1993a). Infrared vibrational spectroscopy of the photosynthetic reaction center. In *The Photosynthetic Reaction Center*, vol. 2 (eds. J. Deisenhofer & J. R. Norris), pp. 239–283. San Diego: Academic Press.

MÄNTELE, W. (1993b). Reaction-induced infrared difference spectroscopy for the study of protein function and reaction mechanisms. *Trends biochem. Sci.* **18**, 197–202.

MÄNTELE, W. (1995). Infrared vibrational spectroscopy of reaction centers. In *Anoxygenic Photosynthetic Bacteria* (eds. E. Blankenship, M. T. Madigan & C. E. Bauer), pp. 627–647. Dordrecht: Kluwer Academic Publishers.

MÄNTELE, W. (1996). Infrared and Fourier-transform infrared spectroscopy. In *Biophysical Techniques in*

Photosynthesis (eds. J. Amesz & A. J. Hoff), pp. 137–160. Dordrecht: Kluwer Academic Publishers.

MÄNTELE, W., SIEBERT, F. & KREUTZ, W. (1982). Kinetic properties of rhodopsin and bacteriorhodopsin measured by kinetic infrared spectroscopy (KIS). *Methods Enzymol.* **88**, 729–740.

MÄNTELE, W. G., WOLLENWEBER, A. M., NABEDRYK, E. & BRETON, J. (1988). Infrared spectroelectrochemistry of bacteriochlorophylls and bacteriopheophytins: implications for the binding of the pigments in the reaction center from photosynthetic bacteria. *Proc. natn. Acad. Sci. USA* **85**, 8468–8472.

MAES, G., SMOLDERS, A., VANDEVYVERE, P., VANDERHEYDEN, L. & ZEEGERS-HUYSKENS, T. (1988). Matrix-isolation IR studies on the basic interaction sites in esters and thiolesters towards proton donors. *J. molec. Struct.* **173**, 349–356.

MAES, G. & ZEEGERS-HUYSKENS, T. (1983). Matrix isolation infrared spectra of the complexes between methylacetate and water or hydrochloric acid. *J. molec. Struct.* **100**, 305–315.

MASUCH, R. & MOSS, D. A. (1999). Stopped flow system for FTIR difference spectroscopy of biological macromolecules. In *Spectroscopy of Biological Molecules: New Directions* (eds. J. Greve, G. J. Puppels & C. Otto), pp. 689–690. Dordrecht: Kluwer Academic Publishers.

METZ, G., SIEBERT, F. & ENGELHARD, M. (1992). High-resolution solid state ^{13}C NMR of bacteriorhodopsin: characterisation of [4-^{13}C]Asp resonances. *Biochemistry* **31**, 455–462.

MIYAZAWA, T. (1960). Perturbation treatment of the characteristic vibrations of polypeptide chains in various configurations. *J. chem. Phys.* **32**, 1647–1652.

MIZUGUCHI, M., NARA, M., KAWANO, K. & NITTA, K. (1997a). FT-IR study of the Ca^{2+}-binding to bovine α-lactalbumin. Relationships between the type of coordination and characteristics of the bands due to the Asp carboxylate groups in the Ca^{2+} binding site. *FEBS Lett.* **417**, 153–156.

MIZUGUCHI, M., NARA, M., KE, Y., KAWANO, K., HIRAOKI, T. & NITTA, K. (1997b). Fourier-transform infrared spectroscopic studies on the coordination of the side-chain carboxylate groups to Ca^{2+} in equine lysozyme. *Eur. J. Biochem.* **250**, 72–76.

MOORE, W. H. & KRIMM, S. (1975). Transition dipole coupling in amide I modes of β-polypeptides. *Proc. natn. Acad. Sci. USA* **72**, 4933–4935.

MOSS, D., NABEDRYK, E., BRETON, J. & MÄNTELE, W. (1990). Redox-linked conformational changes in proteins detected by a combination of infrared spectroscopy and protein electrochemistry. Evaluation of the technique with cytochrome c. *Eur. J. Biochem.* **187**, 565–572.

MUGA, A., MANTSCH, H. H. & SUREWICZ, W. K. (1991). Membrane binding induces destabilization of cytochrome c structure. *Biochemistry* **30**, 7219–7224.

NABEDRYK, E. (1996). Light-induced Fourier transform infrared difference spectroscopy of the primary electron donor in photosynthetic reaction centers. In *Infrared Spectroscopy of Biomolecules* (eds. H. H. Mantsch & D. Chapman), pp. 39–82. New York: Wiley-Liss.

NABEDRYK, E., LEONHARD, M., MÄNTELE, W. & BRETON, J. (1990). Fourier transform infrared difference spectroscopy shows no evidence for an enolization of chlorophyll a upon cation formation either *in vitro* or during P700 photooxidation. *Biochemistry* **29**, 3242–3247.

NAKAMOTO, R. K. & INESI, G. (1984). Studies of the interactions of 2′,3′-*O*-(2,4,6-trinitrocyclohexyldienylidine) adenosine nucleotides with the SR ($Ca^{2+} + Mg^{2+}$)-ATPase active site. *J. biol. Chem.* **259**, 2961–2970.

NARA, M., TANOKURA, M., YAMAMOTO, T. & TASUMI, M. (1995). A comparative study of the binding effects of Mg^{2+}, Ca^{2+}, Sr^{2+}, and Cd^{2+} on calmodulin by Fourier-transform infrared spectroscopy. *Biospectroscopy* **1**, 47–54.

NARA, M., TASUMI, M., TANOKURA, M., HIRAOKI, T., YAZAWA, M. & TSUTSUMI, A. (1994). Infrared studies of interaction between metal ions and Ca^{2+} binding proteins. Marker bands for identifying the types of coordination of the side-chain carboxylate groups to metal ions in pike parvalbumin (pI = 4·10). *FEBS Lett.* **349**, 84–88.

NARA, M., TORII, H. & TASUMI, M. (1996). Correlation between the vibrational frequencies of the carboxylate group and the types of its coordination to a metal ion: an *ab initio* molecular orbital study. *J. phys. Chem.* **100**, 19812–19817.

NAUMANN, D. (2001). FT-infrared and FT-Raman spectroscopy in biomedical research. In *Infrared and Raman Spectroscopy of Biological Materials* (eds. H. U. Gremlich & B. Yan), pp. 323–377. New York: Marcel Dekker Inc.

NETZER, W. J. & HARTL, F. U. (1997). Recombination of protein domains facilitated by co-translational folding in eukaryotes. *Nature* **388**, 343–349.

NEVSKAYA, N. A. & CHIRGADZE, Y. N. (1976). Infrared spectra and resonance interactions of amide-I and II vibrations of α-helix. *Biopolymers* **15**, 637–648.

NODA, I. (1993). Generalized two-dimensional correlation method applicable to infrared, Raman, and other types of spectroscopy. *Appl. Spectrosc.* **47**, 1329–1336.

NOGUCHI, T., INOUE, Y. & TANG, X.-S. (1999). Structure of a histidine ligand in the photosynthetic oxygen-evolving complex as studied by light-induced Fourier transform infrared difference spectroscopy. *Biochemistry* **38**, 10187–10195.

OVERMAN, S. A. & THOMAS, G. J. (1999). Raman markers of nonaromatic side chains in an α-helix assembly: Ala,

Asp, Glu, Gly, Ile, Leu, Lys, Ser, and Val residues of phage *fd* subunits. *Biochemistry* **38**, 4018–4027.

PALAFOX, M. A. (1998). Empirical correlations in vibrational spectroscopy. *Trends Appl. Spectrosc.* **2**, 37–57.

PARRISH, J. R. & BLOUT, E. R. (1972). The conformation of poly-L-alanine in hexafluoroisopropanol. *Biopolymers* **11**, 1001–1020.

PINCHAS, S. & LAULICHT, I. (1971). *Infrared Spectra of Labelled Compounds*. London, New York: Academic Press.

POHLE, W., BOHL, M. & BÖHLIG, H. (1990). Interpretation of the influence of hydrogen bonding on the stretching vibrations of the PO_2^- moiety. *J. molec. Struct.* **242**, 333–342.

POTTER, W. T., TUCKER, M. P., HOUTCHENS, R. A. & CAUGHEY, W. S. (1987). Oxygen infrared spectra of oxyhemoglobins and oxymyoglobins. Evidence of two major liganded O_2 structures. *Biochemistry* **26**, 4699–4707.

PRIBIC, R., VAN STOKKUM, I. H., CHAPMAN, D., HARIS, P. I. & BLOEMENDAL, M. (1993). Protein secondary structure from Fourier transform infrared and/or circular dichroism spectra. *Analyt. Biochem.* **214**, 366–378.

RAHMELOW, K. & HÜBNER, W. (1996). Secondary structure determination of proteins in aqueous solution by infrared spectroscopy: a comparison of multivariate data analysis methods. *Analyt. Biochem.* **241**, 5–13.

RAHMELOW, K., HÜBNER, W. & ACKERMANN, T. (1998). Infrared absorbances of protein side chains. *Analyt. Biochem.* **257**, 1–11.

RAIMBAULT, C., BUCHET, R. & VIAL, C. (1996). Changes of creatine kinase secondary structure induced by the release of nucleotides from caged compounds – an infrared difference-spectroscopy study. *Eur. J. Biochem.* **240**, 134–142.

RAIMBAULT, C., CLOTTES, E., LEYDIER, C., VIAL, C. & BUCHET, R. (1997). ADP-binding and ATP-binding sites in native and proteinase-K-digested creatine kinase, probed by reaction-induced difference infrared spectroscopy. *Eur. J. Biochem.* **247**, 1197–1208.

RASCHKE, T. M. & MARQUSEE, S. (1998). Hydrogen exchange studies of protein structure. *Curr. Opin. Biotechnol.* **9**, 80–86.

RAVA, R. P. & SPIRO, T. G. (1985). Resonance enhancement in the ultraviolet Raman spectra of aromatic amino acids. *J. phys. Chem.* **89**, 1856–1861.

REINSTÄDLER, D., FABIAN, H., BACKMANN, J. & NAUMANN, D. (1996). Refolding of thermally and urea-denatured ribonuclease A monitored by time-resolved FTIR spectroscopy. *Biochemistry* **35**, 15822–15830.

REINSTÄDLER, D., FABIAN, H. & NAUMANN, D. (1999). New structural insights into the refolding of ribonuclease T1 as seen by time-resolved Fourier-transform infrared spectroscopy. *Proteins* **34**, 303–316.

REISDORF, W. C. & KRIMM, S. (1996). Infrared amide I′ band of the coiled coil. *Biochemistry* **35**, 1383–1386.

RIEPE, M. E. & WANG, J. H. (1968). Infrared studies on the mechanism of action of carbonic anhydrase. *J. biol. Chem.* **243**, 2779–2787.

ROBERT, B. (1996). Resonance Raman studies in photosynthesis – chlorophyll and carotenoid molecules. In *Biophysical Techniques in Photosynthesis* (eds. J. Amesz & A. J. Hoff), pp. 161–176. Dordrecht: Kluwer Academic Publishers.

ROEPE, P., AHL, P. L., DAS GUPTA, S. K., HERZFELD, J. & ROTHSCHILD, K. J. (1987). Tyrosine and carboxyl protonation changes in the bacteriorhodopsin photocycle. 1. M412 and L550 intermediates. *Biochemistry* **26**, 6696–6707.

ROTHSCHILD, K. J. (1992). FTIR difference spectroscopy of bacteriorhodopsin: toward a molecular model. *J. Bioenerg. Biomembr.* **24**, 147–167.

ROTHSCHILD, K. J., HE, Y. W., GRAY, D., ROEPE, P. D., PELLETIER, S. L., BROWN, R. S. & HERZFELD, J. (1989). Fourier transform infrared evidence for proline structural changes during the bacteriorhodopsin photocycle. *Proc. natn. Acad. Sci. USA* **86**, 9832–9835.

ROTHSCHILD, K. J., ROEPE, P., AHL, P. L., EARNEST, T. N., BOGOMOLNI, R. A., DAS GUPTA, S. K., MULLIKEN, C. M. & HERZFELD, J. (1986). Evidence for a tyrosine protonation change during the primary phototransition of bacteriorhodopsin at low temperature. *Proc. natn. Acad. Sci. USA* **83**, 347–351.

RÜDIGER, M., HAUPTS, U., GERWERT, K. & OESTERHELT, D. (1995). Chemical reconstitution of a chloride pump inactivated by a single point mutation. *EMBO J.* **14**, 1599–1606.

SARVER, R. W. & KRUEGER, W. C. (1991). An infrared and circular dichroism combined approach to the analysis of protein secondary structure. *Analyt. Biochem.* **199**, 61–67.

SASAKI, J., LANYI, J. K., NEEDLEMAN, R., YOSHIZAWA, T. & MAEDA, A. (1994). Complete identification of C=O stretching vibrational bands of protonated aspartic acid residues in the difference infrared spectra of M and N intermediates versus bacteriorhodopsin. *Biochemistry* **33**, 3178–3184.

SCHEIRLINCKX, F., BUCHET, R., RUYSSCHAERT, J.-M. & GOORMAGHTIGH, E. (2001). Monitoring of secondary and tertiary structure changes in the gastric H^+/K^+-ATPase by infrared spectroscopy. *Eur. J. Biochem.* **268**, 3644–3653.

SCHLERETH, D. D., FERNANDEZ, V. M. & MÄNTELE, W. (1993). Protein conformational changes in tetraheme cytochromes detected by FTIR spectroelectrochemistry: *Desulfovibrio desulfuricans* Norway 4 and *Desulfovibrio gigas* cytochromes c_3. *Biochemistry* **32**, 9199–9208.

SCHLERETH, D. D. & MÄNTELE, W. (1992). Redox-induced conformational changes in myoglobin and hemoglobin: electrochemistry and ultraviolet–visible and Fourier transform infrared difference spectroscopy at

surface-modified gold electrodes in an ultra-thin-layer spectroelectrochemical cell. *Biochemistry* **31**, 7494–7502.

SCHLERETH, D. D. & MÄNTELE, W. (1993). Electrochemically induced conformational changes in cytochrome *c* monitored by Fourier transform infrared difference spectroscopy: influence of temperature, pH, and electrode surfaces. *Biochemistry* **32**, 1118–1126.

SCHULTZ, C. P. (2000). Illuminating folding intermediates. *Nature Struct. Biol.* **7**, 7–10.

SENGUPTA, P. K. & KRIMM, S. (1985). Vibrational analysis of peptides, polypeptides, and proteins. XXXII. α-poly (L-glutamic acid). *Biopolymers* **24**, 1479–1491.

SIEBERT, F. (1990). Resonance Raman and infrared difference spectroscopy of retinal proteins. *Methods Enzymol.* **189**, 123–136.

SIEBERT, F. (1995). Infrared spectroscopy applied to biochemical and biological problems. *Methods Enzymol.* **246**, 501–526.

SIEBERT, F., MÄNTELE, W. & KREUTZ, W. (1980). Flash-induced kinetic infrared spectroscopy applied to biochemical systems. *Biophys. struct. Mech.* **6**, 139–146.

SILVA, R. A. G. D., KUBELKA, J., BOUR, P., DECATUR, S. M. & KEIDERLING, T. A. (2000). Site-specific conformational determination in thermal unfolding studies of helical peptides using vibrational circular dichroism with isotopic substitution. *Proc. natn. Acad. Sci. USA* **97**, 8318–8323.

SLAYTON, R. M. & ANFINRUD, P. A. (1997). Time-resolved mid-infrared spectroscopy: methods and biological applications. *Curr. Opin. struct. Biol.* **7**, 717–721.

SMITH, S. O., BRAIMAN, M. S., MYERS, A. B., PARDOEN, J. A., COURTON, J. M. L., WINKEL, C., LUGTENBURG, J. & MATHIES, R. A. (1987). Vibrational analysis of the all-trans retinal chromophore in light-adapted bacteriorhodopsin. *J. Am. chem. Soc.* **109**, 3108–3125.

SPIRO, T. G. & GABER, B. P. (1977). Laser Raman scattering as a probe of protein structure. *Annu. Rev. Biochem.* **46**, 553–572.

SUREWICZ, W. K., MANTSCH, H. H. & CHAPMAN, D. (1993). Determination of protein secondary structure by Fourier transform infrared spectroscopy: a critical assessment. *Biochemistry* **32**, 389–394.

SUSI, H. & BYLER, D. M. (1987). FTIR study of proteins with parallel β chains. *Arch. Biochem. Biophys.* **258**, 465–469.

SUSI, H., BYLER, D. M. & GERASIMOWICZ, W. V. (1983). Vibrational analysis of amino acids: cysteine, serine, β-chloroalanine. *J. molec. Struct.* **102**, 63–79.

SUSI, H., TIMASHEFF, N. & STEVENS, L. (1967). Infrared spectra and protein conformation in aqueous solutions 1. The amide I band in H_2O and D_2O solutions. *J. biol. Chem.* **242**, 5460–5466.

TACKETT, J. E. (1989). FT-IR characterisation of metal acetates in aqueous solution. *Appl. Spectrosc.* **43**, 483–489.

TAKEUCHI, H. & HARADA, I. (1986). Normal coordinate analysis of the indole ring. *Spectrochim. Acta* (*A*) **42**, 1069–1078.

TAKEUCHI, H., WATANABE, N. & HARADA, I. (1988). Vibrational spectra and normal coordinate analysis of *p*-cresol and its deuterated analogs. *Spectrochim. Acta* (*A*) **44**, 749–761.

TIMASHEFF, S. N., SUSI, H. & STEVENS, L. (1967). Infrared spectra and protein conformations in aqueous solutions. *J. biol. Chem.* **242**, 5467–5473.

TONGE, P. J. & CAREY, P. R. (1989). Direct observation of the titration of substrate carbonyl groups in the active site of α-chymotrypsin by resonance Raman spectroscopy. *Biochemistry* **28**, 6701–6709.

TONGE, P. J. & CAREY, P. R. (1992). Forces, bond lengths, and reactivity: fundamental insight into the mechanism of enzyme catalysis. *Biochemistry* **31**, 9122–9125.

TONGE, P. J., FAUSTO, R. & CAREY, P. R. (1996). FTIR studies of hydrogen bonding between α,β-unsaturated esters and alcohols. *J. molec. Struct.* **379**, 135–142.

TONGE, P., MOORE, G. R. & WHARTON, C. W. (1989). Fourier-transform infrared studies of the akaline isomerization of mitochondrial cytochrome *c* and the ionization of carboxylic acids. *Biochem. J.* **258**, 599–605.

TONGE, P. J., PUSZTAI, M., WHITE, A. J., WHARTON, C. W. & CAREY, P. R. (1991). Resonance Raman and Fourier transform infrared spectroscopic studies of the acyl carbonyl group in [3-(5-methyl-2-thienyl)acryloyl]chymotrypsin: evidence for artefacts in the spectra obtained by both techniques. *Biochemistry* **30**, 4790–4795.

TORII, H. & TASUMI, M. (1992a). Application of the three-dimensional doorway-state theory to analyses of the amide-I infrared bands of globular proteins. *J. chem. Phys.* **97**, 92–98.

TORII, H. & TASUMI, M. (1992b). Model calculations on the amide-I infrared bands of globular proteins. *J. chem. Phys.* **96**, 3379–3387.

TORII, H. & TASUMI, M. (1996). Theoretical analyses of the amide I infrared bands of globular proteins. In *Infrared Spectroscopy of Biolmolecules* (eds. H. H. Mantsch & D. Chapman), pp. 1–18. New York: Wiley-Liss.

TORII, H. & TASUMI, M. (1998). *Ab initio* molecular orbital study of the amide I vibrational interactions between the peptide groups in di- and tripeptides and considerations on the conformation of the extended helix. *J. Raman Spectrosc.* **229**, 81–86.

TORII, H., TATSUMI, T., KANAZAWA, T. & TASUMI, M. (1998a). Effects of intermolecular hydrogen-bonding interactions on the amide I mode of *N*-methylacetamide: matrix-isolation infrared studies and *ab initio* molecular orbital calculations. *J. phys. Chem.* (*B*) **102**, 309–314.

TORII, H., TATSUMI, T. & TASUMI, M. (1998b). Effects of hydration on the structure, vibrational wavenumbers, vibrational force field and resonance Raman

intensities of *N*-methylacetamide. *J. Raman Spectrosc.* **29**, 537–546.

Toyoshima, C., Nakasako, M., Nomura, H. & Ogawa, H. (2000). Crystal structure of the calcium pump of sarcoplasmic reticulum at 2·6 Å resolution. *Nature* **405**, 647–655.

Toyoshima, C. & Nomura, H. (2002). Structural changes in the calcium pump accompanying the dissociation of calcium. *Nature* **418**, 605–611.

Trewhalla, J., Liddle, W. K., Heidorn, D. B. & Strynadka, N. (1989). Calmodulin and troponin C structures studied by Fourier transform infrared spectroscopy: effects of calcium and magnesium binding. *Biochemistry* **28**, 1294–1301.

Troullier, A., Gerwert, K. & Dupont, Y. (1996). A time-resolved Fourier transformed infrared difference spectroscopy study of the sarcoplasmic reticulum Ca^{2+}-ATPase: kinetics of the high-affinity calcium binding at low temperature. *Biophys. J.* **71**, 2970–2983.

Troullier, A., Reinstädler, D., Dupont, Y., Naumann, D. & Forge, V. (2000). Transient non-native secondary structures during the refolding of α-lactalbumin detected by infrared spectroscopy. *Nature Struct. Biol.* **7**, 78–86.

Ungar, D., Barth, A., Haase, W., Kaunzinger, A., Lewitzki, E., Ruiz, T., Reiländer, H. & Michel, H. (2001). Analysis of a putative voltage-gated prokaryotic potassium channel. *Eur. J. Biochem.* **268**, 5386–5396.

Vander Stricht, D., Raussens, V., Oberg, K. A., Ruysschaert, J.-M. & Goormaghtigh, E. (2001). Difference between the E1 and E2 conformations of gastric H^+/K^+-ATPase in a multilamellar lipid film system. Characterisation by fluorescence and ATR-FTIR spectroscopy under a continuous buffer flow. *Eur. J. Biochem.* **268**, 2873–2880.

Venyaminov, S. Y. & Kalnin, N. N. (1990a). Quantitative IR spectrophotometry of peptide compounds in water (H_2O) solutions. I. Spectral parameters of amino acid residue absorption bands. *Biopolymers* **30**, 1243–1257.

Venyaminov, S. Y. & Kalnin, N. N. (1990b). Quantitative IR spectroscopy of peptide compounds in water (H_2O) solutions. II Amide absorption bands of polypeptides and fibrous proteins in α-, β-, and random coil conformations. *Biopolymers* **30**, 1259–1271.

Venyaminov, S. Y. & Prendergast, F. G. (1997). Water (H_2O and D_2O) molar absorptivity in the 1000–4000 cm^{-1} range and quantitative infrared spectroscopy of aqueous solutions. *Analyt. Biochem.* **248**, 234–245.

Vogel, R. & Siebert, F. (2000). Vibrational spectroscopy as a tool for probing protein function. *Curr. Opin. chem. Biol.* **4**, 518–523.

Von Germar, F., Barth, A. & Mäntele, W. (2000). Structural changes of the sarcoplasmic reticulum Ca^{2+} ATPase upon nucleotide binding studied by Fourier transform infrared spectroscopy. *Biophys. J.* **78**, 1531–1540.

Von Germar, F., Galán, A., Llorca, O., Carrascosa, J. L., Valpuesta, J. M., Mäntele, W. & Muga, A. (1999). Conformational changes generated in GroEL during ATP hydrolysis as seen by time-resolved infrared spectroscopy. *J. biol. Chem.* **274**, 5508–5513.

Wang, J. H., Xiao, D. G., Deng, H., Webb, M. R. & Callender, R. (1998). Raman difference studies of GDP and GTP binding to c-Harvey ras. *Biochemistry* **37**, 11106–11116.

Wharton, C. W. (2000). Infrared spectroscopy of enzyme reaction intermediates. *Nat. Prod. Rep.* **17**, 447–453.

White, A. J., Drabble, K., Ward, S. & Wharton, C. W. (1992). Analysis and elimination of protein perturbation in infrared difference spectra of acyl-chymotrypsin ester carbonyl groups by using ^{13}C isotopic substitution. *Biochem. J.* **287**, 317–323.

White, A. J., Drabble, K. & Wharton, C. W. (1995). A stopped-flow apparatus for infrared spectroscopy of aqueous solutions. *Biochem. J.* **306**, 843–849.

White, A. J. & Wharton, C. W. (1990). Hydrogen-bonding in enzyme catalysis. Fourier-transform infrared detection of ground-state electronic strain in acyl-chymotrypsins and analysis of the kinetic consequences. *Biochem. J.* **270**, 627–637.

Wright, W. & Vanderkooi, J. M. (1997). Use of IR absorption of the carboxyl group of amino acids and their metabolites to determine p*K*s, to study proteins, and to monitor enzymatic activity. *Biospectroscopy* **3**, 457–467.

Zhang, M., Fabian, H., Mantsch, H. H. & Vogel, H. J. (1994). Isotope-edited Fourier transform infrared spectroscopy studies of calmodulin's interaction with its target peptides. *Biochemistry* **33**, 10883–10888.

Zscherp, C. & Barth, A. (2001). Reaction-induced infrared difference spectroscopy of the study of protein reaction mechanisms. *Biochemistry* **40**, 1875–1883.

Zscherp, C. & Heberle, J. (1997). Infrared difference spectra of the intermediates L, M, N, and O of the bacteriorhodopsin photoreaction obtained by time-resolved attenuated total reflection spectroscopy. *J. phys. Chem.* (*B*) **101**, 10542–10547.

Zscherp, C., Schlesinger, R., Tittor, J., Oesterhelt, D. & Heberle, J. (1999). In situ determination of transient pK_a changes of internal amino acids of bacteriorhodopsin by using time-resolved attenuated total reflection Fourier-transform infrared spectroscopy. *Proc. natn. Acad. Sci. USA* **96**, 5498–5503.